UNIVERSIDAD DE CONCEPCIÓN
FACULTAD DE CIENCIAS FÍSICAS Y MATEMÁTICAS

Spectroscopic dissection of the Globular Cluster NGC 6569

Unvealing multiple population features based on light and heavy elements as part of the bulge Cluster APOgee Survey(CAPOS)

Por: Nicolas Sebastian Barrera Diaz

Thesis presented to the Faculty of Physical and Mathematical Sciences of the Universidad de Concepción for the academic degree of Magíster in Galactic Astrophysics

Agosto 2024
Concepción, Chile

Profesor Guía: Sandro Villanova

AGRADECIMIENTOS

Quisiera expresar mi más puro agradecimiento a las personas que me acompañaron durante todo este proceso. Incalculable valor motivacional y emocional se lo debo a mis padres, Alejandra y Marcelo, y a mi hermano Cristóbal, quienes confiaron en mí en todo momento. La vida nos ha llevado a estar separados por el mundo, pero gracias a su incondicional apoyo, he logrado superar una de muchas barreras que están por venir.

Además, agradezco a toda mi familia en general que siempre me animaron en momentos de baja expectativa y soledad. Una mención especial se la dedico a mis mascotas, Cosmos, mi perro, y a mi enigmática y anónima gata, conocida como *la gata*. Sin ellos presentes, este proceso no se hubiese finalizado.

Adicionalmente, mi más sincera gratitud a las personas que conocí en Concepción durante estos 6 años y que ahora forman parte de mis lazos íntimos de amistad. Gracias por días y noches repletas de estímulos positivos y resaca. También, una noble mención a mi mejor amigo, Juan Carlos (*el sotac*), a quien le debo estos 14 años de linda amistad, en los cuales he basado gran parte de mi soporte emocional.

Finalmente, agradezco a los académicos que estuvieron presentes en mi proceso de aprendizaje. A mi guía de Tesis, Sandro Villanova, por la confianza que depositó en mí y las enseñanzas que me dejó. A mi prácticamente co-guía de Tesis, Douglas Geisler, por reafirmar su apoyo numerosas veces y confiar en mi conocimiento y habilidades. Al profesor José Fernández Trincado, por brindarme soporte técnico cuando lo necesité para manejar el software involucrado, y al resto del claustro del departamento de Astronomía que, gracias a sus críticas y orientación, pude llegar hasta aquí.

Gracias.

Resumen

Análisis de la evolución quimiodinámica en cúmulos globulares (CGs) ha revelado un fenómeno exclusivo respecto a sus poblaciones estelares, mostrando variaciones anómalas de elementos ligeros de estrella a estrella no esperables de una evolución estelar estándar, conocido como múltiples poblaciones (MPs). Sin embargo, la investigación espectroscópica de MPs, particularmente en la Vía Láctea, se ha centrado en CGs del halo y del disco, descartando casi por completo aquellos del bulbo galáctico, donde los escenarios de formación de MPs aún deben ser probados. Recientemente, el cúmulo globular NGC 6569, con una relativamente alta metalicidad, cumplió con los requisitos para definir MPs mostrando dispersiones anti-correlacionadas de [Na/Fe] y [O/Fe]. No obstante, evita características espectrales clave para explicar sus patrones de abundancia y, por lo tanto, la fuente de material enriquecido. Realizamos un análisis espectral detallado de 10 gigantes rojas utilizando espectros de alta resolución en el infrarrojo cercano recolectados con APOGEE-2S, como parte del bulge Cluster APOgee survey(CAPOS), para caracterizar completamente sus MPs. Usamos el código BACCHUS para obtener simultáneamente abundancias de MPs y elementos de procesos s/r- para investigar las fuentes de contaminación y posibles escenarios de formación de MPs basados en variaciones de abundancia. Derivamos un valor promedio de [Fe/H] = -0.93 $\pm$ 0.05 dex con una dispersión compatible con errores intrínsecos, sin evidencia de dispersión de metalicidad. Las abundancias de elementos α presenta un valor promedio de [α/Fe] = 0.41 dex, compatible con hallazgos previos en este cúmulo. En cuanto a sus MPs, clasificamos por primera vez dos poblaciones estelares distintas basadas en nitrógeno y evidenciamos una clara anti-correlación entre [N/Fe] y [C/Fe]. Además, derivamos valores de [Ce/Fe] y [Nd/Fe] por primera vez en NGC 6569 y apoyamos la idea de un material contaminado dominante por procesos r en la evolución temprana, basado en la razón [Ce/Nd] = -0.20. Además, probamos la calidad de las abundancias obtenidas comparando los parámetros atmosféricos de APOGEE Stellar Parameters and Chemical Abundance Pipeline (ASPCAP) con aquellos de la fotometría de *Gaia* + *2MASS*, resolviendo problemas adjudicados a la sobreestimación de la temperatura de las segundas poblaciones introducida por ASPCAP.

Keywords – NGC 6569, Cumulo Globular, Bulbo Galactico, Tesis de Magister

Abstract

Chemodynamical evolution analysis in globular clusters (GCs) has revealed an exclusive phenomena regarding their stellar populations, exhibiting anomalous star-to-star variations in light elements not expected from standard stellar evolution, known as multiple populations(MPs). However, spectroscopic MPs research, particularly in the Milky way, has focused mainly on halo and disk GCs, almost completely discarding those of the Galactic bulge, where MPs formation scenarios remain to be tested. Recently, the relatively high-metallicity bulge GC NGC 6569 filled the requisites to define MPs showing anti-correlated [Na/Fe] and [O/Fe] spreads. Nevertheless, it avoids key spectral features to explain its abundance patterns and thus the enriched material source. We performed a detailed spectral analysis of 10 red giants members using high-resolution near-infrared spectra collected with Apache Point Observatory Galactic Evolution Experiment II(APOGEE-2S), as part of the bulge Cluster APOgee Survey(CAPOS) project, to fully characterize its MPs. We use the Brussels Automatic Code for Characterizing High accuracy Spectra(BACCHUS) code to obtained simultaneously MPs and s/r-process elements abundances to investigate pollution sources and possible MPs formation scenarios based on abundance variations. We derived a mean value of [Fe/H] = -0.93 ± 0.05 dex with star-to-star spread compatible with intrinsic errors, finding no evidence of metallicity spread. α-elements enhancement preclude a mean value of [α/Fe] = 0.41 dex, compatible with previous findings on this cluster. Regarding their MPs, we classify for the first time two distinct stellar population based on nitrogen and evidence a clear anti-correlation between [N/Fe] and [C/Fe]. In addition, we derived values of [Ce/Fe] and [Nd/Fe] for the first time in NGC 6569 and support the idea of dominant r-process polluted material on the early evolution based on the ratio [Ce/Nd] = -0.20. Moreover, we test the quality of the obtained abundances comparing the atmospheric parameters from APOGEE Stellar Parameters and Chemical Abundance Pipeline(ASPCAP) to those from *Gaia* + *2MASS* photometry, disentangling problems adjudicated to the overestimation of temperature of second population introduced by ASPCAP.

Keywords – NGC 6569, Globular Cluster, Galactic Bulge, Master thesis

Contents

List of Tables

List of Figures

Chapter 1

Introduction and context

1.1 Milky Way assembly history and the Galactic Bulge

It is one of the main goals in modern astronomy studies to reconstruct and understand the assembly histories of galaxies, especially the Milky Way(MW), which is especially useful because it offers the possibility of studying galaxy-like properties with unprecedented detail. The MW is host to a number of companions that are gravitationally bound that include a population of about ~ 150 Globular clusters(GCs) and some ~ 30 dwarf galaxies that provides a tangible and verifiable prediction of structure formation in the cold dark matter(Λ CDM) cosmology (Fattahi et al., 2020). This implies that galaxies are surrounded by a diffuse stellar halo formed by the accretion and disruption of lower mass galaxies(Cattaneo et al., 2011). This formation mechanism indicates that the halo is composed of relatively old, metal-poor stars, many still part of substructures associated with accretion events(Tumlinson, 2009). Such is the case of the Galactic halo.

In this context, Galactic GCs are powerful cosmological archaeology probes as they are among the objects for which we can measure their age, metallicity and other properties with high precision (De Angeli et al., 2005), tracing back the history of the Galaxy formation bringing insights of *in situ* and accreted structures that are keys to form a picture of the primordial Universe(Massari et al., 2019).

Nevertheless, as we now know much about the history of the galactic halo and even about the disk, there remains a component of the galaxy in which dust-obscured objects near the galactic center awaits to be detected or studied more deeply. Such is the case of the Galactic Bulge(GB). This component is fundamental to recreate the formation of our Galaxy and other structures like the bar and inner disk. It contains more than a quarter of the total mass of the Galaxy (Valenti et al., 2016) and its believe to host a very important number of GCs($\sim$ 30) even at the metal-rich end because of the rapid chemical evolution in its deep potential well (Horta et al., 2021). These metal-rich GCs share the kinematics, spatial distribution, and composition of the bulge field stars (Bica et al., 2006) allowing to trace the bulge stellar population by means of its GCs (Minniti and Zoccali, 2007). Direct comparison of bulge field stars with metal-rich GCs has result in an age estimation of $\sim$ 10-13 Gyr for the bulk of its stellar population(Rich, 2001; Joyce et al., 2023; Catchpole et al., 2016). Also, element abundances of bulge giants shows that bulge stars have larger [O/Fe] and [Mg/Fe] than both thin and thick disk stars(e.g. Lecureur et al., 2007). This is the signature of a chemical enrichment by massive stars, progenitors of SNII, with little or no contribution from SNIa, and thus of a shorter formation timescale(below $\sim$ 2 Gyr) of the bulge with respect of both disk components(Minniti and Zoccali, 2007). In this context, GB and its globular clusters represent the most extreme population within the Galaxy. However, there are not a strong census on formation of galaxy bulges based on observational data of the GB or nearby galaxies. Ongoing burst of star formation in the center of high-redshift galaxies seems to be in contrast with secular formation or rapid and violent merging events in the primordial gas that have been proposed based on the morphology of nearby galaxies bulges (Kormendy and Kennicutt, 2004; Tadaki et al., 2017). In addition, there is not self-consistent chemodynamical Bulge model that support fully a current Bulge-formation scenario based on observational data(Barbuy et al., 2018). Fortunately, looking forward to improve constrains on formation models, now the historical observational caveats of the GB related with crowding and extinction are avoided by observing in the near-IR, together with precise astrometry, (Gaia Collaboration et al., 2016, 2023) minimizing dramatically contamination problems creating a precise three-dimensional map concerning the bulge area (Surot et al., 2020). Among other things, this allow to extract high-resolution spectra of individual stars (e.g. APOGEE, Majewski et al., 2017) to obtain precise element abundances to improve the chemical dimension. This is critical to understand the evolutionary history of the GB since its offer the possibility to trace back the conditions present in the early Universe. Therefore, we focus in one of the principal GB component, its globular clusters, which also allow us to explore their own formation and self-enrichment(and thus the one of the bulge).

1.2 Globular Clusters

As we briefly reviewed, globular clusters offer insights into stellar evolution and dynamics. Therefore, studying these clusters as a system provides a fossil record of a galaxy's formation, helping to constrain models of galactic formation and evolution. (Ashman and Zepf, 2008).

1.2.1 General properties of GCs

Star clusters distinguishing themselves from stellar associations and moving groups by their gravitational binding. Also, they distinguish themselves from galaxies as the first are contained into the other. Although there are exceptions as some galaxies do not host any clusters (Forbes et al., 2000) and also some GCs are even more massive that some dwarf galaxies (Belokurov et al., 2007). Globular clusters are dense and spherical collections of large groups of stars($\sim 10^4 - 10^6$) that are all gathered together in the shape of a globe concentrated toward their centers where the stellar density can range from 100 to 10000 stars per cubic parsec (Mackey and van den Bergh, 2005). Moreover, in comparison with another usual classification of stellar clusters, the Open Clusters(OCs), GCs are found to be very old(usually more than 10 Gyr) and massive system($\sim 10^4 - 10^6 M_{\odot}$) located mainly in the halo and the bulge with no presence of gas, dust or young stars(Mackey and van den Bergh, 2005). OCs on the other hand are younger systems with ages below 1 Gyr, subtended in the galactic disk and with ongoing star formation inferred from the presence of dust and gas within them (Paunzen et al., 2006).

In terms of metallicity, GCs span over a wide range(-2.5 $<$ Fe/H $<$ 0.5 dex) with a bimodal distribution but, mostly at the metal-poor end, while OCs are metal-rich($>$-0.8 dex), with some overlapping in between $\sim$ -0.8 dex (Muratov and Gnedin, 2010). Also, as we will see, one of the most fundamental characteristic of GCs are the presence of Multiple population(MPs) found in almost all ancients

GCs studied spectroscopically, while no evidence of this phenomenon has been found in any OC (Gratton et al., 2012b). MPs manifested in terms of light elements(sometimes heavy) star-to-star variations that are not produced by standard stellar evolution processes but through a very complex chemical history that changes from one GC to another (Gratton et al., 2012a) establishing more than one generation of stars contrary to the classical view of GCs as single coeval stellar populations. This has increased the importance of the chemical dimension since this phenomena is still puzzling.

1.2.2 Globular clusters in the Milky Way

The Milky Way's globular cluster system comprises over 150 identified members (Harris, 2010), though it's likely that some remain undetected due to obscuration by the Galactic bulge. The estimated total population is approximately 180 objects (Bica et al., 2016). These clusters exhibit a central concentration, with around half residing within 5 kpc of the Galactic center(Massari et al., 2019). Notably, some clusters extend beyond 100 kpc from the Galaxy's center (Pal 4, van Loon et al., 2009).

The system can be viewed as two or more distinct subsystems, with the majority forming a spherical, metal-poor halo distribution and a smaller subset of relatively metal-rich clusters that displays characteristics aligning with a thick disk population as well as part of the Milky Way's bulge population (Binney and Wong, 2017).

Also, there is a bimodality observed in the colour and metallicity of GCs, the blue, metal-poor clusters form in satellite galaxies which are accreted onto the Milky Way, while the red, metal-rich clusters form mostly in situ or, to a lower extent in massive, self-enriched galaxies merging with the Milky Way (Agertz and Gieles, 2016). This merging processes in the early epochs of the MW assembly reveal the true nature of the stellar populations in our Galaxy (Kruijssen et al., 2020, 2019). Some commonly known *cannibal* events include Gaia-Enceladus-Sausage (e.g. Grand et al., 2020), Sequoia (Myeong et al., 2019), Helmi streams (Helmi et al., 1999), Kraken (Kruijssen et al., 2020) and the Sagittarius dwarf galaxy(e.g. Johnston et al., 1999).

Figure 1.2.1: The globular cluster NGC 6569. Source: ESA/Hubble & NASA, R. Cohen

1.3 Thesis layout: NGC 6569

NGC 6569 is an old(12.8 ± 0.1 Gyr, Saracino et al. (2019)), massive ($2.29 \pm 0.21 \times 10^5 M_\odot$, Baumgardt and Vasiliev (2021)) globular cluster situated in the constellation Sagittarius, located in the Galactic bulge($l^\circ, b^\circ = 0.487, -6.676$) at approximately 3 kpc from the Galactic center (Baumgardt and Vasiliev, 2021) and ≈ 10 kpc from the Sun (Saracino et al., 2019). It has a relatively wide range of metallicity estimation [Fe/H] ∼ -0.87 to -0.76 (Zinn, 1985; Bica and Pastoriza, 1983; Valenti et al., 2005; Valenti et al., 2011; Johnson et al., 2018) coming from deep photometry and high resolution spectroscopy, along a region of high foreground interstellar reddening E(B-V) ∼ 0.49 - 0.55 (Zinn, 1985; Bica and Pastoriza, 1983; Valenti et al., 2005).

Recently internal kinematics an influence from the Galactic bar structure have identified at least 23 extra-tidal stars up to 5 tidal radii from the cluster, with radial velocities and metallicities matching NGC 6569, suggesting significant tidal interactions with the Galactic bulge (Hughes et al., 2023). The cluster's orbits, analyzed using spectral dynamics methods, indicate a significant influence of the galactic bar, with a capture probability of 0.2 (Bajkova et al., 2023). Integration of its orbit in a non-axisymmetric potential shows regular, stable motion over long periods, supporting the bar's impact.

Photometrically, this cluster exhibits a peculiar well studied double horizontal branch (Mauro et al., 2012), with two distinct groups of stars, separated by about 0.1 magnitudes in the K_s band, suggesting the presence of multiple stellar populations within the cluster. However, although the two HB groups are composed of cluster members, the luminosity difference is likely due to slight variations in helium content rather than differences in metallicity or light element abundances, indicating intrinsic features of the cluster rather than observational errors or field contamination (Johnson et al., 2018).

On the other hand, high resolution near infrared spectroscopy have revealed the chemical composition of NGC 6569, finding enhanced α-elements([α/Fe] $\sim$ 0.43), indicative of rapid early enrichment dominated by type II supernovae (Valenti et al., 2011). Moreover, clear (anti-)correlations between [O/Fe], [Na/Fe], [Al/Fe], and low $^{12}C/^{13}C$ ratios suggest at least two distinct stellar populations, indicating the presence of extra mixing during the red giant branch phase, supporting the evidence of multiple populations in NGC 6569 (Johnson et al., 2018). Additionally, (Johnson et al., 2018) found that NGC 6569 exhibits significant enrichment in heavy elements, with [La/Fe] = +0.38 dex and [Eu/Fe] = +0.49 dex. The moderately depleted mean [La/Eu] ratio of -0.11 dex suggests significant pollution via the r-process, though the cluster also experienced some s-process enrichment as indicated by the higher [La/Eu] values compared to more metal-poor systems (e.g. Yong et al., 2005).

However, GCs like NGC 6569 has not been fully characterized in terms of their chemistry, lacking fully elemental abundances obtained simultaneously to form a integrate picture of their stellar populations. In this respect, taking advantage of the recent capabilities of near infrared spectroscopy (e.g. APOGEE-2S, Majewski et al., 2017), the bulge Cluster APOgee Survey (CAPOS, Geisler et al., 2021) aim to investigate Bulge globular clusters(BGCs) penetrating obscuring dust toward the bulge to find key spectral features in the H-band and build a definitive database of the BGCs system for the first time. In order to do so, element abundances has to be obtained as precise as possible. In the case of NGC 6569, as part of

CAPOS targeting field, has a decent sample from where we can extract it spectra. In this study, we reinforce the chemical dimension on this cluster regarding its multiple population and complex and anomalous star-to-star light elements pattern within clusters stars. Based on the correlated spectral features supporting at least two populations of stars within NGC 6569, we aim to characterized them by other crucial multiple population elements, such as Nitrogen. Moreover, we expect to find anti- and correlated features in [N/Fe], [C/Fe] and [Al/Fe] and crucial information of first generation progenitors origin by their heavy element content(e.g. [Ce/Fe] and [Nd/Fe]), where we expected to find a clear r-process domination. Moreover, we compare our results to disk and halo counterpart to reveal the possible differences of this two distinct GCs systems.

Chapter 2

Stellar populations in Globular clusters

2.1 GCs as single stellar populations

To fully understand the complexity of stellar populations in GCs, we must understand historically how our view of their structure has changed. This is key to understand the current view of GCs because, although there is a paradigm shift around stellar populations in globular clusters, we cannot leave behind what has transcended, as it has laid the foundations of stellar evolution for decades. This change refers to the classical paradigm of globular clusters as single stellar populations.

A single stellar population(SSP) is a set of coeval (i.e., born in a single star formation burst)stars having the same age, initial chemical composition (in terms of both He and metal abundances), and different mass, distributed according to an initial mass function (IMF) (Gratton et al., 2012). While the range in [Fe/H] covered by Galactic GCs is very large, with values between $\sim$ -2.3 and +0.07 (e.g. Harris, 2010), nearly all GCs appear to be fairly homogeneous in heavy elements (i.e., Fe-peak, neutron-capture, and alpha-elements, see e.g. Carretta et al. (2009), with the exception of the most massive ones like ω Cen (e.g. Villanova et al., 2014); M22 or M54 (e.g. Da Costa et al., 2009; Carretta et al., 2010). In this context, it was believed that GCs did not experience any chemical changes internally. The proto-GC cloud inherited its metals from progressive metal-enrichment during the evolution of halo chemistry, rather than producing them in situ(James et al., 2004). Also, there were no dramatic dynamical events that could have caused a significant alteration in their mass throughout their lifetime. With this definition, an usual interpretation of SSP is defined by a single isochrone in the color-magnitude diagram (CMD)(see Section 2.1.5).

Therefore, with thousand hundreds to millions of stars with similar ages and metallicities bonded together since formation, single GCs have long been seen as the best laboratories for low-mass star physics and stellar evolution theory(see Section 2.1.1), taking advantage of the comparison of the observed positions of the stars in clusters' CMDs with the predicted paths of the stellar evolution models in the Hertzsprung-Russell diagram(Isochrones), leading also to some of the most significant progresses in the understanding and the description of convection, atomic diffusion, rotation-induced mixing, hydrodynamical instabilities, equation of state, opacities, mass loss, model atmosphere (e.g. Lebreton et al., 2014; Heasley and Mengel, 1972), and nuclear reactions in stellar interiors(Nucleosynthesis, see Section 2.1.2). In this context, by embracing the SSP paradigm, we shall review how this view has led to the development of some of the fundamental principles of stellar astrophysics.

2.1.1 Stellar evolution

As far as we know, stars undergo several process during their lifetime characterized by specific physical processes occurring in their interiors. The development in stellar evolution has been made possible to test and calibrate, on the one hand, by observations of star clusters. In particular, GCs, given their longevity, have the potential to develop a complete picture of all phases of stellar evolution. In Figure 2.1.1a, we can see the CMD of a typical GC, that theoretically we known as the Hertzsprung-Russel(H-R) diagram(Luminosity-Temperature). In it, we find a specific morphology from which we infer the different phases of stellar evolution, characterizing it through evolution models with which we base our knowledge to construct a stellar evolutionary tracks (See Fig 2.1.1b, an evolutionary track for a sun-like star). Thus, we separate the stellar paths in different phases or branches that gives us some certainties of how stars evolve[1].

- **Zero-Age Main Sequence (ZAMS)**: defined as the phase in stellar

[1]Here we only refer to stellar stages from hydrogen burning.

Figure 2.1.1: Example of a GC CMD morphology and evolutionary track of a low-mass star

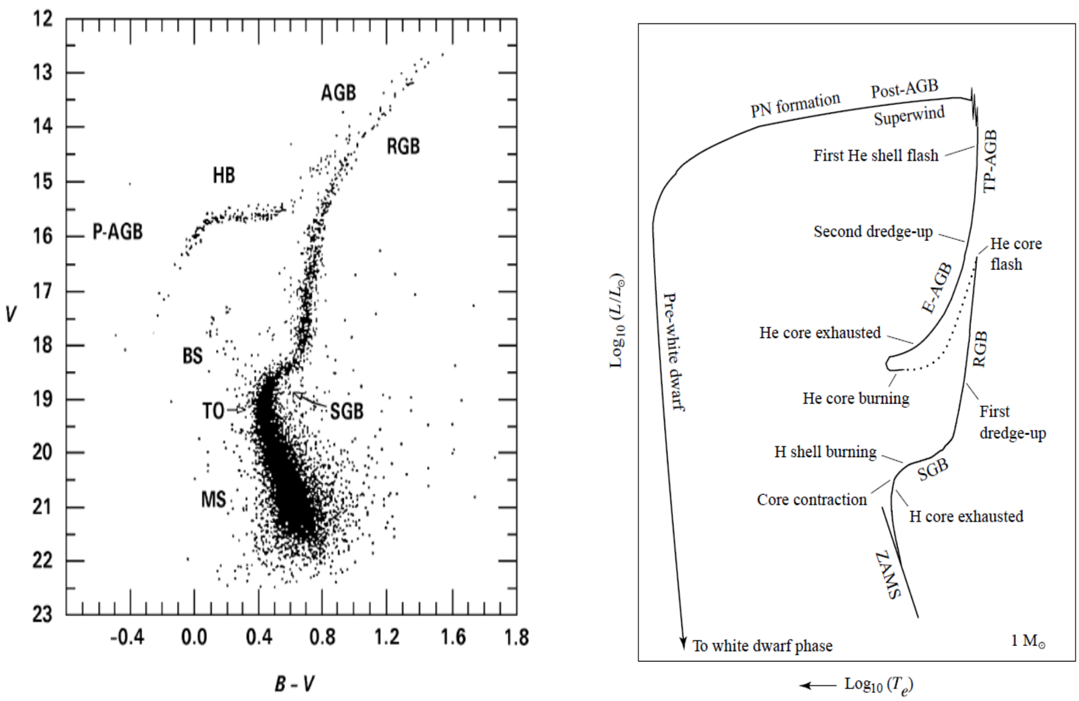

(a) Color-magnitude diagram for a typical globular cluster. Essentially the color index B-V of the stars is shown on the x-axis, while the y-axis denotes the surface brightness V.

(b) A schematic diagram of the evolution of a low-mass star of 1 $M_\odot$ from the zero-age main sequence to the formation of a white dwarf star evolution where stars are at the beginning of their main sequence lifetime. During this phase, stars are fusing hydrogen into helium in their cores and have not yet undergone significant nuclear burning processes. The ZAMS marks the point at which stars have just formed and are in a state of equilibrium between gravitational collapse and nuclear fusion (Douglas, 2024).

- **Main sequence (MS)**: defined as the phase where a star initiates hydrogen fusion in its core, which is sustained by the energy released from this process (Beccari and Carraro, 2014). This stage is characterized by the ignition of hydrogen in the core and the presence of CNO cycle-processed material at the surfaces of stars, indicating fast rotation and efficient mixing processes (Gouliermis et al., 2006).

- **Turn-off(TO) point**: defined as the stage where stars are departing from the main sequence phase and progressing into more advanced stages as a result of hydrogen exhaustion in their cores (Campbell et al., 2013).

- **Sub-Giant Branch (SGB)**: stage in the evolution of stars occurring after they leave the main sequence. During this phase, the core of the star contracts while the envelope expands (Goodarzi et al., 2021). This results in a decrease on the surface temperature, moving horizontally through the H-R diagram. The SGB is also where mass loss can occur, affecting the subsequent stages of stellar evolution (Salaris et al., 2016).

- **Red-Giant Branch (RGB)**: defined as stars with a helium core that is not burning, surrounded by hydrogen undergoing fusion (a hydrogen-burning shell). Stars are much more luminous than main sequence stars, having larger radii, i.e., giant stars. Their higher luminosity is due to their greater energy production, more than during their main-sequence phase, due to the region of hydrogen fusion being larger (Zhou et al., 2022), scaling vertically through the HR diagram. In this phase occurs the *first dredge-up*: as a result of strong convective mixing between layers, the outer atmosphere will display the spectral signature of hydrogen fusion (Carretta et al., 1999). The RGB is also characterized by mass loss (Salaris et al., 2016).

- **Horizontal Branch (HB)**: this stage is characterized by the commencement of the helium fusion through the triple-alpha process(see Section 2.1.2) in the stellar core(known as the helium flash [2]) and causes the temperature to increase while the radius decreases, thus the luminosity remains constant, moving roughly horizontally(and to the left) in the HR diagram (Salaris and Cassisi, 2005). It is a period of stable helium core burning distributing stars according to their envelope mass. The left end of the branch corresponds to stars with lower mass envelopes and the right end to stars with higher mass envelopes [3]. An interesting feature in this branch is a prominent gap in the HB. The gap occurs at the instability strip, a region of the Hertzsprung–Russell diagram largely occupied by several related classes of pulsating variable stars (Gautschy and Saio, 1996). These pulsating horizontal-branch stars are known as RR Lyrae variable stars.

- **Asymptotic-Giant Branch (AGB)**: During this phase, stars ascend towards the HR diagram burning hydrogen and helium in concentric shells around a degenerate core leading to the expansion and cooling of the star (Marigo et al., 2013). A common process occurs in stars with 4–8 $M_{\odot}$ at the early phases of the AGB(Early-AGB) when helium fusion comes to an end at the core and convection mixes the products of the CNO cycle known as the *second dredge-up*[4] (Lambert, 1992). Moreover, a *third dredge-up* can occur in evolved AGB stars and the elemental abundances at the envelope are altered by the mixing of CNO and s-process products to the outer layers of the star following thermal pulses (TPs), as a consequence of helium production in the hydrogen shell and subsequent periodic helium flashes (Uttenthaler et al., 2019). This process typically occurs several times on the AGB.

- **Final stages(Post-AGB)**: In the final stages of stellar evolution, stars undergo dramatic transformations leading to phenomena such as white dwarfs and supernovae. White dwarfs are the remnants of low-mass stars that have exhausted their nuclear fuel, contracting again to produce a planetary nebula with an extremely hot central star and then leaving behind a cooling core (Hansen, 1998). On the other hand, supernovae are powerful explosions that mark the end of a star's life. Every observed supernova has

[2]Non-degenerate cores initiate fusion more smoothly, without a flash.
[3]The spread of stars along the horizontal branch at constant luminosity also depends on metallicity, much stronger at lower metallicities.
[4]Some lower-mass stars experience the first and third dredge-ups in their evolution without ever having gone through the second.

being considered the terminal explosion of a star (Arcavi et al., 2017). These explosions can be triggered by core collapse in massive stars or interactions between ejecta and companion stars (Hirai and Yamada, 2015) leaving possible stellar remnants such as neutron stars or black holes.

2.1.2 Nucleosynthesis

Based on the well-understood Standard Model physics (Wagoner et al., 1967), predictions of the abundances of the light elements, D, ^{3}He, ^{4}He, and ^{7}Li, synthesized at the end of the 'first three minutes', are in good overall agreement with the primordial abundances inferred from observational data, thus validating the standard hot Big-Bang cosmology (e.g. Schramm and Turner, 1998). The nucleosynthesis chain begins with the formation of deuterium in the process $p(n,\gamma)$D[5]. Then it follows the 2-body reactions D$(p,\gamma)^3$He and ^{3}He(D, $p)^4$He. Heavier nuclei do not form in significant quantity because of the absence of stable nuclei with mass number 5 or 8 (which impedes nucleosynthesis via n^4He, p^4He or ^{4}He^{4}He reactions), and the large Coulomb barriers for reactions such as ^{3}He(^{4}He, $\gamma)^7$Li and ^{3}He(^{3}He, $\gamma)^7$Be (Fields et al., 2014). Therefore, heavier elements could not have their origin in the nucleosynthesis of the big bang and, in fact, we know that they are created through nuclear processes inside the interior of the stars and during the end of their life as we shall see.

2.1.3 Stellar Nucleosynthesis

Stellar nucleosynthesis is the nuclear process by which new nuclei are produced in stars during stellar evolution. These processes develop through the different phases of stellar evolution as they involve different physical inputs to generate the necessary conditions for the formation of heavier and heavier elements, therefore, they are directly related to what was discussed in section 2.1.1.

2.1.3.1 Hydrogen burning

The first set of nuclear reactions in stellar evolution involves hydrogen burning through the *pp* chains and the CNO bi-cycle. The first two reactions of the *pp* chains are

$$^1\mathrm{H} +^1\mathrm{H} \longrightarrow^2 \mathrm{D} + e^+ + \nu + \gamma \tag{2.1.1}$$

[5]We use this notation to represent the reaction $p + n \longrightarrow \gamma$+D

where e^+ accounts for the positron(that is then annihilated) and ν for the neutrino(which is then lost taking energy). And

$$^2\mathrm{D} + ^1\mathrm{H} \longrightarrow ^3\mathrm{He} + \gamma \tag{2.1.2}$$

After this, the main link of the *pp* chain($pp-1$) that occurs 86 % of the time is followed by

$$^3\mathrm{He} + ^3\mathrm{He} \longrightarrow ^4\mathrm{He}^{6} + 2^1\mathrm{H} + \gamma \tag{2.1.3}$$

There is also two more alternatives very unlikely to happen after reaction 2.1.2, the $pp-2$ chain(14 %): $^3\mathrm{He}(\alpha,\gamma)^7\mathrm{Be}(e^-,\nu)^7\mathrm{Li}(p,\alpha)^4\mathrm{He}$ and the $pp-3$ chain(0.02 %): $^3\mathrm{He}(\alpha,\gamma)^7\mathrm{Be}(p,\gamma)^8\mathrm{B}(e^+,\nu)^8\mathrm{Be}^*(\alpha)^4\mathrm{He}$.

The complete chain releases a net energy of 26.732 MeV but 2.2 % of this energy (0.59 MeV) is lost to the neutrinos that are produced. The main branch($pp-1$) is dominant at temperatures of 10 to 14 MK (Pagel, 1997). At higher temperatures, hydrogen burning takes place more rapidly (see Figure 2.1.2, including the triple α process, see section 2.1.3.2) by a catalytic cycle involving the CNO elements that, in fact, have to be already present, therefore this is not a primordial cycle involving first generation stars. The main part of the cycle involves C and N, while the ON cycle usually contributes little energy, but becomes significant at high temperatures. At temperatures of several $\times 10^7$ K, the CNO cycle breaks out into third and fourth branches(Pagel, 1997)(see Figure 2.1.3). Because of the differing rates of the component reactions, the CNO cycle modifies the initial composition of the material, which typically has O > C > N, making more ^{14}N at the expense of carbon and (at the higher temperatures) oxygen.

At still higher temperatures ($> 10^8$K), nuclear reactions become so fast that there is not enough time for β-decays(e.g. that of ^{13}N) and begins a so-called fast CNO process leading into hot Ne–Na and Mg–Al cycles. The $^{22}\mathrm{Ne}(p,\gamma)^{23}\mathrm{Na}$ reaction takes part in the neon-sodium cycle of hydrogen burning. This cycle plays a crucial role for the synthesis of the elements with mass A = 20-25 in asymptotic giant branch stars, classical novae explosions and type Ia supernovae, where hydrogen burning occurs at high temperatures (Depalo, 2015). The Mg-Al chain becomes active at higher temperature (> 80MK) and the two most fragile isotopes ^{25}Mg and ^{26}Mg are the first ones to be destroyed. $\sim$ 70 MK are required

[6] That we refers hereafter as α particle

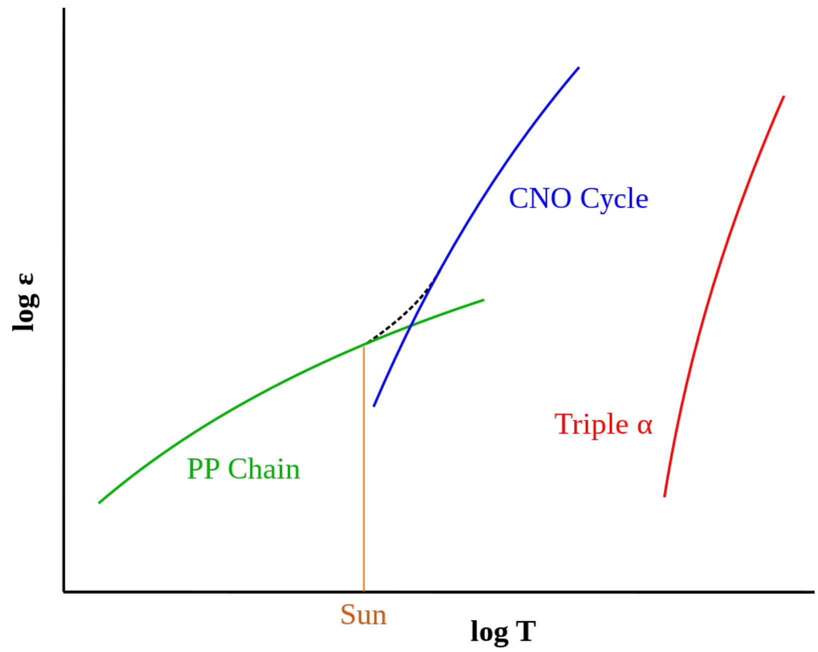

Figure 2.1.2: Logarithm of the relative energy output (ϵ) of *pp* chain, CNO and triple-α fusion processes as a function of T (Adelberger et al., 2011).

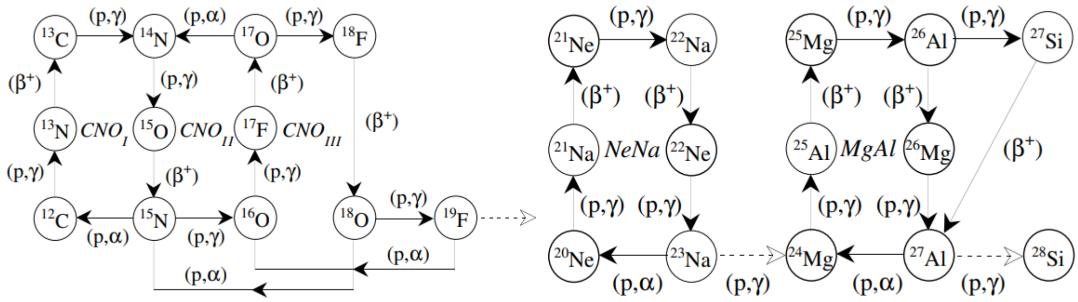

Figure 2.1.3: CNO-cycle and the NeNa- and MgAl-chains (Arnould et al., 1999).

to start depleting ^{24}Mg and substantial amounts of ^{27}Al are produced through this chain. Also, at sufficient temperatures there is ^{28}Si production.

2.1.3.2 Helium burning

At the RGB phase, the H-exhausted core continues to contract in radius (while expanding as the H-burning shell make its way outwards in mass) and heat up[7]. At some point, helium-burning, sets in at temperatures of the order of 10^8K and densities $\sim 10^4$gmcm^{-3} through the triple α reaction ^{4}He(^{4}He)^{8}Be(^{4}He, γ)^{12}C(Pagel, 1997). The net energy liberated in the process is 7.275 MeV. Other important He-burning reactions involve heavier elements. ^{12}C$(\alpha, \gamma)^{16}$O converts a substantial fraction of the carbon from triple-α into oxygen. More advanced He-burning reactions may take place at $T \sim 10^9$K at shell-burning stages and explosive nucleosynthesis, such as ^{16}O$(\alpha, \gamma)^{20}$Ne$(\alpha, \gamma)^{24}$Mg(Charbonnel, 2016). Moreover, He-burning from pre-processed H-burning material (like ^{14}N) can lead to reactions that serve as a source of free neutrons for the neutron capture processes in massive stars ^{14}N$(\alpha, \gamma)^{18}$F$(\beta^+\nu)^{18}$O$(\alpha, \gamma)^{22}$Ne$(\alpha, n)^{25}$Mg. In low mass stars there is also an important neutron source involving He-burning e.g. ^{13}C$(\alpha, n)^{16}$O.

2.1.3.3 Later burning stages

In low mass stars ($M < 8M_\odot$), core-burning cease by the formation of a degenerate CO core. Massive stars ignite carbon in the non-degenerate core leading to main reactions involving several elements up the iron peak.

- Carbon-burning ($T \sim 10^9$K)

$$
\begin{aligned}
{}^{12}\mathrm{C}({}^{12}\mathrm{C})^{24}\mathrm{Mg}^* \longrightarrow & \alpha +^{20}\mathrm{Ne} \\
& p +^{23}\mathrm{Na} \\
& n +^{23}\mathrm{Mg}
\end{aligned}
\tag{2.1.4}
$$

- Neon-burning ($T \sim 1.5 \times 10^9$K)

$$
{}^{20}\mathrm{Ne}(\gamma, \alpha)^{16}\mathrm{O}; \quad {}^{20}\mathrm{Ne}(\alpha, \gamma)^{24}\mathrm{Mg} \tag{2.1.5}
$$

[7]This process is slowed down by degeneracy in the case of low-mass stars

Figure 2.1.4: Binding energy of nuclei and interior structure of evolved stars.

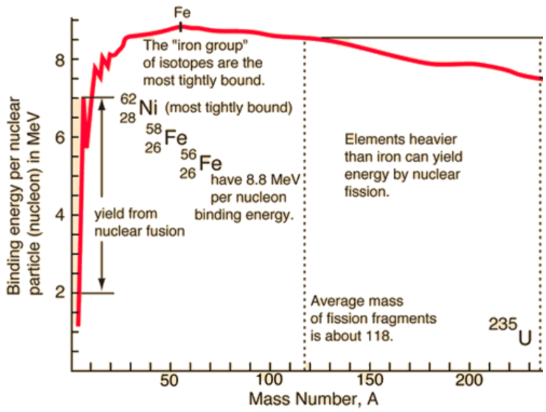

(a) Binding energy per nucleon as a function of mass number (Nave, 2010).

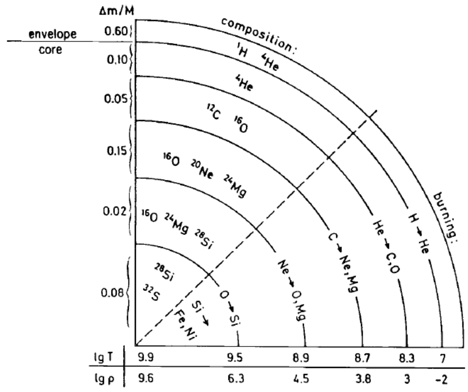

(b) Adapted schematic illustration of the 'onion-like' structure in the interior of evolved high mass stars (Kippenhahn et al., 2013).

- Oxygen-burning ($T \sim 2 \times 10^9$K)

$$\mathrm{O} + \mathrm{O} \longrightarrow \mathrm{Si}, \mathrm{S}, \mathrm{etc} \tag{2.1.6}$$

- Silicon-burning ($T \sim 3 \times 10^9$K)

$$^{28}\mathrm{Si}(\gamma, \alpha)^{24}\mathrm{Mg} \tag{2.1.7}$$

followed by

$$^{28}\mathrm{Si} + \alpha + p + n \longrightarrow \text{iron peak elements.} \tag{2.1.8}$$

At this last point, a large number of reactions will be subject to photodisintegration leading to free n, p and α particles. These react with ^{28}Si building up heavier nuclei up to ^{56}Fe. Due to its strong binding energy[8](see Figure 2.1.4a), this nuclei becomes the dominant species in the core. Here, the star ends to have an 'onion-like' structure consisting of the resulting products of the previous burning phases(see Figure 2.1.4b). Finally, there is a dynamical collapse of the core which lead to photodisintegration that even breaks the ^{56}Fe nuclei into α particles reversing the effect of all prior burning phases. Such processes can occur during supernovae explosions (Kippenhahn et al., 2013).

[8]Technically this refers to the binding energy per nucleon, which is the binding energy divided by number of nucleons.

2.1.4 Neutron-capture nucleosynthesis

The nuclear burning we discussed in section 2.1.3 is able to produce only elements up to iron, since the creation of heavier elements is endothermic. Elements above the iron group are not effectively produced by reactions between charged particles, they result from neutron captures on a seed nucleus(predominantly ^{56}Fe). There are two main neutron-capture processes. If the neutron-capture time is long compared to the β-decay time, the process is called the slow neutron-capture process(s-process). If it is rapid, it is called the rapid neutron-caputre process(r-process). The s-process occurs during mixing episodes in the course of AGB evolution where there are sources of free neutrons due to He-burning(see Figure 2.1.5a); (e.g. Ratkiewicz et al., 2019), whereas the r-process may occur during SN II outbursts, or possibly in other high-energy events related to neutron stars (e.g. Kasen et al., 2017). The s-process typically progresses along the valley of β stability(stable nuclide, see Fig 2.1.5b), where neutron captures occur at a rate regulated by β-decay processes (Lugaro and Herwig, 2001). On the other hand, the r-process involves rapid neutron captures that move material far from the valley of stability(to the neutron rich portion) and these newly synthesized unstable nuclei eventually decay back to stability, forming stable r-process nuclei (Sneden et al., 2008).

2.1.5 Isochrones

With the dual combination of how stars evolved(stellar evolution) and internal structure and processes(nucleosynthesis) it becomes possible the modeling of stellar populations in GCs(but also in Open clusters). Such models are called Isochrones. Isochrones are a set of stellar models compute at the same(iso) age(chrone), which considers both the dynamic dimension (initial mass, mass loss, etc.) and the chemical composition, typically using [Fe/H] and [α/Fe] values(see Figure 2.1.6a). As we mentioned in section 2.1, GCs as SSPs have been useful to constrain these stellar models to such point where we describe its stellar populations with a single isochrone(see Fig 2.1.6b), process called isochrone fitting. Remarkably, through the fitting in the TO point, we can estimate the age of the cluster and on the other hand, we use other stellar stages to fix and thus estimate the chemical composition (e.g. Gontcharov et al., 2023).

Figure 2.1.5: S-process production and the valley of stability.

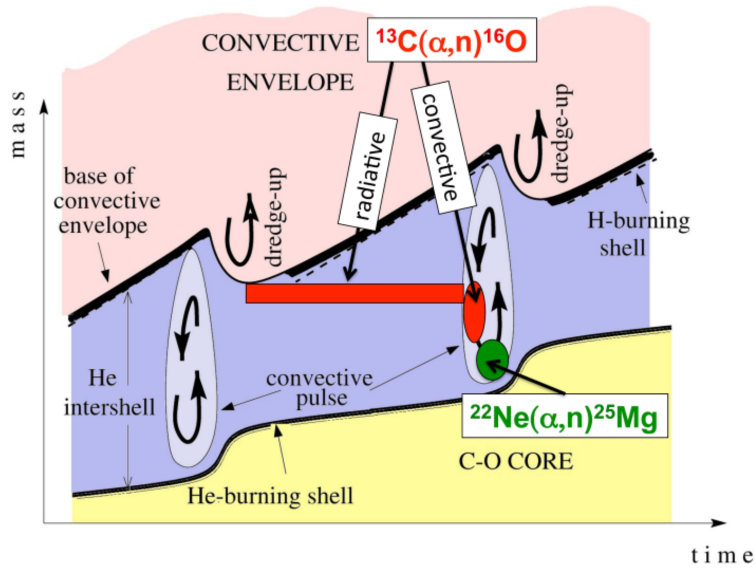

(a) Schematic illustration of the evolution of the internal structure of an AGB star where neutrons are released for the s process (Maria, 2016).

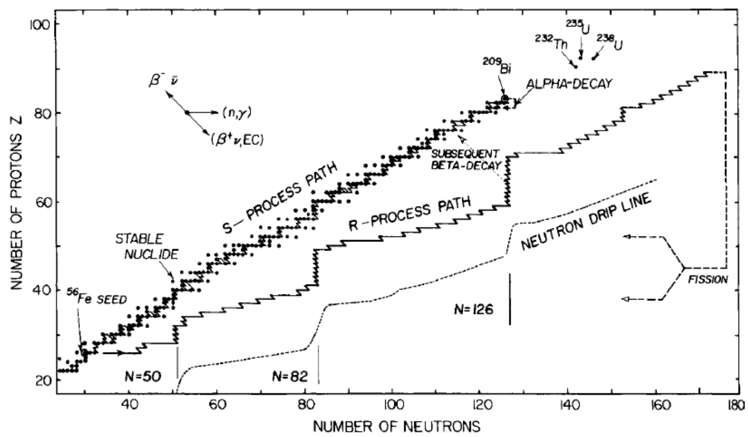

(b) Neutron capture paths in the N, Z plane (Pagel, 1997).

Figure 2.1.6: S-process production and the valley of stability.

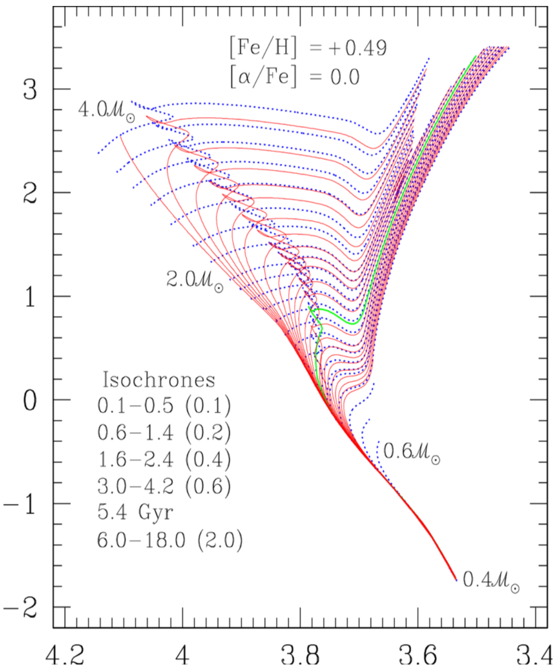

(a) Grid of evolutionary tracks with fixed [Fe/H]. The isochrones span the range of ages from 0.1 to 18.0 Gyr and masses from 0.1 $M_{\odot}$ to 4.0 $M_{\odot}$ (VandenBerg et al., 2006).

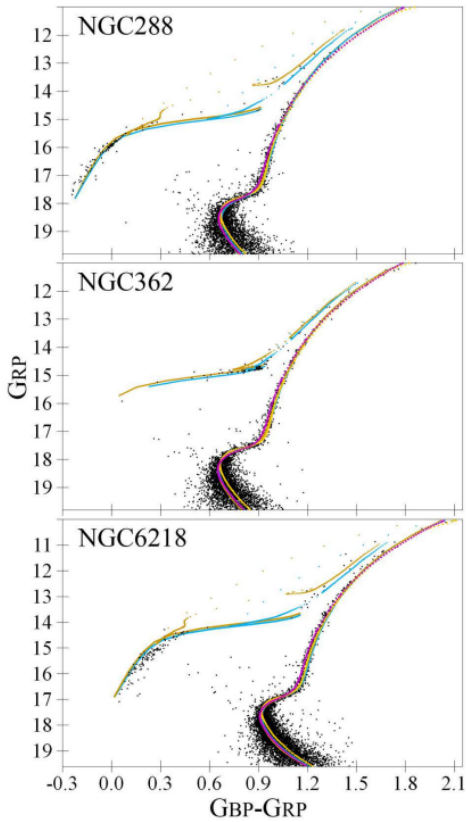

(b) BaSTI-IAC isochrone fitting example of 3 globular clusters with GAIA filters (Gontcharov et al., 2021).

2.2 The multiple population phenomenom in GCs

As we have seen, globular clusters (GCs) were traditionally thought to be single stellar populations (SSPs) (Renzini, 1988), but nowadays we know that they consist of multiple generations of stars (??). In principle, the fact that real clusters are not exactly single stellar populations should be obvious, because their formation is not predicted to be instantaneous (typically spanning over a few million years) (Elmegreen, 2000) (thus all stars having the same age) or completely homogeneous (the original molecular cloud is not fully chemically homogeneous, with variations in metallicity up to ~ 0.1 dex) (Bland-Hawthorn and Freeman, 2010). However, the differences that we find between generations of stars in GCs are much more significant than simply a small spread of the formation epoch or original inhomogeneities (Piotto, 2009). In fact, within what we call the second generation, we can define subpopulations with characteristics that challenge the classical paradigm of stellar populations in GCs (Milone, 2017). In this context, instead of separating the populations generationally, we will use the terms first population (1P) and second population (2P) for stars that share signatures typical of field stars (hence of the original molecular cloud composition) and anomalous or enriched stars (in specific elements such as Na, O, Mg, and Al, with differences in [Na/Fe] and [O/Fe] of up to ~ 0.5 dex) (Carretta et al., 2009b). This is because, although there is a generational difference (with age differences usually less than 1 Gyr), it is not significant compared to the chemical and spatial differences that exist (D'Antona, 2016). In addition, the generational terminology generates a direct link to their origin, which has not been determined so far. As a consequence, this phenomenon has historically been referred to as multiple populations (MPs) (Gratton, 2019). In the following sections, we describe the phenomenology of GC MSPs.

2.2.1 Star-to-star abundance variations

MPs are defined as the presence of star-to-star variations in chemical abundances, not expected from stellar evolutionary processes (Bastian and Lardo, 2018). These variations, in particular in light elements(e.g. He, C, N, O, Na, Mg and Al), are imprinted in GCs CMDs causing complexities in explaining the phenomena with single stellar models. These variations are used to separate populations.

2.2.1.1 Observational evidence of MPs through stellar evolution

Since the pioneer study of Osborn (1971), who discovered two N-enhanced stars in M 10 and M 5, there has been plenty of evidence of MPs not only coming from brighter and evolved stars(e.g. RGB), but in all evolutionary stages. Also, MPs are reproduce in GCs CMDs as multiple branches that are not produce by age differences and this also has been seen through all main stellar stages.

Distinct CN band strengths in seven MS stars of 47 Tuc was found by Hesser and Bell (1980), similar to those in giant stars. Since there is no mechanism able to mix Nitrogen to the surface in MS stars(MS low-mass stars do not have a convective envelope able to transport the nuclearly processed material to the atmosphere), this implies a primordial origin. Later, Gratton et al. (2001) discovered anti-correlated Na-O and Mg-Al abundances for a few main sequence turn-off stars in NGC 6752 and NGC 6397. Since the temperature at which the reactions that produce Na and destroy Mg (see section 2.1.3) can not be reached by MS stars, this was a clear indication of an external origin. Photometrically, the first evidence of multiple MSs was in ω Cen, showing up to three distinct sequences(Villanova et al., 2007), differentiated in their He content with the bluer sequence enriched to $Y \sim 0.38$(Norris, 2004). Later, Piotto et al. (2007b) presented a colour-magnitude diagram of NGC 2808 based on HST filters showing three distinct MSs in this cluster with the same age and metallicity but three different He abundances(See Fig. 2.2.1a). Moreover, complementing less evolved MS stars, SGB stars contribute to a more definitive acceptance of primordial origin since before the first dredge up no efficient mixing is possible (e.g. Milone et al., 2008).

In the case of RGB stars, these have been by far the most studied mainly because they are the most accessible due to their brightness. CN and CH bimodalities distributions has been found in several clusters together with relations between C and N and heavier elements such as Na and Al (e.g. Norris et al., 1981; Gratton et al., 2004). Also, several anti-correlations between Na-O and Al-Mg remains as the famous ones since they are directly linked to the MPs phenomena(See section 2.2.1.2) (e.g Carretta et al., 2009a; Pancino et al., 2017a). Remarkably, the Na-O anticorrelation has been proposed to be caused by peculiar evolution of RGB stars. However, the fact that this feature is also found in unenvolved stars, primordial differences within GC stars remains as the only possibility with the MPs phenomena being the only possible scenario able to explain it. In addition, multiple photometric sequences(See Fig. 2.2.1b) have also been found first in massive clusters (ω Cen, M 54, NGC 2808, NGC 6388, 47 Tuc) and only later in more average globular clusters (NGC 1851, NGC 6752, M 22, or the Magellanic Clouds ones)(see e.g. Gratton et al., 2012b, and references therein).

Evidence of MPs along the HB relate the He content variations with this phenomena, also showing split branches(See Fig. 2.2.1c). This splitting of the HB has long been related to the so-called second parameter problem that state that the colour of the HB is determined not only by metallicity (e.g. Caloi and D'Antona, 2005). In addition, variations in proton-capture elements are expected to be correlated with variations of the He content (Piotto et al., 2007a). This is a common signature present also in AGB stars in several individual cluster (like M 3, M 92, NGC 362, NGC 1851, NGC 6752, NGC 2808, and NGC 6121, Gruyters et al. (2017)), where multiple AGB have also been detected(See Fig. 2.2.1). Moreover, MPs have been detected also in the white-dwarf cooling sequence by their He content (Gruyters et al., 2017).

2.2.1.2 Light elements abundance variations

MPs are characterized mainly by variations in light element abundances. However, only some elements show changes that are common among all GCs and, in other cases, although the evidence is scarce, the direct relationship that they have in the phenomenology of the MPs cannot be disentangled. Nevertheless, these variations features are not found in the field or OCs (e.g. Martell et al., 2011), implying that some unique chemical enrichment mechanism is operating in GCs and can be unambiguously understood as the result of H-burning through the CNO-cycle and the NeNaMgAl-chains(See section 2.1.3). We will consider in the following the elements from He to Si.

- **Helium**: Helium abundance variations among GCs stars comes from high-precision photometry and direct measurements in RGB and HB stars (Charbonnel, 2016). The maximum helium spread on helium determined is 0.13 dex in NGC 2808 in MS stars (Milone et al., 2012). However, as we mentioned, He spread is found along several stellar stages.
- **Lithium, beryllium and Flourine**: In some clusters it is found Li and F anti-correlated with Na and also the presence of Be (Lind et al., 2009;

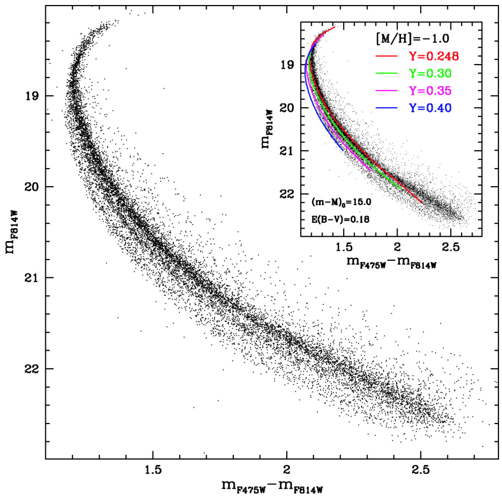

(a) Observed NGC 2808 MS CMD fitted with four 12.5 Gyr isochrones, with different color code He content (Piotto et al., 2007b).

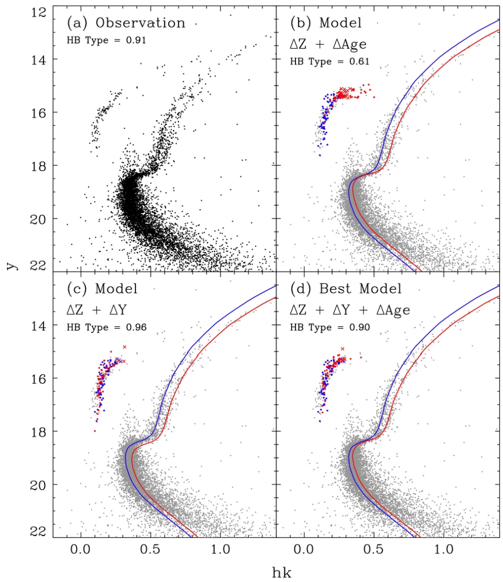

(b) Population models for NGC 288 compared with the observed CMD. Red lines and symbols are for the metal-rich second generation population, while the blue lines and symbols are for the metal-poor population (Roh et al., 2011).

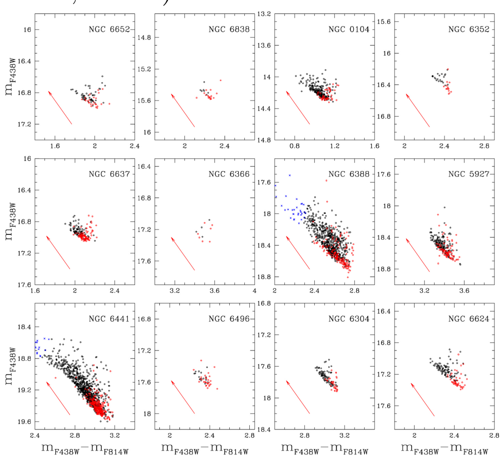

(c) CMDs for the red HB stars of the Galactic GCs studied in Dondoglio et al. (2021). 1P and 2P stars are colored red and black, respectively. Blue crosses represent the blue HB stars.

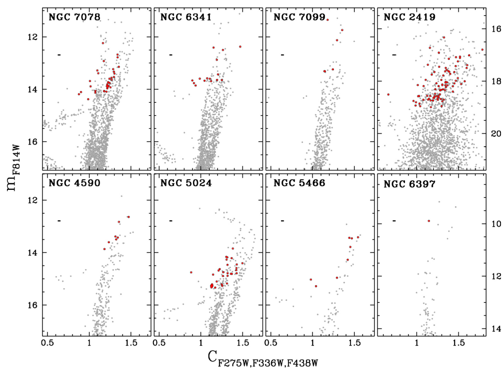

(d) CMD of several clusters studied in Lagioia et al. (2021) for AGB stars.

Figure 2.2.1: MPs as seen throught GCs CMDs.

Pasquini et al., 2007; Denissenkov et al., 2006; Smith et al., 2005). If the 2P low-mass star that we see today were formed from the pure ejecta from 1P stars, we would not see these elements, since they are destroyed early in stellar interiors. This implies a complex mixing episode occurring during the 2P stars formation with pristine gas (Prantzos and Charbonnel, 2006).

- **CNO**: The vast majority of GCs display N anti-correlated with C (e.g. Mészáros et al., 2020). However, the sum C+N+O remain constant in most globular cluster stars (e.g. Mészáros et al., 2015). This implies a recycle of only H-burning products, otherwise (e.g. He-burning) we will see an increase in the N values.
- **Sodium**: The abundances of Na are found to be anti-correlated with O(See Fig. 2.2.2a) in almost all globular cluster studied (Carretta et al., 2009). Such is this feature that Carretta et al. (2009) proposed a new definition of GCs as stellar clusters showing the Na-O anti-correlation.
- **Magnesium and Aluminium**: Mg and Al appeared to be anti-correlated(See Fig. 2.2.2b) to different extent depending on the cluster, while the metal-poor and more massive cluster shows this feature indistinctly, this is not the case for the metal-rich end and less massive clusters (e.g. Mészáros et al., 2020).
- **Silicon**: Si-Mg anticorrelations are found in massive and metal-poor GCs. This implies leakage from the MgAl chain into Si production through the $^{26}\mathrm{Al}(p,\gamma)^{27}\mathrm{Si}(e-,\nu)^{27}\mathrm{Al}(p,\gamma)^{28}\mathrm{Si}$ reactions. Without this leakage, we would expect a simple correlation between Mg and Si since they are both alpha elements (e.g. Mészáros et al., 2020).
- **Potassium**: Large range of K have been found in some clusters (e.g. NGC 2419 Mucciarelli et al., 2012). Some weak Mg-K exist in a few clusters, but the K enhancement is no understood (e.g. Mészáros et al., 2020).

2.2.1.3 Fe-peak elements

Evolutionary models of GCs predict that generations of stars within clusters will experience significant Fe enrichment from the ejecta of the earliest, massive core collapse SNe (e.g. Parmentier et al., 1999). However, overall, GCs are found to be fairly homogeneous in iron-peak elements (Gratton et al., 2004), with some

Figure 2.2.2: Light elements NaOMgAl anti-correlations.

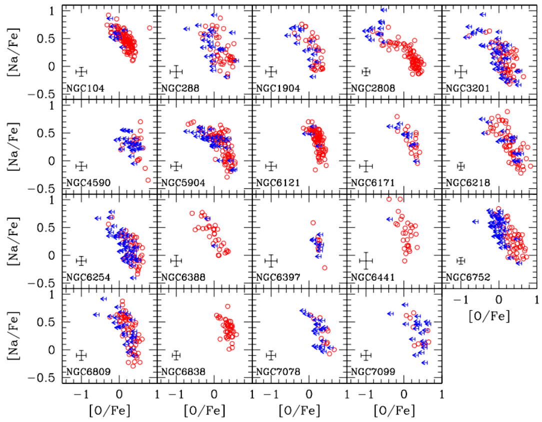

(a) The Na-O anti-correlation observed in all the 19 GCs of Carretta et al. (2009).

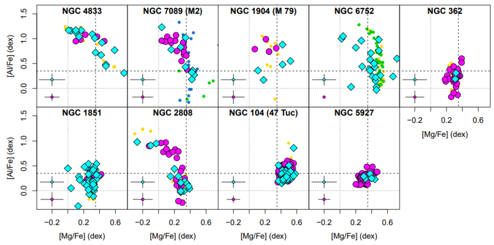

(b) Mg-Al anti-correlation of 9 GCs from Pancino et al. (2017b) color-code by instruments(GES UVES(cyan),GIRAFFE(magenta) and FLAMES(gold)).

remarkable exceptions of ω cen(suspected to be the stripped remnant of an accreted dwarf galaxy (Meylan, 2003)), M54 (associated with the nucleus of Sagittarius dwarf spheroidal galaxy (Layden and Sarajedini, 1997)), NGC 3201 (Gonzalez and Wallerstein, 1998), NGC 1851 (Carretta et al., 2012), M22 (Marino et al., 2011), Terzan 5 (Ferraro et al., 2009b) and NGC 6273 (Yong et al., 2016). Such is the case for Fe (e.g. Mészáros et al., 2020) and Ni, Cu and Mn showing no significant spread through several [Fe/H] values (Gratton et al., 2004).

2.2.1.4 n-capture elements

Because globular cluster (GC) abundance studies focus primarily on cool giants (the brightest members), there is a lack of reported n-capture element abundances since most strong transitions of n-capture elements occur at wavelengths below 5000 $\mathring{A}$ (Gratton et al., 2004). The reported n-capture elements include mostly Ba, La, and Eu, and to a lesser extent Y, Zr, Ce, and Nd (Gratton et al., 2004). Ba and Eu have served to estimate the s-process ([Eu/Ba] $\sim +1$) and r-process ([Eu/Ba] ~ -1) dominance among field and GC stars (Busso and Wasserburg, 1999). Overall, n-capture element star-to-star variation in field stars spans a wide range in the metal-poor end, [Fe/H] < -2.5 dex, and it is less extreme for metal-rich stars (Sneden and Gallino, 2008). This trend is similar to cluster-to-cluster variations, and it has been proposed that original inhomogeneities in the proto-GC are responsible. However, star-to-star variations among GCs are more prominent, with differences up to ~ 1.0 dex in [Ba/Fe] and [Eu/Fe] (e.g., Johnson et al., 2018).

In general, these variations do not correlate with light element variations, but recently there is strong evidence of a Ce-N correlation in a few clusters (e.g., Ton 2 and NGC 6380) (e.g., Fernández-Trincado et al., 2022, 2021) that may indicate the pollution of intermediate-mass AGB stars to the second population (2P).

2.2.1.5 Relation with GCs properties

Independently of GCs extension, 2P are systematically more concentrated than 1P stars (e.g. Lardo et al., 2011), only with a few exceptions (See e.g. NGC 6362 Miholics et al., 2015). Also 2P stars show more radially anisotropic velocity distribution, low binary fraction and are more numerous than 1P stars (Bastian and Lardo, 2018). Standard stellar evolution state that the stellar ejecta released into the cluster should not depend on cluster properties (Bastian and Lardo, 2018). However, an important role is achieved by the cluster mass related to the MPs phenomenology, where it has been found a general relation between larger extents in the Na-O anti-correlation(and He spread (Milone, 2015)) and cluster mass and magnitude(See Fig. 2.2.3a), presumably because GCs deep enough potential well able to retain more efficiently the stellar ejecta to form the enriched 2P stars(reason why we do not found MPs in OCs). In addition, nearly all of the ancient GCs that have been deeply studied seems to show MPs, but it appears to be a limit where massive old clusters older than $\sim$ 6 Gyr host MPs (Hollyhead et al., 2017) while those young clusters younger than $\sim$ 2 Gyr do not (Martocchia et al., 2018). Moreover, there seems not to be a metallicity dependence since MPs are found in the full range of GC metallicities, from [Fe/H] $\sim$ -2.5 to near solar metallicity(See Fig. 2.2.3b).

2.2.2 The polluters and MPs formation scenarios

At the time that only elemental abundances of RGB stars were determined, it was proposed that GC stars modify their surface composition along this branch invoking deep mixing theories between the stellar convective envelope and the H-burning shell (Denisenkov and Denisenkova, 1990). Observation of C, N and Li can be well explained by thermohaline mixing, but the presence of heavier light elements such as Na, Mg and Al and the efficiency of the mixing process is debatable since this not reach deep enough hot layers to induce variations in the RGB. Additionaly, in low-mass red giants the temperature is not high enough

Figure 2.2.3: Relations between GCs properties and MPs

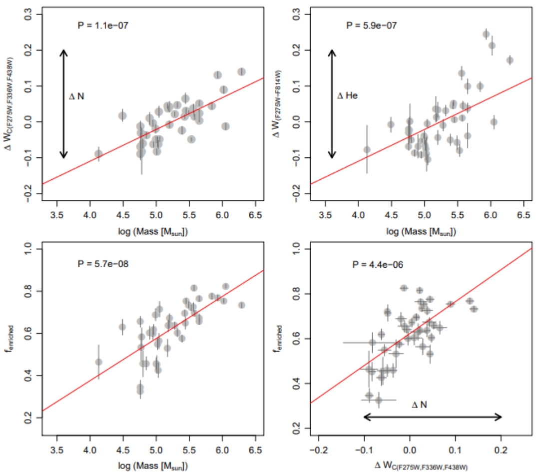

(a) MP properties variations with the present day GC mass and HST UV Legacy survey colors. $f_{enriched}$ is the fraction of 2P stars relative to the total number of stars. Data from Milone et al. (2017).

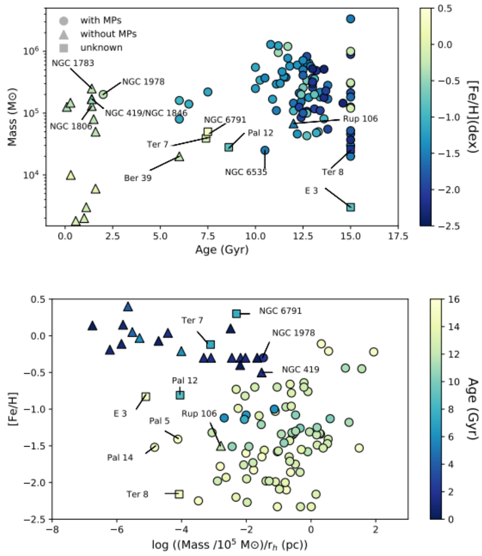

(b) Mass-Age-[Fe/H] relations from literature where MPs are present withing clusters. Data from Krause et al. (2016) and Bastian and Lardo (2018).

to activate the Mg-Al chain. Moreover, light elements variation found in less evolved stars at MS and SGB completely contradict these assumptions (Gratton et al., 2001). Therefore, the observed abundances cannot come from natural evolutionary processes within GCs stars, and the only possible solutions has to involve a complex GCs self enrichment process. The different scenarios where this have developed involve what we call the "polluters", massive short-lived 1P stars that enhance the intracluster environment with H-burning products to create 2P stars. In this context, polluters not only must be able to bring the processed material from the core to the stellar surface but expel it trough the intracluster medium slow enough to retain it and without contributing iron-peak elements.

2.2.2.1 Intermediate-mass AGB stars

In this scenario AGB stars of $\sim$ 5-10 $M_\odot$ are proposed to be the source of the enriched material to form 2P stars. In particular, Na and Al enrichment correlated with high values of N are produced by neutron capture within thermal pulses (Cottrell and Da Costa, 1981) to directly affect the envelope composition with H-burning products of CNO, NeNA and MgAl cycles. AGB stars loss mass via slow winds that could be retained by the cluster (D'Ercole et al., 2008). Moreover, He

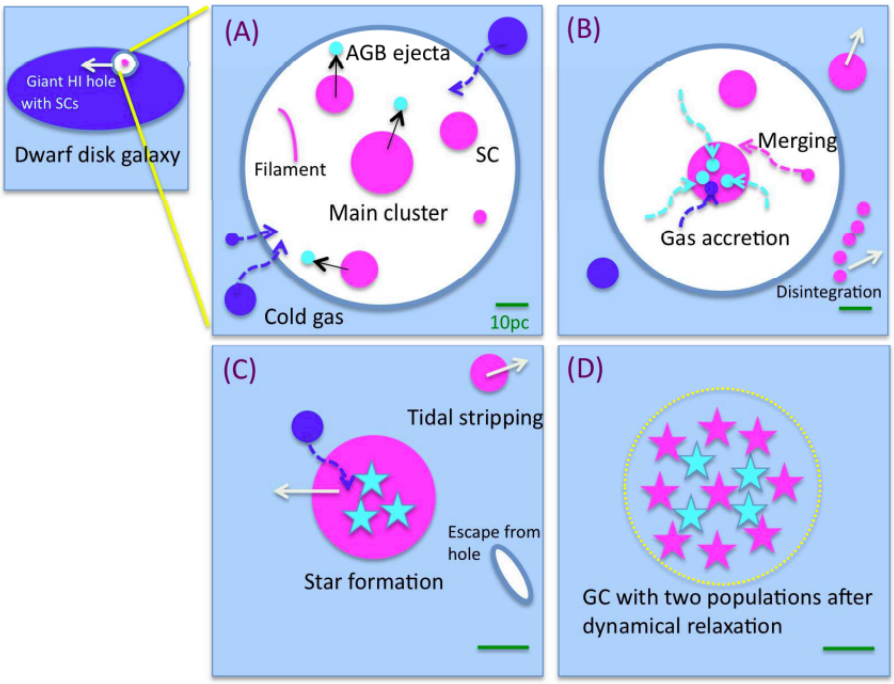

Figure 2.2.4: A brief illustration of the scenario of GC formation and AGB polution to form 2P stars (Bekki, 2017).

enrichment is accounted before stars reach the AGB through the second dredge-up. However, this model fail to reproduce the abundance trends observed in GCs. In particular, it is not possible to obtain O depletion and Na enrichment without increasing the sum of C+N+O (Slemer et al., 2017). Low values of O would lead necessarily to low Na for very high temperatures (Denissenkov and Herwig, 2003).

The very basic form of this scenario start with a first generation forming as a SSP. High mass stars and their associated SNe clear the gas from within the cluster expelling all the enriched material feedback. This is required to have no iron-peak spreads. Eventually, 1P stars evolve through the AGB and pollute the intracluster medium accumulating the enriched material towards the center after it cools down. After a critical density is reached, 2P stars begin to form out of this material(See Fig. 2.2.4).

2.2.2.2 Fast rotating massive stars

Massive stars ($> 15 - 25 M_\odot$) have been proposed to account for the CNONaAl variations since they reach the high temperatures required early in the MS (Maeder and Meynet, 2006). In particular, there is a developed advanced model that involves fast rotation, allowing the transport of MP elements from the convective core to the radiative envelope while lossing mass. This scenario involve Fast Rotating Massive Stars (FMRS, Decressin et al., 2007). Here, the O-Na and the C-N anti-correlations built up relatively easy as a consequence of the equilibrium of the CNO cycle and the early efficiency of NeNa cycle. 2P stars are then formed in an outflowing equatorial disc that surrounds the massive star(See Fig. 2.2.5). However, in top of the production of the necessary MPs elements, including even Al, the reaction rate to deplete Mg(via ^{24}Mg(p,γ)), and therefore be able to match observations, has to be increase by three order of magnitudes with respect to nominal values (Iliadis et al., 2001). With nominal values, FMRS reproduce a Mg-Al correlation. Moreover, Si-Mg could not be established since the high temperatures to produce Si is not reached. In the case of the He content, FMRS are able to show He-enriched 2P stars, but their values are too high compare to observations (Chantereau et al., 2016).

2.2.2.3 Other candidate polluters

- **Supermassive stars(SMS)**: SMS ($\sim 10^4$M$_\odot$) have been proposed to be the source of H-burning products to self enrich GCs to form 2P stars (Denissenkov and Hartwick, 2014). They formed via runaway collisions or monolithic collapse of the proto-cluster cloud. SMS reach high enough central temperatures for CNO, NaNe and MgAl cycles at the beginning of the MS, and form 2P stars mixing H-burning ashes with pristine gas. However, these objects are hypothetical and have very inconveniences with the input physics related with their formation and evolution.

- **Interacting binaries**: Another possible way to release enriched material from the cores of massive stars involve binary interactions proposed by de Mink et al. (2009a). Here, an interaction between a 20 and 15 M$_\odot$ leads to a 10 M$_\odot$ yield material that reproduce well N-enriched and O-depleted 2P stars as well as other MPs elements. However, the amount of yields could depend on the evolutionary stages of the stars, their total mass and their ratios (Bastian and Lardo, 2018). As a consequence, this model is not reproducible as a general trend and do not account for the particularities of each GC.

- **Early Disc accretion Disc**: Bastian et al. (2013) proposed a model

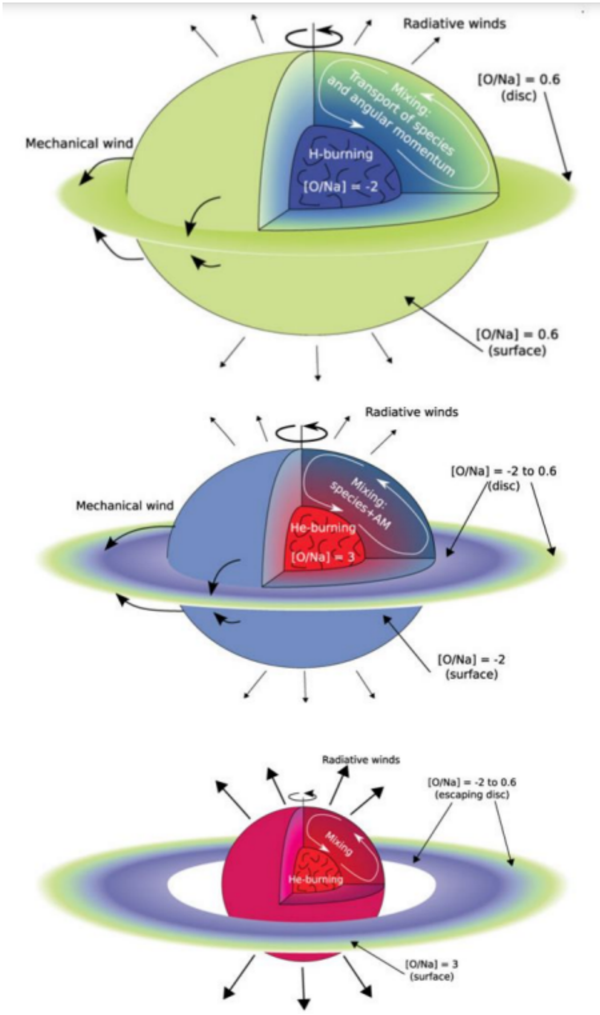

Figure 2.2.5: Schematic view of the evolution of FMRS (Lardo, 2013).

for multiple populations in young massive clusters (YMCs) that did not involve multiple star-formation epochs. Instead, enriched material from high-mass interacting binary stars and fast-rotating massive stars (FRMS) polluted low-mass stars forming at the same time. These low-mass stars, retaining protoplanetary discs for about 10 million years, would sweep up this material as they passed through the cluster core, assuming early mass segregation. However, the model's need for fully convective accreting stars with short accretion timescales (1-3 million years) limited material supply. Hydrodynamical simulations showed that discs accreted material quickly but lost it just as rapidly, stopping further accretion within about 10,000 years, much shorter than needed (Wijnen et al., 2016).

- **Turbulent Separation of Elements During GC Formation**: Hopkins (2014) suggested that MPs arise from cloud physics during the earliest phases of GC formation, where large dust grains become aerodynamic and move separately from gas and small dust grains in turbulent environments. This separation leads to the formation of stars with different elemental enhancements depending on the dust distribution. However, this model fails to explain the Na-O anticorrelation and He spreads observed in GCs and predicts symmetrical elemental spreads that are not seen in observations (Bastian and Lardo, 2018).

- **Reverse Population Order For GC Formation Scenarios**: To address the mass-budget problem(See section 2.2.2.4), Marcolini et al. (2009) proposed that star abundances evolve from 2P to 1P during cluster formation. This model envisions GC formation from gas enriched by a single Type Ia supernova and asymptotic giant branch (AGB) yields, with star formation occurring in this enriched region, reproducing observed anti-correlations but requiring assumptions about the interstellar medium's iron content and inner region size, and relying on unlikely stellar configurations (Bastian and Lardo, 2018).

2.2.2.4 Observational constrains

The suggested stellar sources for the origin of the polluted material have difficulties reproducing some observed abundance trends. To address these problems, most models have adopted some form of dilution, mixing the enriched material produced by first-generation stars with primordial material. For example, despite nuclear processing of C, N, O, and Na resulting in Li-free material, observations show that Li remains constant or only slightly varies from star to star in globular clusters (e.g. Salaris and Cassisi, 2014). The presence of 2P stars with depleted Li abundance is surprising because 2P stars with intermediate chemical variations share the same Li abundance as 1P stars, suggesting a mechanism like dilution or Li production by AGBs must restore the initial Li abundance in intermediate 2P stars without affecting extreme 2P stars.

In any case, dilution of a fixed set of yields does not help in explaining the full set of observations, the predicted yields of AGBs, FRMS, interacting binaries, or very massive stars and the observed distributions claim for the need of stochasticity (Bastian et al., 2015). Whatever the polluting source, it needs to produce a high degree of cluster-to-cluster variations in order to explain the observations.

For models that propose massive stars($> 15\mathrm{M}_\odot$) as the origin of enriched material, a large reservoir of primordial material is assumed to remain within the cluster, but for AGB star models, the origin of diluted material is harder to explain due to core-collapse supernovae expelling leftover material. Conroy and Spergel (2011) suggested that clusters could accrete material from their host galaxy, but this process, combined with AGB yields, does not reproduce observed abundance distributions unless the timing of dilution is very specific, with material accretion increasing after the most massive AGB stars have shed their material.

The presence of Al and Mg anti-correlated ranges among cluster stars argues against the FRMS scenario, as the necessary temperatures to destroy ^{24}Mg occur only in the cores of massive stars at the end of their main sequence evolution, which would also cause a significant He enrichment. Pollution from AGB stars can more naturally reproduce these observations, with Mg depletion and Al production being sensitive to AGB metallicity, though the resulting Na, Mg, Al, and Si correlations depend heavily on mixing with He-burning material (Ventura et al., 2016).

While most globular clusters (GCs) show 1P and 2P stars distributed continuously in the Na-O plane; O, Na, and Al abundances cluster around certain values, suggesting multimodal sub-populations (e.g. Carretta, 2014). This observed discreteness disfavors formation scenarios based on accretion onto pre-existing stars or 2P stars forming within the disk of fast rotating massive stars, as these processes would result in continuous rather than discrete abundance variations.

Moreover, A key challenge with all proposed self-enrichment scenarios in globular clusters is that the enriched populations (2P stars) often equal or exceed the primordial population (1P stars), revealing a "mass budget problem". The "mass budget problem" in GCs arises from the discrepancy between the observed fraction of enriched stars and the amount of material that could have been processed through 1P stars under standard initial mass functions (IMFs). Models invoking AGB stars or other scenarios struggle to explain how 2P stars, which can make up around two-thirds of a typical GC population, could have formed given the limited mass available from 1P stars. For example, for a standard IMF, only ∼7% of the stellar mass in a 1P is in stars with masses between $5 - 9M_{\odot}$ (i.e., stars that pass through the AGB phase often associated with the AGB scenario). Low mass ($< 0.8M_{\odot}$) stars, on the other hand, make up ∼40% of the initial mass fraction. For a typical GC, 2P stars represent ∼67% of cluster stars, while 1P stars make up the remaining ∼33%. Assuming that 100% of the mass of every AGB star gets used to make 2P stars (an extreme assumption) and that the 2P has a standard IMF, AGB stars can only account for 4 - 5% of the population of 2P stars. If we assume that, on average, 50% of the mass of each 2P star comes from diluting material, then AGB stars can account for 8 - 10% of the 2P stars (Prantzos and Charbonnel, 2006). Proposed solutions include limiting the mass range of 2p stars or assuming that GCs were significantly more massive at birth and lost a large fraction of their stars over time.

Chapter 3

Observations and Data description

3.1 Source catalogs

3.1.1 Gaia Data Release 3

The Gaia mission, launched by the European Space Agency (ESA), aims to create the most precise three-dimensional map of our galaxy. Since its launch, Gaia has produced several data releases, with Data Release 3 (DR3) being one of the most comprehensive and detailed to date, released on June 13, 2022 (Gaia Collaboration, 2022a,b).

GAIA DR3 includes a wide range of astrometric, photometric, and spectroscopic data. This release builds upon the Early Data Release 3 (EDR3) and adds new data products, such as: complete astrometric solutions (position, parallax, and proper motion) for around 1.46 billion sources. G magnitudes for approximately 1.806 billion sources. G_{BP} and G_{RP} magnitudes for around 1.54 billion and 1.55 billion sources, respectively. Object classifications and astrophysical parameters (such as T_{eff}, $\log g$, [M/H], A_G, and distance) derived for 470 million objects.

GAIA DR3 represents a significant advancement over previous releases. Compared to GAIA DR1 and DR2, DR3 includes improved astrometric precision, expanded temperature intervals for radial velocity measurements, and new spectroscopic data. DR3 extends the magnitude range for radial velocity measurements and introduces new functionality for de-blending overlapping spectra, thus improving the completeness and accuracy of the data (Gaia Collaboration, 2016, 2018, 2022a,b).

For the study of multiple populations in the globular cluster NGC 6569, proper motions and photometry were extracted from GAIA DR3. Proper motions help identify cluster member stars and , while photometry provides information on the age of the stars.

3.1.2 The Apache Point Observatory Galactic Evolution Experiment II: APOGEE-2

The Apache Point Observatory Galactic Evolution Experiment (APOGEE) is a high-resolution (R$\sim$22,500), H-band (1.5-1.7 μm) spectroscopic survey of the Milky Way and its nearby dwarf galaxies (Majewski et al., 2017). The survey began as APOGEE-1 under SDSS-III (Eisenstein et al., 2011) and continued into SDSS-IV with APOGEE-2 (Blanton et al., 2017). APOGEE-2 expanded the survey to include the Southern Hemisphere (APOGEE-2S) and used the 2.5-meter du Pont telescope at Las Campanas Observatory (Bowen and Vaughan, 1973). Spectra are observed with custom-built, multi-object spectrographs, which record the spectra of 300 targets simultaneously (Wilson et al., 2019).

DR17 is the final release of APOGEE-2 data from SDSS-IV. This release includes all APOGEE data, incorporating observations taken at Apache Point Observatory (APO) through November 2020 and at Las Campanas Observatory (LCO) through January 2021. The dual APOGEE-2 instruments have observed more than 650,000 stars throughout the Milky Way. The data reduction process is detailed in Nidever et al. (2015), and the spectra are analyzed using the APOGEE Stellar Parameters and Chemical Abundances Pipeline (ASPCAP) (García Pérez et al., 2016a), with synthetic spectra libraries described in Zamora et al. (2015). The accuracy and precision of the derived atmospheric parameters and chemical abundances are extensively analyzed in Holtzman et al. (2018), Jönsson et al. (2018), and Jönsson et al. (2020). The customized H-band line list used is detailed in Shetrone et al. (2015), Hasselquist et al. (2016), Cunha et al. (2017), and Smith et al. (2021).

For this study, we utilized the spectra and radial velocities from this final data release of the APOGEE-2S survey.

3.1.3 The bulge Cluster APOgee Survey: CAPOS

The bulge Cluster APOgee Survey (CAPOS, Geisler et al., 2021) aims to study Bulge Globular Clusters (BGCs) focusing on their chemodynamics. CAPOS seeks to obtain detailed abundances and kinematics for a comprehensive sample of bona fide members in true BGCs, with the capabilities of APOGEE-2S. The primary goals include gathering a definitive database on the BGC system, searching for the oldest objects in the Galaxy, studying the complex nature of the Galactic Bulge, uncovering correlations, determining BGC velocities and orbits, investigating MPs in the BGC system, and comparing them to their halo and disk counterparts .

CAPOS originally targeted 20 cataloged BGCs(including NGC 6569), aiming to increase the number of observed bona fide BGCs by APOGEE to 28, with CAPOS contributing nearly three-fourths of this observed sample. This project, in conjunction with SDSS-IV data, will provide a legacy database of the BGC system, offering much better and self-consistent spectroscopic metallicities and detailed abundances for up to 20 elements, with a precision of 0.05 dex (Geisler et al., 2021). Many BGCs have limited or nonexistent velocity information, which CAPOS aims to address. CAPOS aims to observe 5-10 members per cluster to derive accurate mean abundances, characterize MPs, and constrain MP formation scenarios. Figure 3.1.1 illustrates the spatial distribution of CAPOS targets within the bulge, highlighting the 20 cataloged BGCs and their positions relative to the Galactic center.

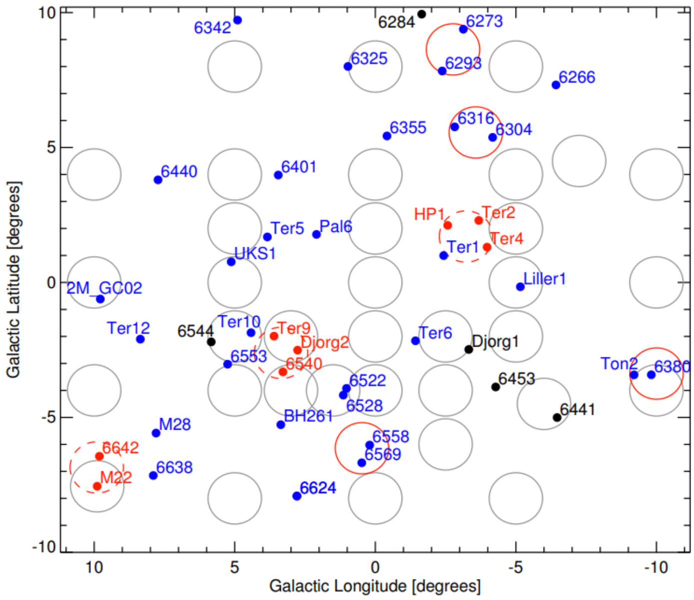

Figure 3.1.1: Central ± 10deg × ± 10deg around the Galactic center. BGCs (i.e., with RGC < 3.5kpc) are identified (generally with their NGC number) in blue and red, while other GCs with RGC > 3.5 kpc are labeled in black. Gray circles show the locations of the SDSS-IV APOGEE-2S survey fields, while CAPOS fields are shown in red, with the dashed circles illustrating the CAPOS fields presented here. All CAPOS clusters are BGCs except for M22, which was observed simultaneously with the BGC NGC 6642 (Geisler et al., 2021).

Chapter 4

Membership analysis

4.1 Sample selection

Having established the accessibility of the data that concern our analysis, the most important part of which begins with obtaining the abundances needed to characterize the MPs in NGC 6569, we must find and determine the most likely members.

4.1.1 Likely members

Targets were aim towards galactic coordinates (l°,b° = 0.48,-6.68) according to Vasiliev and Baumgardt (2021) and selected on the basis on *Gaia* DR3 spatial position and proper motions and APOGEE DR17 radial velocities(RVs) and metallicity. For this purpose, we follow a similar methodology as Geisler & Muñoz et al. (In preparation) target selection and select stars that lies within the tidal radii of 7.15", according to Harris (2010). Additionally, we have used the PM from *Gaia* DR3 using the determination of the center for each CAPOS GCs in a proper motion diagram determined by Vasiliev and Baumgardt (2021). We used a radius of 0.5 [mas/yr] from the nominal value for NGC 6569($\mu_\alpha \cos\delta$[mas/yr], μ_δ[mas/yr], $-4.125, -7.354$). This radius is optimal for maximizing members and at the same time avoid contamination from field stars. In this case, we selected stars with signal-to-noise ratio (SNR) > 50 to maximize the precision on the abundance determination. Then, our next criteria is based on RVs. We have considered stars within 2σ from the mean of -49.83 [km/s] and using the dispersion of Vasiliev and Baumgardt (2021). The last criteria was metallicity. For this, we use the value estimate the values both of Harris (2010) and García Pérez et al. (2016b) which is the APOGEE pipeline(See section 4.2), obtaining the same results. In total, we have obtained ten stars that satisfy our criteria (see Table 4.1.1).

Table 4.1.1: Astrometric, photometric and kinematic properties of NGC 6569 members.

APOGEE ID	α [deg]	δ [deg]	G_{bp} [mag]	K_s [mag]	$\mu_\alpha \cos\delta$ [mas/yr]	μ_δ [mas/yr]	RV [km/s]	SNR [pixel^{-1}]
2M181339403150132	273.414	-31.837	15.29	9.24	-4.167	-7.483	-48.64	222
2M181340253149477	273.418	-31.830	15.06	10.04	-4.047	-7.835	-50.45	174
2M181333243150194	273.389	-31.839	16.03	10.93	-4.062	-7.366	-54.96	153
2M181337893147295	273.408	-31.792	15.76	10.86	-4.196	-7.416	-50.32	171
2M181330833148103	273.378	-31.803	15.62	10.63	-3.866	-7.492	-49.30	130
2M181341513148556	273.423	-31.815	15.63	10.68	-4.167	-7.273	-55.72	119
2M181420653147172	273.586	-31.788	16.78	11.83	-4.225	-7.193	-47.16	92
2M181347253147570	273.447	-31.799	16.64	12.28	-4.23	-7.366	-46.46	64
2M181351543151406	273.465	-31.861	16.68	12.29	-3.993	-7.498	-47.48	60
2M181333293146211	273.389	-31.773	16.71	12.70	-4.416	-7.713	-51.42	51

In Fig. 4.1.2 we can see the spatial distribution of the ten stars towards the cluster center color and sized coded by SNR and K_s magnitude. Note that only one star do not lie within the tidal radii(black dashed circle). This star did not satisfy the fourth criteria of our membership analysis and although this could represent a sufficient enough criteria to discard this star, we decided to keep it in the sample since it could be associated anyway to the cluster 1P or 2P membership. Moreover, recently Hughes et al. (2023) discover 23 extra-tidal stars around NGC 6569 that extent up to 5 tidal radii. Unfortunately, none of their stars match with our possible extra tidal one. However, it is worth to say that tidal tails of NGC 6569 have been simulated with Gala python package and show extreme complexity due to dynamical stirring from the bulge potential (Silva et al., 2023). In fact, Bajkova et al. (2023) quantify the influence of the Galactic bar on the Dynamics of NGC 6569 showing that the probabilities of capturing this cluster(therefore, its stars) is > 0.2.

In Fig. 4.1.1 we see the proper motion distribution of NGC 6569 likely members. Here all stars lies within 0.5 mas/yr from the center of the nominal value, including the possible extra-tidal star.

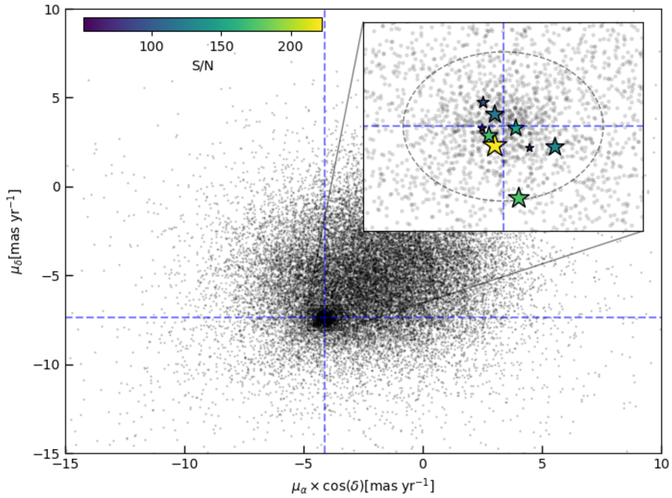

Figure 4.1.1: Proper motion distribution of NGC 6569 likely members color and sized coded by SNR and K_s magnitude. The box zoom inset represent 0.7 X 0.7 mas/yr and the black dashed circle the maximum radius of 0.5 mas/yr. The blue dashed lines are centered on the proper motion nominal value.

Radial velocity and metallicity criteria is shown in Fig. 4.1.3. The ten member stars are clustering inside a red box, a typical behavior related to selection of globular clusters stars (See e.g. González-Díaz et al., 2023). The red points are stars that satisfy our RV criteria but have proper motion > 0.5 mas/yr from the nominal value, thus they are not NGC 6569 members.

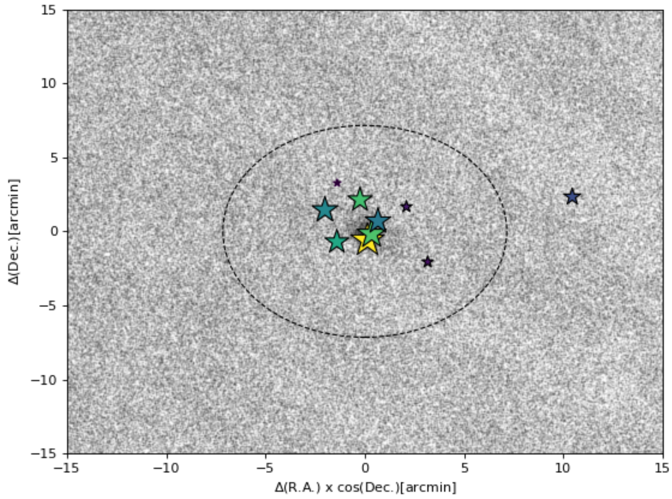

Figure 4.1.2: Spatial distribution of NGC 6569 likely members color and sized coded by SNR and K_s magnitude. The black dashed circle and the grey points represent the tidal radii and field stars within 15" from the cluster center, respectively.

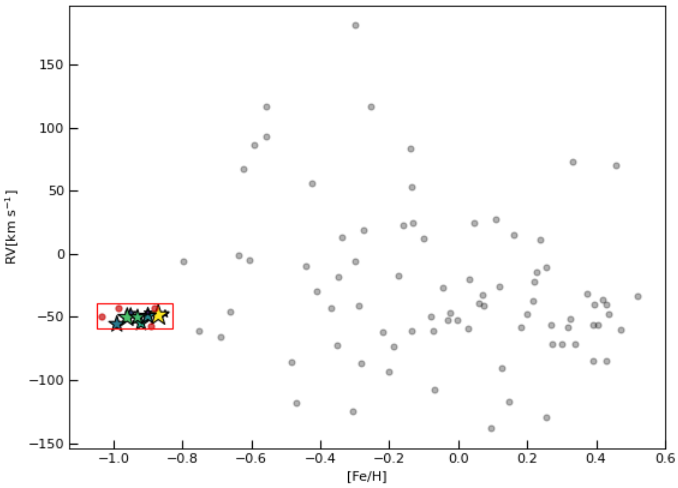

Figure 4.1.3: Radial velocity versus metallicity space of NGC 6569. Likely members are color and sized color as in Fig. 4.1.1 inside a red box. Red point inside this box have similar RVs values but do not satisfy the proper motion criteria. Grey points represents field stars.

4.2 Atmospheric parameters

The next fundamental step is to obtain atmospheric parameters which give us the physical input for each star on which the spectral analysis can be developed. This is a requirement for generating any atmospheric model and synthesized spectrum and, in particular, is necessary for the use of BACCHUS(See section 4.3.1). In this context we have to be aware from were we extract or infer these parameters. In the context of CAPOS, Geisler et al. (2021) tested the reliability of the APOGEE Stellar Parameter and Chemical Abundances Pipeline (ASPCAP, García Pérez et al., 2016b) for several CAPOS clusters. ASPCAP consists of a fortran90 code that determines atmospheric parameters and chemical abundances from observed spectra by comparing observed spectra to libraries of theoretical spectra, using χ^2 minimization in a multidimensional parameter space and it is fairly establish in the literature how well atomic species are measured with APOGEE spectra (e.g. Mészáros et al., 2020). Therefore, for a first guess, we decided to extract the uncalibrated and calibrated values of atmospheric parameters, effective temperature(T_{eff} [K]) and surface gravity($\log g$ [m/s^2]) from ASPCAP.

Nevertheless, a systematic effect on chemical abundances with ASPCAP effective temperature has been studied in GCs and the field (Masseron et al., 2019; Zasowski et al., 2019). ASPCAP tends to overestimate both T_{eff} and $\log g$ of 2P stars. In particular, a MP indicator, such as N abundance, is increased from 1P to 2P stars(by almost 1 dex). Although N tends to increase naturally in RGB dredge-up episodes this do not affect metallicity. This is a direct consequences of overestimated values of T_{eff}, since higher T_{eff} means fainter spectral lines and in order to fit a line, the metallicity value tends to be higher Geisler et al. (2021). In Fig. 4.2.1, this trend is shown, where the difference in metallicity for 2P stars(here defined as [N/Fe > 0.7] is significantly higher than 1P stars, that in fact, is not supported by observations(Mészáros et al., 2020), i.e., there is no metallicity spread within MPs in GCs(with the exception of the most massive ones, as mentioned early). For this reason, abundances for 2P stars was derived using independent atmospheric parameters than those from APOGEE.

In this context, we decided to inferred effective temperature and surface gravity through isochrone fitting using giant stars. With the first two criteria, spatial distribution and proper motion, we were able to construct the CMD of NGC 6569

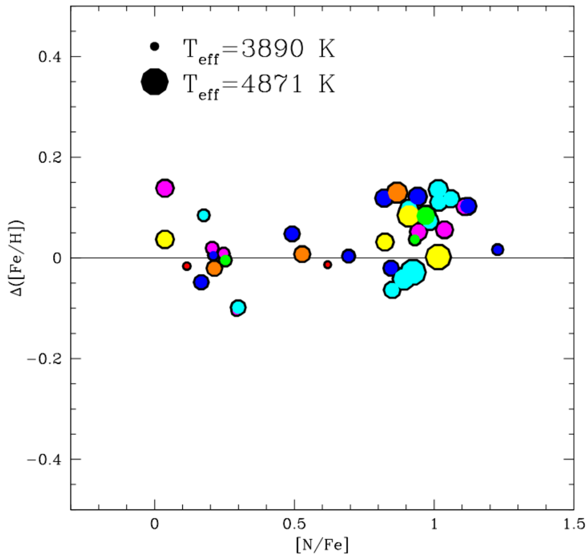

Figure 4.2.1: Difference in [Fe/H] as a function of [N/Fe], with the cluster mean for 1P and 2P stars as derived from ASPCAP.

with *Gaia* and 2MASS(contained in *Gaia* data) photometry, blue filter G_{bp} and K_s filter. We plotted G_{bp} - K_s for color and K_s for magnitude. This combination is commonly used in CAPOS (e.g. González-Díaz et al., 2023)(See Fig. 4.2.2). Then we corrected the CMD using giant stars. For this purpose, we selected all RGB stars within a radius of 3.5 arcmin from the cluster center and that have proper motions compatible with that of NGC 6569. First, we draw a ridge line along the RGB, and for each of the selected RGB stars we calculated its distance from this line along the reddening vector(calculated as $A_K/(A_{Bp} - A_K)$. The vertical projection of this distance gives the differential interstellar absorption at the position of the star, while the horizontal projection gives the differential Optical+NIR reddening at the position of the star. After this first step, for each star of the field we selected the three nearest RGB stars, calculated the mean interstellar reddening and absorption, and finally subtracted these mean values from its Optical+NIR colours and magnitudes. We underline the fact that the number of reference stars used for the reddening correction is a compromise between having a correction affected as little as possible by photometric random error and the highest possible spatial resolution (Fernández-Trincado et al., 2022). In order to estimate the distance of the cluster we performed an isochrone fitting of the RGB using the PARSEC[1] database. We had to consider that Bulge clusters are

[1]http://stev.oapd.inaf.it/cgi-bin/cmd

affected by high reddening, generally exceeding E(B-V)> 0.50(Valenti et al., 2005). The reddening correction highly depends on the spectral energy distribution (SED) of the star, i.e. on its temperature. For this reason, the extinction correction was applied point-by-point to the isochrone using the extinction law of (Cardelli et al., 1989). The free parameters for this fitting are the true distance modulus, $(m\text{-}M)_0$ (or the equivalent distance in pc), the interstellar absorption in the V band, AV, and the reddening-law coefficient, RV(See Fig. 4.2.2). These three parameters were estimated simultaneously using the Bp-K vs. K shown in Fig. 4.2.2 assuming an age of 12 Gyrs(within the errors of Saracino et al. (2019) of 12.8 $\pm$ 1 Gyr) and a global metallicity [M/H] = 0.8 that considers the α-enhancement of the cluster according to the relation by Salaris et al. (1993). Finally, the interstellar absorption and the extinction law coefficient we found can be translated to E(B-V)= 0.682 $\pm$0.061 for NGC 6569, higher than derived before; E(B-V) $\sim$ 0.49 - 0.55 (Zinn, 1985; Bica and Pastoriza, 1983; Valenti et al., 2005). In order to obtain Teff and log g from photometry, we first derived the differential-reddening corrected CMD of Fig. 4.2.2 and we then horizontally projected the position of each observed star until it intersected the isochrone and assumed Teff and logg to be the temperature and gravity of the point of the isochrones that have the same Ks magnitude as the star. The corrected magnitude and color values as well as the inferred extinction and distances are listed in table ??

Table 4.2.1: Corrected photometric values and inferred extinction and distance of NGC 6569 members

APOGEE ID	K_{s0}	$(G_{bp} - K_s)_0$	Av	Distance[pc]
2M181351543151406	12.287	4.374	0.025	12450.35
2M181420653147172	10.756	4.922	0.112	12450.67
2M181333243150194	10.907	4.95	0.185	12451.06
2M181339403150132	9.24	6.027	0.024	12450.44
2M181340253149477	10.789	4.876	-0.098	12450.12
2M181330833148103	10.636	5.059	-0.084	12451.09
2M181341513148556	10.683	5.022	-0.079	12450.77
2M181347253147570	12.283	4.374	-0.016	12450.65
2M181337893147295	10.853	4.871	0.039	12450.03
2M181333293146211	10.987	4.469	0.025	12451.15

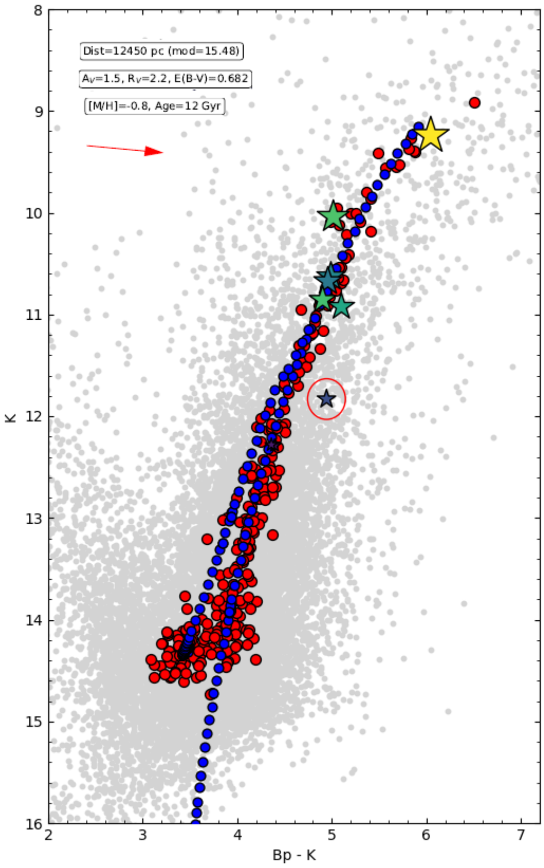

Figure 4.2.2: Colour-magnitude diagram corrected by differential reddening and extinction-corrected in the Gaia bands of our sample and stars within 15'. NGC 6569 members are color and sized coded as 4.1.1. The best fit isochrone is represented in red while blue points are stars that satisfy the first two criteria on our analysis. Grey points are field stars and the possible extra-tidal star is marked inside a red circle.

4.2.1 Microturbulence ξ_{micro}

The third atmospheric parameter that is fundamental in our analysis is the microturbulence or microturbulence velocity ξ_{micro}. Microturbulence can cause broadening of the absorption lines in the stellar spectrum and depends on effective temperature and surface gravity. The microturbulent velocity is the non-thermal component of the photospheric velocity field which has a correlation length smaller than the size of the line forming region (Cantiello et al., 2008). In the 1D models(see Section 4.3.1), the small-scale velocity fields in the stellar photosphere is represented by this parameter .For FKG stars like NGC 6569 members, we used the definition given by Mott et al. (2020):

$$\xi_{micro} = 0.998 + 3.16 \times 10^4 \mathrm{X} - 0.253\mathrm{Y} - 2.86 \times 10^4 \mathrm{XY} + 0.165\mathrm{Y}^2 \quad (4.2.1)$$

where X = Teff - 5500 [K] and Y = logg - 4.0. From here, the inferred and

Table 4.2.2: Adopted atmospheric parameters inferred from photometry, and spectroscopy(Uncalibrated and calibrated).

	Photometry			Uncalibrated			Calibrated		
APOGEE ID	Teff[K]	logg[m/s^2]	ξ [km/s]	Teff[K]	logg[m/s^2]	ξ [km/s]	Teff[K]	logg[m/s^2]	ξ [km/s]
2M181351543151406	4427.3	1.57	1.50	4259.9	1.58	1.33	4419.8	1.58	1.49
2M181420653147172	4316.7	1.37	1.54	4274.4	1.3	1.55	4442.4	1.30	1.73
2M181333243150194	4089.8	0.97	1.61	4083.4	1.13	1.47	4239.8	1.13	1.65
2M181339403150132	3679.8	0.21	1.78	3851.1	0.3	1.93	4010.7	0.30	2.15
2M181340253149477	3885.1	0.59	1.69	3831.5	0.86	1.39	3994.6	0.86	1.59
2M181330833148103	4025.2	0.85	1.64	4019.8	0.85	1.63	4020.0	0.93	1.56
2M181341513148556	4036.5	0.87	1.63	3955.2	1.11	1.34	4117.7	1.11	1.53
2M181347253147570	4424.8	1.57	1.50	4525.5	1.85	1.40	4670.6	1.85	1.53
2M181337893147295	4076.6	0.94	1.62	4082.7	0.96	1.61	4247.9	0.96	1.81
2M181333293146211	4526.9	1.75	1.47	4835.7	1.69	1.81	4954.2	1.69	1.93

extracted atmospheric parameters used in this work are listed in table ??.

4.2.2 APOGEE spectra conversion

The wavelength calibration of the APOGEE data is done using vacuum wavelengths. However, the wavelengths of atomic transitions are usually quoted at standard temperature and pressure(S.T.P.).Thus, recognizing spectral lines associated with specific atomic transitions may require converting the SDSS data to the equivalent values at S.T.P. For APOGEE data, we have used the conversion from Ciddor (Ciddor, 1996) to convert between vacuum and air wavelengths. For a vacuum wavelength (λ_v) in Ångstroms, convert to air wavelength (λ_a) using the equation:

$$\lambda_a = \lambda_v/(1.0+5.792105\times10^{-2}/(238.0185-(10^4/\lambda_v)^2)+1.67917\times10^{-3}/(57.362-(10^4/\lambda_v)^2) \tag{4.2.2}$$

4.3 Spectral analysis

Modeling atmospheres for late-type stars requires extensive physical data, including ionization and dissociation equilibrium for atoms and molecules, chemical compositions, ionization and dissociation energies, partition functions, and continuous absorption and scattering coefficients. However, the most critical and demanding requirement is accurate data for calculating line absorption processes. Once we have an extensive atomic and molecular line list it is possible to recreate the spectrum. To account for the most precise abundance determination, we performed our spectral analysis based on synthetic spectra. Spectral synthesis is a powerful technique to determine the chemical compositions of stars based on their observed spectra. It involves modeling the physical conditions (like temperature, gravity, and chemical composition) of a star's atmosphere theoretically. These models are then used to generate synthetic spectra, which predict how the star's spectrum should appear under these conditions. The general physical assumptions relevant to atmosphere model are the following:

- **Stratification and hydrostatic equilibrium**: Assuming spherical symmetry by describing how pressure balances gravitational forces within stellar atmospheres, the equation of hydrostatic equilibrium states that

$$\nabla P_{\mathrm{tot}} = -\rho \frac{G M_{\mathrm{r}}}{r^2} \tag{4.3.1}$$

  where P_{tot} is the total pressure(gas, radiative and turbulence), ρ the matter density, G Newton's constant of gravity and M_r the stellar mass inside radius r.

- **Mixing length convection**: Mixing length convection (Henyey et al., 1965) assumes that convective elements in stellar atmospheres behave like bubbles of hot gas rising through cooler layers, influencing the transport of energy and elements. It usually gives the convective energy flux as a function of density, temperature, pressure, specific heat and mixing length, the length of the "bubbles". The convective flux is added to the radiation energy flux, and we may then write the energy equilibrium equation

$$F_{\text{conv}} + F_{\text{rad}} = \frac{L}{4\pi r^2} \tag{4.3.2}$$

The total radiative flux F_{rad}, is non-local functional of the model structure and can be calculated from a solution of the transfer equation. In spectral synthesis this invoke a radiative transfer code.

- **Local Thermal Equilibrium(LTE)** : All atomic and molecular number densities are assumed to adhere to the laws of thermal equilibrium, including the Saha equation for ionization states and chemical equilibrium equations for molecules while excitation equilibrium and partition functions are determined using the Boltzmann distribution.

The analytic dissection of these assumptions yields to a closed system of equations, of approximately 7, for determining dependent variables. Essentially, a standard multidimensional Newton-Raphson method is applied to solve the highly non-linear system.

4.3.1 Brussels Automatic Code for Characterizing High accUracy Spectra: BACCHUS

For our analysis, we use the Brussels Automatic Code for Characterizing High accUracy Spectra (BACCHUS Masseron et al., 2016) that measures line-by-line elemental abundances from on-the-fly spectral synthesis and provides additional quality flags for each line it analyzes (e.g., identifying when a line is severly blended, too weak to be measured, etc.). More specifically, this BACCHUS module consists of a shell script code that computes on the fly synthetic spectra for a range of abundances and compares these syntheses to observational data on a line-by-line basis, deriving abundances from different methods. Since BACCHUS is primarily a line-by-line base code, it is intended to work for high enough resolution spectra so that individual lines are resolved, such as the APOGEE spectra. The synthetic spectra are calculated using the 1D-LTE Turbospectrum radiative transfer code (Gustafsson et al., 2008), with spherically symmetric radiative transfer for giants, and the MARCS model atmosphere grids (Gustafsson et al., 2008). A custom line list has been created as described in Smith et al. (2021). The parameter range is limited to the model atmosphere grid in the model path, hence currently F, G, K, and M type star, special to our red giants members.

The BACCHUS code utilizes synthetic spectra to identify continuum points for normalizing observed spectra and defines specific spectral regions (termed "mask" or "window") for determining abundances from each spectral line. Normalization involves selecting continuum wavelengths in synthetic spectra and fitting a linear relation within a 30 Å range around the line of interest in observed spectra. The spectral window for each line is determined by comparing how variations in elemental abundance affect synthetic spectra with the second derivative of observed flux to locate local maxima adjacent to the line of interest. SNR is estimated from the rms of the continuum point (if any). If there are not enough continuum point the SNR is derived from the ratio of the synthesis and the observed spectrum. The distinguishing feature of this code lies in its utilization of four methods to compare observed and synthetic spectra within the specified window, enabling it to derive an abundance measurement from each method. In the following section we review these methods in details.

4.3.2 Abundance estimation

From the *bacchus.abund* module of BACCHUS, we obtained several spectral features centered in specific lines of each element showing the results of the synthesis. For each page, it shows the result of individual line fitting and abundance determination("log A"). An example for Mg is shown in Fig. 4.3.1. The figure is divided into three panels:

- **Upper Panel:** This panel displays the observed normalized spectrum (black) alongside the synthetic spectra generated with various abundances (colored), as detailed at the top. The long dashed line traces the continuum fit over the continuum points (red dots). The short-dashed line(s) indicate the input wavelength to be studied. Additional information includes the estimated SNR, the reduced χ^2 of the line best fit, and the pseudo-equivalent width value.

- **Bottom Panel:** This panel shows the same normalized observed spectrum and synthesis as in the upper panel but zoomed in on the line of interest. The short-dashed line(s) indicate the input wavelength. The horizontal

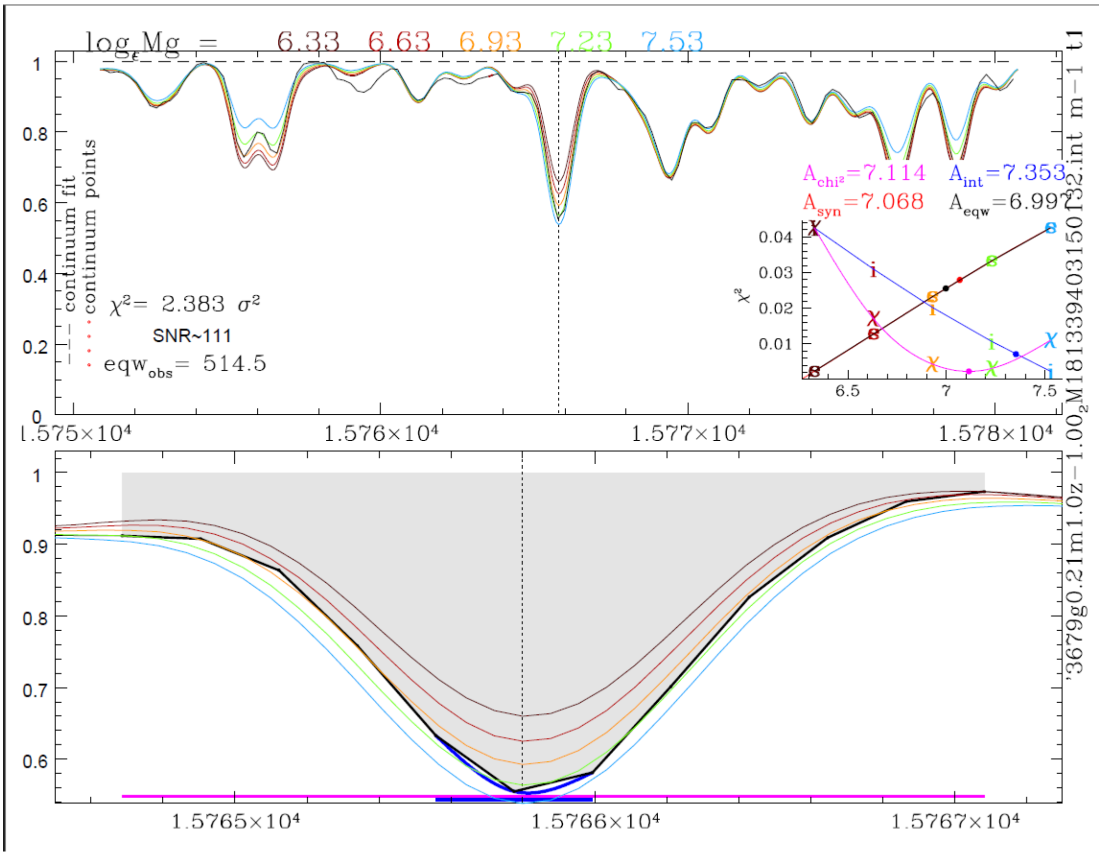

Figure 4.3.1: Example of Mg line spectral fit synthesis with BACCHUS. Description are found in the text.

magenta line shows the selected region for the "χ^2" and the "syn" abundance determination methods, while the blue line indicates the region for the "int" method. The points for the abundance determination are shown by a thickened line on the observed spectrum. The shaded area represents the pseudo-equivalent width. The blue parabolic line indicates the points used for the fit of the "intensity" method. The short-dashed line indicates the input wavelength. Continuum points are indicated by red dots.

- **Third Panel:** This panel, inserted in the upper panel, shows the diagram for the four methods of abundance determination. Each method is represented by a different color (χ^2: magenta, synthesis: red, equivalent width: black, and intensity: blue) and by a letter for each input abundance (χ^2: "χ", synthesis: "s", equivalent width: "e", and intensity: "i"). The final interpolated abundance value for each method is indicated by a dot. Finally, the model used is mentioned on the right-hand side.

The four methods are:

- **the eqw method**: determines the abundance needed to match the equivalent widths of the synthetic spectra to the observations. The code compute for each input abundance A the following:

$$\Delta eqw(A) = eqw_{syn}(A) - eqw_{obs} \tag{4.3.3}$$

  where eqw_{obs}(observed) and $eqw_{syn}(A)$(synthetic) are respectively defined by the n observed points defined by the line mask as described above. Then the code interpolate the $\Delta eqw(A)$ against log(A) and numerically search for the null solution. While this method is known to be independent of stellar rotation, macroturbulence, or instrument resolution -hence convolution-, it can be greatly affected by badly-fitted blending lines.

- **the syn method**: looks for the abundance that makes the difference between the synthetic and the observed points zero. the code compute for each input abundance A the following:

$$\Delta syn(A) = \sum_{n}(x_o - x_i(A)) \tag{4.3.4}$$

  whre x_o and x_i are respectively the n observed points defined by the line mask as described above. Then the code interpolate the $\Delta syn(A)$ against log(A) and numerically search for the null solution. While this method is mathematically similar to the "eqw" method and offers similar advantages, but can numerically provide slight different results. Moreover, this method allows some extrapolation as well as estimates for upper limits. But the accuracy of this method depends on the quality of fit, hence the quality of line physical parameters (hfs, NLTE, collisionnal broadening, ...).

  .

- **the int method**: measures abundances by matching the line core in the synthetic and observe spectra. The code first select five points around the line center. A polynomial fit is computed over those points(displayed as a blue line at the bottom of Fig. 4.3.1). The line intenisities (or depths) are then computed by averaging the value of the five selected points for both the syntheses $I(A)$ and the obs I_{obs}. Then the code interpolate the $I(A)$ - I_{obs}

against log(A) and numerically search for the null solution. This method is not expected to be quite insensitive to blends as long as the selected line is not in the wing of another stronger line. However, it is extremely sensitive to the convolution parameter. To determine the convolution parameter, which is used to encompass the instrumental, rotational, and macroturbulence broadening with a Gaussian profile, Si lines are used rather than more typical Fe lines because the former are generally cleaner and stronger in the APOGEE spectra, even at low metallicities. We use a constant convolution parameter of -12.

- **the χ^2 method**: determines an abundance by minimizing the squared differences between synthetic and observed spectra. the code compute for each input abundance A the following:

$$\chi^2(A) = \sum_n (x_o - x_i(A))^2 \tag{4.3.5}$$

where x_o and x_i are respectively the n observed points defined by the line mask as described above. Then the code fit a polynome to the χ(A) against log(A) and numerically find the minimum. This method is the default method, because it shown present a good compromised among the other methods strengths and weaknesses (mildly sensitive to convolution and mildly sensitive to the line physical parameters.

We inspected carefully line by line for each element and each stars and based on abundance estimation flags of BACCHUS, we rejected the bad lines and we keep only lines with reliable measurements. The estimation flags for each method range an integer number from 0 to 2(or 3 in the syn/eqw method). Where 0 Indicates when BACCHUS is only measuring an upper limit with this method or the measurement is beyond the synthesized range of abundances in the case of χ^2 method. Number 1 indicates that the measurement from the method is okay. Number 2 indicates that the measurement is an extrapolation outside of the synthesized range of abundances for the syn/eqw methods, that large (wavelength) offset between the observed and synthesized line cores or strong line (line intensity is below 0.4 of the continuum) for the int method and that the method crashed in the case of χ^2 method. There is an extra number 3 flag for syn/eqw that indicate large (wavelength) offset between the observed flux minimum (nominally the line

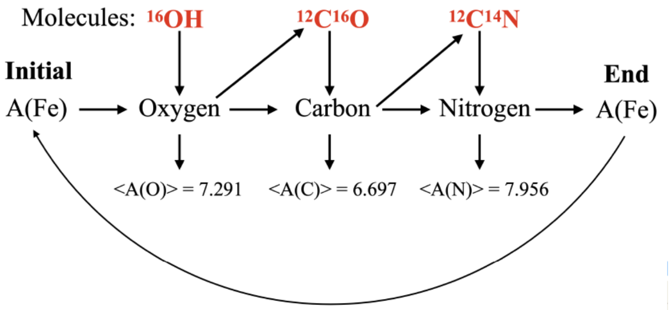

Figure 4.3.2: Self consistency as described by Smith et al. (2013)

core) and the synthetic flux minimum.

Based on these flags, we only kept lines where all methods converge, i.e., the flag has the value of 1. From here an initial abundance is determined based on column density of each element scale to that of hydrogen represent as $\log(N_{\rm X}/N_{\rm H})$, where X represent each chemical species. To express our abundances as [X/H] we scale to the sun values

$$[{\rm X/H}] = \log(N_{\rm X}/N_{\rm H})_{*} - \log(N_{\rm X}/N_{\rm H})_{\odot} \tag{4.3.6}$$

where $\log(N_{\rm X}/N_{\rm H})_{\odot}$ are extracted from Asplund et al. (2005) for light elements and from Grevesse et al. (2015) for heavier than Cu. Finally, from the value of [Fe/H] we scale all the abundances as [X/Fe].

4.3.2.1 Self consistency: CNO

CNO requires an special treatment. Abundances for ^{12}C, ^{14}N, ^{16}O are derived from combinations of vibration–rotation lines of CO and OH, and electronic transitions of CN. The procedure used for the CNO analysis, is to use CO to set the carbon abundance. With that carbon abundance, OH provides an O abundance, which, if different from the initial value (taken to be the solar value scaled by the stellar value of [Fe/H]), is used to re-analyze the CO lines. This process is repeated until the C and O abundances yield consistent abundances from CO and OH. With these values of C and O, the CN lines are used to derive the abundance of nitrogen. In general, the abundance of N has little to no effect on the CO and OH lines, however, the respective final C, N, and O abundances all provide self-consistent results from CO, OH, and CN (Smith et al., 2013). From here, we extracted the molecular dependence of CNO.

4.3.2.2 Error estimation

The uncertainties are calculated as the root sum square of the individual uncertainties from errors in each independent atmospheric parameter.

$$\sigma^2 = \sigma^2_{\text{mean}} + \sigma^2_{[\text{X/H}],\xi_t} + \sigma^2_{[\text{X/H}],\log g} + \sigma^2_{[\text{X/H}],T_{\text{eff}}} \tag{4.3.7}$$

where each deviation σ represents the change in our initial central value estimation after running BACCHUS with atmospheric parameters varied by $T_{\text{eff}} \pm 100$ K, $\log g \pm 0.3$ m/s^2, and $\xi_{\text{micro}} \pm 0.05$ km/s. This implies running BACCHUS for each of the different atmospheric parameters and statistically measure the variations. Errors are detailed in table 4.3.2.

Table 4.3.1: Typical abundance uncertainties determined for stars in our sample.

Abundance	$\Delta T_{\rm eff}$ (K)	$\Delta \log g$ (dex)	$\Delta\xi_t$ (km s^{-1})	**Mean** (dex)	$(\Sigma x^2)^{1/2}$ (dex)
2M181339403150132					
[C/Fe]	0.02	0.02	0.03	0.09	0.1
[N/Fe]	0.02	0.02	0.06	0.09	0.11
[O/Fe]	0.05	0.05	0.14	0.03	0.16
[Mg/Fe]	0.08	0.09	0.05	0.07	0.15
[Al/Fe]	0.06	0.03	0.16	0.05	0.18
[Si/Fe]	0.07	0.04	0.02	0.05	0.1
[Ca/Fe]	0.08	0.02	0.03	0.09	0.13
[Ti/Fe]	0.06	0.04	0.02	0.04	0.08
[Fe/H]	0.04	0.03	0.01	0.01	0.05
[Ni/Fe]	0.06	0.04	0.08	0.1	0.15
[Ce/Fe]	0.04	0.08	0.07	0.03	0.12
[Nd/Fe]	0.13	0.1	0.07	0.04	0.18
2M181340253149477					
[C/Fe]	0.03	0.04	0.09	0.05	0.11
[N/Fe]	0.05	0.11	0.06	0.09	0.16
[O/Fe]	0.05	0.16	0.05	0.04	0.18
[Mg/Fe]	0.11	0.1	0.07	0.04	0.17
[Al/Fe]	0.05	0.08	0.04	0.06	0.12
[Si/Fe]	0.05	0.16	0.02	0.07	0.18
[Ca/Fe]	0.09	0.05	0.04	0.03	0.11
[Ti/Fe]	0.06	0.04	0.07	0.09	0.13
[Fe/H]	0.04	0.05	0.01	0.02	0.07
[Ni/Fe]	0.03	0.03	0.06	0.05	0.09
[Ce/Fe]	0.07	0.02	0.08	0.04	0.12
[Nd/Fe]	0.03	0.11	0.08	0.04	0.14
2M181337893147295					
[C/Fe]	0.01	0.06	0.1	0.04	0.12
[N/Fe]	0.1	0.07	0.08	0.09	0.17
[O/Fe]	0.07	0.13	0.07	0.07	0.18
[Mg/Fe]	0.08	0.13	0.02	0.07	0.15
[Al/Fe]	0.1	0.05	0.06	0.05	0.14
[Si/Fe]	0.03	0.07	0.08	0.07	0.13
[Ca/Fe]	0.07	0.01	0.02	0.03	0.08
[Ti/Fe]	0.07	0.02	0.02	0.04	0.09
[Fe/H]	0.06	0.03	0.02	0.04	0.08
[Ni/Fe]	0.02	0.05	0.05	0.04	0.08
[Ce/Fe]	0.09	0.03	0.07	0.08	0.15
[Nd/Fe]	0.05	0.01	0.04	0.03	0.08

Table 4.3.2: Table 4.3.2 continued.

Abundance	ΔT_{eff} (K)	$\Delta \log g$ (dex)	$\Delta\xi_t$ (km s^{-1})	**Mean** (dex)	$(\Sigma x^2)^{1/2}$ (dex)
2M181333243150194					
[C/Fe]	0.03	0.03	0.08	0.09	0.13
[N/Fe]	0.02	0.03	0.01	0.1	0.1
[O/Fe]	0.02	0.06	0.09	0.07	0.13
[Mg/Fe]	0.02	0.05	0.07	0.05	0.1
[Al/Fe]	0.06	0.07	0.05	0.03	0.1
[Si/Fe]	0.09	0.13	0.07	0.06	0.18
[Ca/Fe]	0.08	0.07	0.16	0.09	0.21
[Ti/Fe]	0.12	0.09	0.04	0.06	0.16
[Fe/H]	0.03	0.04	0.03	0.05	0.07
[Ni/Fe]	0.09	0.08	0.02	0.07	0.13
[Ce/Fe]	0.06	0.06	0.07	0.04	0.12
[Nd/Fe]	0.12	0.03	0.02	0.05	0.14
2M181330833148103					
[C/Fe]	0.01	0.05	0.02	0.04	0.07
[N/Fe]	0.08	0.09	0.01	0.08	0.13
[O/Fe]	0.04	0.02	0.06	0.03	0.08
[Mg/Fe]	0.04	0.02	0.07	0.04	0.09
[Al/Fe]	0.06	0.08	0.06	0.05	0.12
[Si/Fe]	0.03	0.06	0.02	0.08	0.11
[Ca/Fe]	0.07	0.05	0.06	0.03	0.1
[Ti/Fe]	0.02	0.05	0.04	0.07	0.1
[Fe/H]	0.06	0.01	0.05	0.01	0.08
[Ni/Fe]	0.04	0.04	0.03	0.02	0.06
[Ce/Fe]	0.07	0.07	0.06	0.08	0.14
[Nd/Fe]	0.05	0.02	0.01	0.03	0.07

Table 4.3.3: Table 4.3.2 continued.

Abundance	ΔT_{eff} (K)	$\Delta \log g$ (dex)	$\Delta\xi_t$ (km s^{-1})	**Mean** (dex)	$(\Sigma x^2)^{1/2}$ (dex)
2M181341513148556					
[C/Fe]	0.07	0.08	0.02	0.11	0.14
[N/Fe]	0.02	0.03	0.04	0.14	0.15
[O/Fe]	0.05	0.13	0.04	0.1	0.18
[Mg/Fe]	0.17	0.08	0.1	0.07	0.22
[Al/Fe]	0.03	0.02	0.06	0.03	0.08
[Si/Fe]	0.02	0.03	0.03	0.01	0.05
[Ca/Fe]	0.04	0.1	0.08	0.03	0.14
[Ti/Fe]	0.02	0.05	0.18	0.07	0.2
[Fe/H]	0.03	0.02	0.06	0.03	0.08
[Ni/Fe]	0.11	0.07	0.08	0.09	0.18
[Ce/Fe]	0.12	0.01	0.03	0.03	0.13
[Nd/Fe]	0.04	0.06	0.05	0.03	0.09
2M181420653147172					
[C/Fe]	0.04	0.08	0.03	0.02	0.1
[N/Fe]	0.09	0.05	0.01	0.08	0.12
[O/Fe]	0.06	0.09	0.06	0.05	0.13
[Mg/Fe]	0.02	0.02	0.01	0.06	0.07
[Al/Fe]	0.04	0.05	0.04	0.09	0.12
[Si/Fe]	0.02	0.07	0.04	0.08	0.12
[Ca/Fe]	0.03	0.04	0.01	0.04	0.06
[Ti/Fe]	–	–	–	–	–
[Fe/H]	0.04	0.07	0.01	0.01	0.08
[Ni/Fe]	0.07	0.05	0.03	0.04	0.09
[Ce/Fe]	0.1	0.02	0.04	0.03	0.11
[Nd/Fe]	0.05	0.08	0.01	0.05	0.1
2M181347253147570					
[C/Fe]	–	–	–	–	–
[N/Fe]	–	–	–	–	–
[O/Fe]	–	–	–	–	–
[Mg/Fe]	0.04	0.02	0.06	0.1	0.13
[Al/Fe]	0.04	0.02	0.03	0.18	0.19
[Si/Fe]	0.09	0.06	0.08	0.02	0.13
[Ca/Fe]	0.02	0.02	0.12	0.05	0.13
[Ti/Fe]	0.09	0.04	0.05	0.02	0.11
[Fe/H]	0.01	0.03	0.03	0.07	0.08
[Ni/Fe]	0.1	0.02	0.08	0.03	0.13
[Ce/Fe]	–	–	–	–	–
[Nd/Fe]	–	–	–	–	–

Table 4.3.4: Table 4.3.2 continued.

Abundance	ΔT_{eff} (K)	$\Delta \log g$ (dex)	$\Delta \xi_t$ (km s^{-1})	**Mean** (dex)	$(\Sigma x^2)^{1/2}$ (dex)
2M181351543151406					
[C/Fe]	0.07	0.08	0.02	0.02	0.11
[N/Fe]	0.02	0.08	0.06	0.05	0.11
[O/Fe]	0.09	0.01	0.02	0.07	0.12
[Mg/Fe]	0.1	0.02	0.07	0.09	0.15
[Al/Fe]	0.09	0.13	0.03	0.05	0.17
[Si/Fe]	0.08	0.05	0.06	0.08	0.14
[Ca/Fe]	0.07	0.03	0.08	0.04	0.12
[Ti/Fe]	0.06	0.03	0.05	0.06	0.1
[Fe/H]	0.05	0.04	0.02	0.05	0.08
[Ni/Fe]	0.01	0.03	0.02	0.12	0.13
[Ce/Fe]	0.03	0.05	0.05	0.04	0.09
[Nd/Fe]	0.04	0.08	0.09	0.03	0.13
2M181333293146211					
[C/Fe]	–	–	–	–	–
[N/Fe]	–	–	–	–	–
[Mg/Fe]	0.16	0.03	0.05	0.04	0.17
[Al/Fe]	0.07	0.06	0.09	0.08	0.15
[Si/Fe]	0.02	0.14	0.03	0.06	0.16
[Ca/Fe]	0.04	0.05	0.02	0.01	0.07
[Ti/Fe]	0.02	0.12	0.07	0.03	0.14
[Fe/H]	0.03	0.03	0.05	0.02	0.07
[Ni/Fe]	0.07	0.06	0.03	0.03	0.1
[Ce/Fe]	–	–	–	–	–
[Nd/Fe]	–	–	–	–	–

Chapter 5

Discussion

5.1 Elemental abundances

From APOGEE-2 spectra, most of the atomic and molecular lines are very weak and heavily blended. In many cases, this blending is too severe to produce reliable abundances in cool, relatively metal-rich bulge GC stars. Therefore, a careful visual inspection of all our spectra was conducted. We provide reliable abundance determinations for eleven selected chemical species, including those from the iron-peak (Fe, Ni), odd-Z (Al), light elements (C, N), α-elements (O, Mg, Si, Ca, Ti), and s-process elements (Ce, Nd). Notably, we did not include sodium in our analysis, a typical species used to separate GC populations, due to its reliance on two atomic lines (Na I: 1.6373μm and 1.6388μm) in the H-band of the APOGEE-2 spectra. These lines are generally very weak and heavily blended by telluric features, making it impossible to produce reliable [Na/Fe] abundance determinations in GCs with the typical $T_{\rm eff}$ and metallicities of NGC 6569. A similar approach follows for [Li/Fe]. For this reason, we place greater emphasis on the elemental abundances of Al, Mg, C, N, and O, which are typical chemical signatures used to distinguish (at least) two main groups of stars with different chemical compositions in the multiple population phenomenon. The final values of each elemental abundance are summarized in table 5.1.1. Here we show the central value for each elements that show good lines for each adopted atmospheric parameters, photometry and uncalibrated and calibrated values from APOGEE DR17. Also we compare with the values estimated by ASPCAP and the mean values determined by Johnson et al. (2018) and Valenti et al. (2011), the only two high resolution studies for NGC 6569.

Table 5.1.1: Elemental abundances of NGC 6569 members. For each specie we show the mean value and the standard deviation. We compare with values estimated with ASPCAP and the adopted atmospheric parameters. We also compare with previous high-resolution studies on this cluster.

Apogee ID	SNR	[C/Fe]	[N/Fe]	[O/Fe]	[Mg/Fe]	[Al/Fe]	[Si/Fe]	[Ca/Fe]	[Ti/Fe]	[Fe/H]	[Ni/Fe]	[Ce/Fe]	[Nd/Fe]
Photometry													
2M181339403150132	222	-0.56	0.99	0.16	0.46	0.78	0.63	0.33	0.56	-0.87	0.07	0.43	0.51
2M181340253149477	174	-0.11	0.34	0.32	0.34	0.21	0.39	0.15	0.13	-0.96	-0.01	0.19	0.48
2M181337893147295	171	-0.48	1.09	0.30	0.54	0.41	0.58	0.17	0.13	-0.93	0.07	0.35	0.49
2M181333243150194	153	-0.29	1.24	0.38	0.49	0.49	0.59	0.35	0.43	-0.92	0.10	0.32	0.46
2M181330833148103	130	-0.26	0.90	0.26	0.39	0.40	0.62	0.10	0.55	-0.90	-0.10	0.34	0.25
2M181341513148556	119	-0.12	0.53	0.49	0.34	0.21	0.39	0.38	0.17	-0.99	0.04	0.24	0.51
2M181420653147172	92	-0.19	0.53	0.55	0.46	0.22	0.71	0.24	–	-0.95	0.03	0.25	0.50
2M181347253147570	64	–	–	–	0.40	0.37	0.58	0.35	0.62	-0.90	0.10	–	–
2M181351543151406	60	-0.02	0.41	0.68	0.58	0.35	0.56	0.40	0.37	-0.85	0.10	0.18	0.46
2M181333293146211	51	–	–	–	0.29	0.22	0.49	0.30	–	-1.02	-0.04	–	–
Mean		-0.25	0.75	0.39	0.43	0.37	0.55	0.28	0.37	-0.93	0.04	0.29	0.46
Std		0.19	0.34	0.17	0.09	0.18	0.10	0.11	0.20	0.05	0.07	0.09	0.09
ASPCAP DR17													
Mean		-0.21	0.66	0.30	0.32	0.33	0.29	0.28	0.12	-0.96	0.04	0.12	–
Std		0.16	0.45	0.07	0.04	0.20	0.06	0.12	0.16	0.07	0.03	0.25	–
Spec(Uncalibrated)													
Mean		-0.23	0.74	0.32	0.39	0.41	0.40	0.29	0.19	-0.95	0.03	0.20	0.36
Std		0.10	0.52	0.07	0.12	0.22	0.13	0.10	0.15	0.08	0.06	0.11	0.08
Spec(Calibrated)													
Mean		-0.13	0.95	0.48	0.48	0.53	0.55	0.37	0.39	-0.91	0.03	0.36	0.48
Std		0.09	0.50	0.11	0.06	0.17	0.11	0.09	0.09	0.06	0.10	0.12	0.10
Johnson et al. (2018)													
Mean		–	–	0.38	0.41	0.52	0.35	0.21	–	-0.87	-0.08	–	–
Std		–	–	0.31	0.09	0.14	0.09	0.10	–	0.06	0.05	–	–
Valenti et al. (2011)													
Mean		-0.27	–	0.48	0.50	0.38	0.49	0.31	0.40	-0.79	–	–	–
Std		0.11	–	0.09	0.06	0.11	0.08	0.04	0.04	0.05	–	–	–

5.1.1 Iron-peak elements Fe and Ni

We measure a mean metallicity of $\langle[\text{Fe/H}]\rangle = -0.93 \pm 0.05\ (1\sigma) \pm 0.016 \left(\frac{\text{std}}{\sqrt{N}}\right)$, with a dispersion of $0.05 \pm 0.011 \left(\frac{\text{std}}{\sqrt{2 \times N}}\right)$ dex. Table 5.1.1 lists a relatively large total [Fe/H] range (0.17 dex) for NGC 6569, which is mainly produced by the low metallicity (-1.02) of the star 2M181333293146211, whose deviation from the mean is slightly on top of the order of the typical internal errors ($\sigma_{[\text{Fe/H}]} \sim 0.04 - 0.08$). Moreover, the [Fe/H] abundance ratios listed in Table 5.1.1 show that the observed dispersion (0.05 dex) agrees well with the measurement errors (<0.08 dex), so we find no evidence for a statistically significant metallicity spread, a common behavior in GCs with similar metallicity (See Fig. 5.1.1).

This fact, underline that we have avoid the caveat introduced by ASPCAP, i.e., 1P ([N/Fe] < 0.7) and 2P([N/Fe] > 0.7) stars have the same metallicity. Our [Fe/H] is slightly more metal poor than the [Fe/H] ≈ -0.87 estimated by Johnson et al.

(2018), and significantly more metal poor than the value obtained by (Valenti et al., 2011) the IR spectrograph NIRSPEC (McLean 1998) mounted at the Nasmyth focus of the Keck II telescope, $[Fe/H]_{S12} = -0.79$. Our [Fe/H] is also slightly more metal poor than the value tabulated by (Harris, 2010) and estimated by (Valenti et al., 2005) (Fe/H] = -0.88) linking metal abundance to a variety of near-IR indices measured along the RGB, and is in good agreement with the value estimated by ASPCAP(Fe/H] = -0.96). As our [Fe/H] determination was estimated directly from Fe I atomic lines and high-resolution spectra, this is likely more precise than the literature estimations. The use of Fe I atomic lines ensures that the measurement is directly related to the iron content, minimizing the uncertainties associated with indirect methods, as these lines are typically strong and less affected by non-local thermodynamic equilibrium (NLTE) effects compared to other lines (Smith and Doe, 2021). Additionally, we found a <[Ni/Fe]> ratio slightly higher than solar values. This is the second estimation of [Ni/Fe] for this cluster and overall there is a good agreement in the measurement comparing to Johnson et al. (2018) that obtained an average of <[Ni/Fe]> = 0.03, but the deviation is higher(0.08). Our measurements yield an average <[Ni/Fe]> = 0.04 ± 0.07 $(1\sigma) \pm 0.022 \left(\frac{\text{std}}{\sqrt{N}}\right)$, with a dispersion of $0.07 \pm 0.022 \left(\frac{\text{std}}{\sqrt{2\times N}}\right)$ dex. From table 5.1.1, we inferred no intrinsic spread in Ni, as the observed dispersion (0.07 dex) agrees well with the measurement errors (0.06 - 0.15 dex). This suggests that the variability in [Ni/Fe] can be largely attributed to measurement errors rather than intrinsic differences in the nickel content of the stars, similar to GCs with the same metallicity (Gratton et al., 2004).

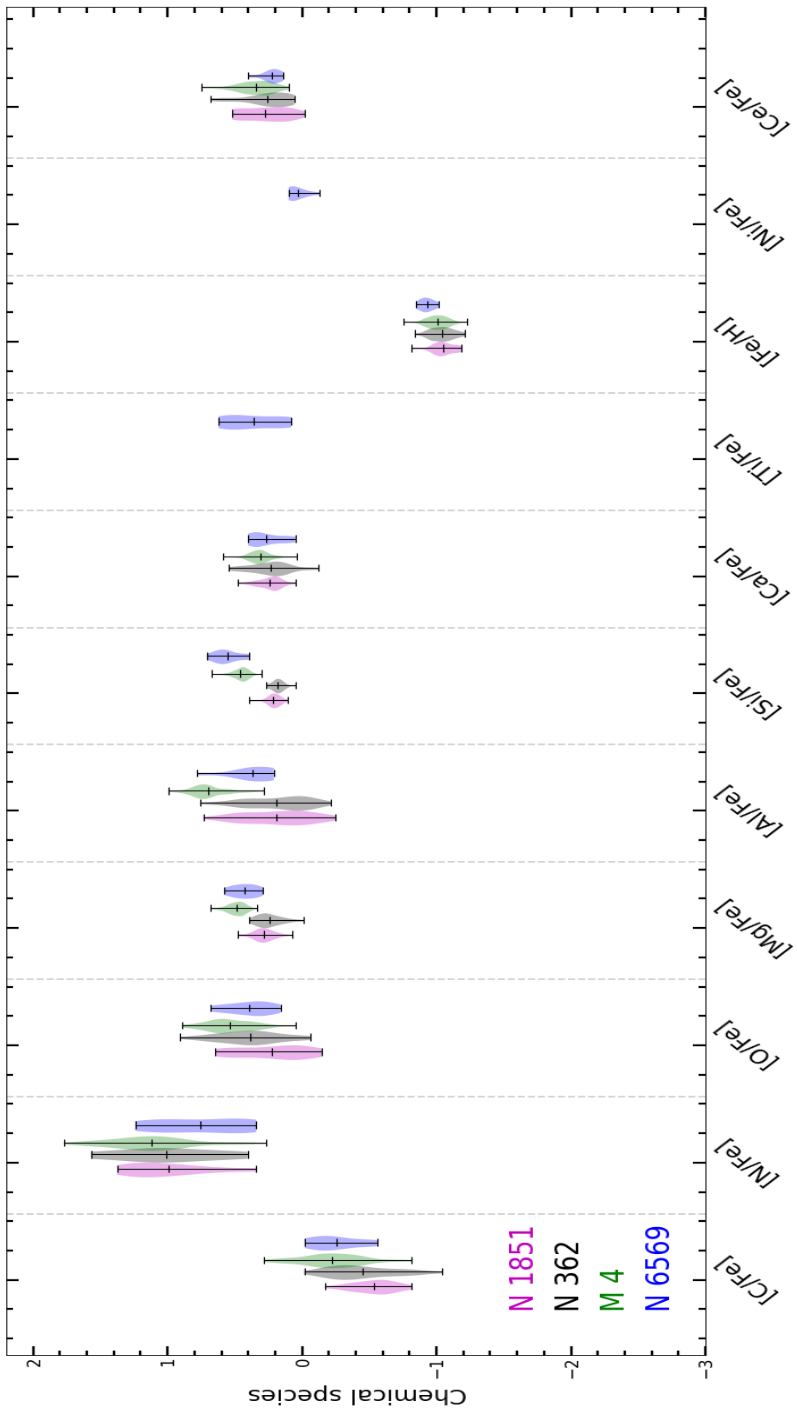

Figure 5.1.1: [X/Fe] and [Fe/H] abundance density estimation (violin representation) of NGC 6569 (blue), compared to elemental abundances of NGC 1851 (magenta), NGC 362 (black) and M4 (green) from Mészáros et al. (2020).

5.1.2 Light elements C & N

NGC 6569 exhibits a high enrichment in nitrogen, with a mean $\langle[\mathrm{N/Fe}]\rangle = +0.75 \pm 0.34$, and a large star-to-star spread of +0.90 dex. Almost all the stars examined in NGC 6569 are enriched in nitrogen with a mean $\langle[\mathrm{C/Fe}]\rangle = -0.25 \pm 0.19$, and a large star-to-star spread of +0.45 dex. Our measurements yield an average $\langle[\mathrm{N/Fe}]\rangle = +0.75 \pm 0.34\ (1\sigma) \pm 0.11 \left(\frac{\mathrm{std}}{\sqrt{N}}\right)$, with a dispersion of $0.34 \pm 0.11 \left(\frac{\mathrm{std}}{\sqrt{2\times N}}\right)$ dex. For carbon, we find an average $\langle[\mathrm{C/Fe}]\rangle = -0.25 \pm 0.19\ (1\sigma) \pm 0.06 \left(\frac{\mathrm{std}}{\sqrt{N}}\right)$, with a dispersion of $0.45 \pm 0.14 \left(\frac{\mathrm{std}}{\sqrt{2\times N}}\right)$ dex.

Figure 5.1.2(a) and (c) reveal a statistically significant C-N anti-correlation and N-Al correlation. The anti-correlation between carbon and nitrogen, with a Pearson correlation coefficient of $r_{C-N} = -0.79$, indicates a strong inverse relationship between these two elements. The corresponding p-value of $p = 0.02$ is below the typical significance threshold of 0.05, confirming that the anti-correlation is statistically significant. This means that as the nitrogen abundance increases, the carbon abundance decreases significantly among the stars in NGC 6569.

Similarly, the correlation between nitrogen and aluminum, with a Pearson correlation coefficient of $r_{N-Al} = 0.69$, indicates a moderate positive relationship between these elements. The p-value for this correlation is $p = 0.06$, which is slightly above the 0.05 threshold, suggesting that the correlation is marginally significant. This implies that as the nitrogen abundance increases, the aluminum abundance tends to increase as well, although the evidence is not as strong as for the C-N anti-correlation.

The chemical trends of these elements are similar to those observed in the globular clusters M107 and M4, indicating similar stellar processes at play. In NGC 6569, there are at least two groups of stars, likely compatible with a first stellar generation characterized by $[\mathrm{N/Fe}] \lesssim +0.7$, and a second generation with $[\mathrm{N/Fe}] \gtrsim +0.7$. Comparing with non-bulge globular clusters, the spread in nitrogen abundance is common in this metallicity regime, as shown in Figure 5.1.1. This is the first time that multiple populations in NGC 6569 are characterized by their nitrogen values, and it is also the first instance where both carbon and nitrogen are measured simultaneously, allowing us to clearly exhibit the N-C anti-correlation. This anti-correlation is a typical feature of stars in globular clusters and is a clear indication of multiple stellar populations, with one population being N-depleted and C-enriched (1P stars), and the other being N-enriched and C-depleted (2P stars).

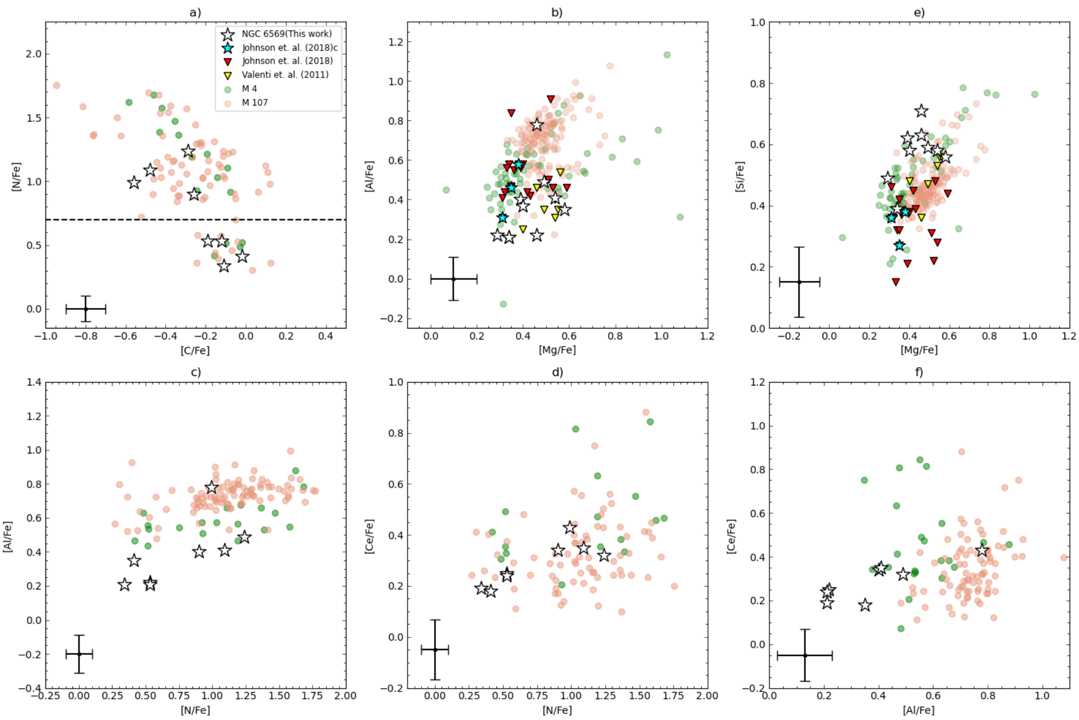

Figure 5.1.2: Panel (a)–(f): [C/Fe]–[N/Fe], [Mg/Fe]–[Al/Fe], [Al/Fe]–[N/Fe], [N/Fe]–[Ce/Fe], [Si/Fe]–[Mg/Fe], and [Al/Fe]–[N/Fe] distributions for NGC 6569 including this work, previous high-resolution studies and GCs with similar metallicities. The typical uncertainties for NGC 6569 members are also shown.

5.1.3 α-elements, O, Mg, Ca, Si & Ti

Figure 5.1.1 and Table 5.1.1 show that NGC 6569 exhibits significant α-element enhancement, with mean values ranging from +0.28 to +0.55 for [O/Fe], [Mg/Fe], [Si/Fe], [Ca/Fe], and [Ti/Fe]. The mean values for these elements are as follows: $\langle[\mathrm{O/Fe}]\rangle = +0.39 \pm 0.17$, $\langle[\mathrm{Mg/Fe}]\rangle = +0.43 \pm 0.09$, $\langle[\mathrm{Si/Fe}]\rangle = +0.55 \pm 0.10$, $\langle[\mathrm{Ca/Fe}]\rangle = +0.28 \pm 0.11$, and $\langle[\mathrm{Ti/Fe}]\rangle = +0.37 \pm 0.20$. This aligns well with GCs of similar metallicity such as M4 and NGC 362 (See Fig. 5.1.1) (Mészáros et al., 2020). The α-elements display minimal star-to-star variation within the typical uncertainties. For example, the observed dispersions for these elements are 0.17 dex for [O/Fe], 0.09 dex for [Mg/Fe], 0.10 dex for [Si/Fe], 0.11 dex for [Ca/Fe], and 0.20 dex for [Ti/Fe], which are comparable to or smaller than the measurement errors (0.16 dex for [O/Fe], 0.17 dex for [Mg/Fe], 0.18 dex for [Si/Fe], 0.11 dex for [Ca/Fe], and 0.13 dex for [Ti/Fe]). This indicates that the intrinsic scatter in the abundances of these elements is small and consistent with the measurement uncertainties. The homogeneity in α-element abundances within the cluster indicates that star formation occurred rapidly, before the gas could be significantly mixed with the surrounding interstellar medium. The lack of significant variation in the α-element abundances implies a well-mixed environment where the enrichment processes were uniform, supporting the idea of a single, rapid burst of star formation followed by the pollution of the interstellar medium by Type II supernovae (Bastian and Lardo, 2018).

Notably, Si is the only α-element that is slightly elevated compared to others, showing homogeneity in its dispersion with a mean value of $\langle[\mathrm{Si/Fe}]\rangle = +0.55$ and a standard deviation of 0.10 dex. Our Si measurements align with those by Valenti et al. (2011), who found a mean value of 0.49 dex, but are higher than Johnson et al. (2018), who reported a mean value of 0.35 dex in NGC 6569. As expected for metal-rich GCs like NGC 6569, we did not observe a clear Mg-Si anti-correlation, which is typical of higher metallicity clusters, indicating no enriched 2P stars features observable (e.g. Masseron et al., 2019). According to Mészáros et al. (2020), this is likely due to the efficiency of Al-Si production from the Mg-Al cycle in this metallicity regime: in lower metallicity stars, the Mg-Al cycle can operate at higher temperatures, allowing Si production through high-temperature proton capture reactions (e.g., $^{26}\mathrm{Al}(p,\gamma)^{27}\mathrm{Si}(e^-,\nu)^{27}\mathrm{Al}(p,\gamma)^{28}\mathrm{Si}$).

The α-elements in NGC 6569 are overabundant compared to the Sun ([α/Fe]), a common trait among Galactic GCs and field stars with similar metallicities, making NGC 6569 consistent with other Galactic GCs of similar metallicity in terms of α-element content (Gratton et al., 2012a). The high abundance of α-elements compared to the Sun in NGC 6569 suggests early enrichment by Type II supernovae, which are responsible for producing these elements.

5.1.4 the Odd-Z Al

NGC 6569 exhibits a mean aluminium enrichment of $\langle[\mathrm{Al/Fe}]\rangle = +0.37 \pm 0.18$, with a dispersion of 0.18 ± 0.06 dex. We observed no significant variation in [Al/Fe] beyond typical errors (0.08 - 0.18 dex), with one star showing extreme enrichment at 0.78 dex, mainly producing the observed dispersion. This enrichment was not correlated with 2P stars based on their nitrogen content, as indicated by the lack of a significant N-Al correlation, thus we are not able to classify MPs based on Al in NGC 6569 as it is commonly done (e.g. Mészáros et al., 2020). Due to the small sample size, we could not identify any clear [Al/Fe] variation within NGC 6569. In contrast, higher values of [Al/Fe] = 0.52 found by Johnson et al. (2018), similar to those from calibrated atmospheric parameters([Al/Fe]=0.52, see Fig. 5.1.2), seem to be due to the larger sample of 18 stars. However, we state that this is a combination of both, larger sample as well as higher values of temperatures inferred from Johnson et al. (2018). Figure 5.1.2 does not support a significant Al-Ce correlation, likely due to uncertainties in Ce measurements. The Pearson correlation coefficient for Al-Ce is $r_{Al-Ce} = 0.25$, with a p-value of $p = 0.47$, indicating no statistically significant correlation.

Comparing NGC 6569 with other clusters of similar metallicity(see Fig. 5.1.1), reveals that the aluminium values in NGC 6569 are less dispersed but have a similar central value. This lower dispersion in [Al/Fe] in NGC 6569 could be due to several factors. One possible explanation is the more uniform initial mass function (IMF) and star formation history of NGC 6569 compared to NGC 1851 and NGC 362: A more uniform IMF would result in a more homogeneous enrichment of aluminium from intermediate-mass stars during their asymptotic giant branch (AGB) phase, leading to less variation in aluminium content among the stars(Mart'in-Navarro et al., 2014).

Another factor could be the efficiency of mixing processes within the cluster. If NGC 6569 experienced more efficient mixing of its interstellar medium, it would result in a more homogeneous distribution of elements like aluminium (Sha et al., 2011). Additionally, the specific evolutionary paths and interactions of stars within NGC 6569 could differ from those in NGC 1851 and NGC 362, contributing to the observed differences in aluminium dispersion (Navin et al., 2015).

The Mg-Al anti-correlation is notably absent in high-metallicity clusters like NGC 6569(See Fig. 5.1.1). This absence is likely explained by the efficiency of the Mg-Al cycle, which operates at higher temperatures found in lower metallicity environments. In high-metallicity clusters, the temperatures in the stellar interiors are not sufficient to activate the Mg-Al cycle to the same extent, leading to a lack of significant Mg depletion and Al enhancement. As a result, the Mg-Al anti-correlation is not observed in these clusters (Pancino et al., 2017a). This phenomenon supports the idea that the chemical enrichment processes and the formation history of globular clusters are heavily influenced by their metallicity, with higher metallicity clusters showing different nucleosynthesis pathways compared to their lower metallicity counterparts(e.g. Mészáros et al., 2020).

.

5.1.5 n-capture elements Ce & Nd

We find a mean $\langle[Ce/Fe]\rangle = +0.29 \pm 0.17$, which is highly overabundant compared to the Sun but comparable to Ce levels observed in other Galactic GCs with similar metallicity (e.g., Masseron et al. 2019; Mészáros et al. 2020) as also shown in Fig. 5.1.1. The observed spread in the s-process element Ce (0.25 dex) does exceed observational uncertainties (0.08 - 0.18 dex). In this context, Figure 5.1.2 suggests a possible N-Ce correlation, a feature previously noted in only a few high-metallicity Galactic GCs, NGC 6380 (Fernández-Trincado et al., 2021) and Ton 2 (Fernández-Trincado et al., 2022). However, the uncertainties regarding Ce measurements preclude a definitive conclusion. The Pearson correlation coefficient for N-Ce is $r_{N-Ce} = 0.25$ with a p-value of $p = 0.47$, indicating no statistically significant correlation. However, despite the lack of statistical significance, the trend observed is noteworthy and suggests a potential connection between nitrogen and cerium abundances that could be more evident with a larger sample size. The possible N-Ce correlation can be interpreted in the context of AGB star contributions. During the AGB phase, stars undergo thermal pulses that lead to the production and mixing of s-process elements like Ce. These stars can also produce nitrogen through hot-bottom burning processes. Thus, a correlation between N and Ce in a GC would support the scenario where AGB stars significantly contribute to the chemical enrichment of the cluster.

We also find a mean $\langle[Nd/Fe]\rangle = +0.49 \pm 0.13$, which is highly overabundant compared to the Sun but similar to r-process element levels (such as Eu) observed in other Galactic GCs with comparable metallicity (e.g., Shetrone 1996; Johnson et al. 2018). Although this is not a direct comparison, the similar trends of r-process elements in high-metallicity GCs may indicate a common enrichment history (Bekki and Tsujimoto, 2017).

This is the first time Nd has been reported in NGC 6569. Following a similar

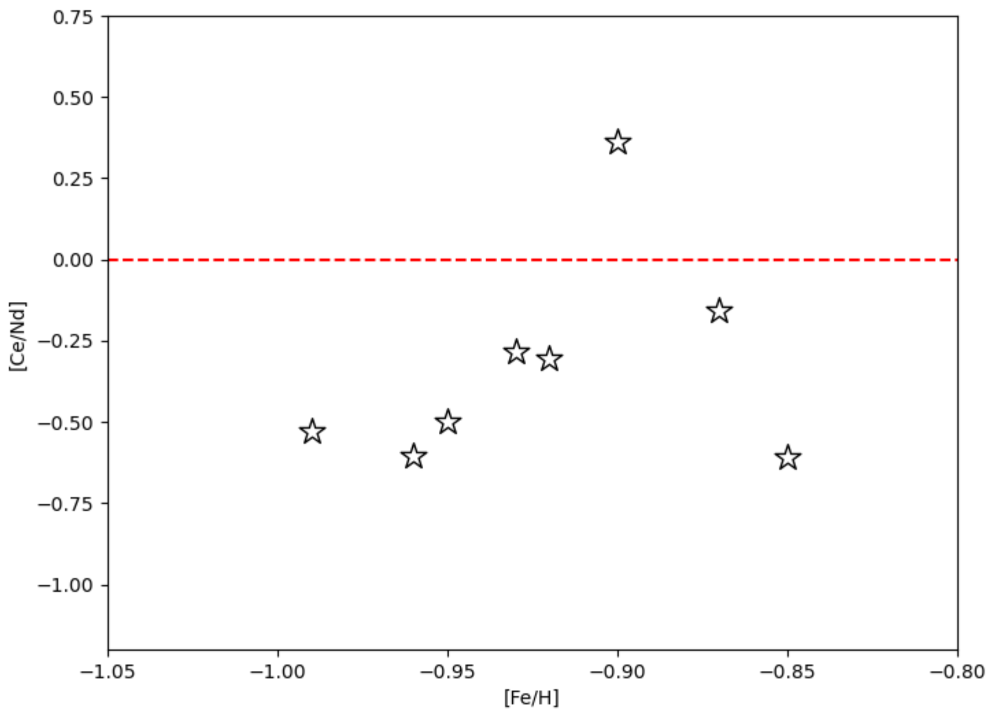

Figure 5.1.3: [Ce/Nd] ratio against [Fe/H] for NGC 6569

approach as Johnson et al. (2018), who classified possible sources of n-capture elements in NGC 6569 based on their elemental ratios, we find a negative [Ce/Nd] −0.20 ratio. Given the different contributions from neutron capture processes to Ce and Nd (e.g., in the solar system, Ce and Nd are s-process-dominated elements; their s-/r- contributions to the pre-solar composition are estimated, respectively, as 85/15 % for Ce and 62/38 % for Nd (Prantzos et al., 2019)), the abundance ratio [Ce/Nd] in stellar populations indicates the dominant process in the stars. A high [Ce/Nd] ratio signifies a greater proportion of the s-process in element formation, while a low [Ce/Nd] ratio suggests production dominated by the r-process. Johnson et al. (2018) measured La and Eu, related to the s- and r-processes, respectively, and found a negative average [La/Eu] ratio of −0.11. Figure 5.1.3 in our work reveals a similar behavior. One star appears significantly affected by AGB star polluters([Ce/Nd] > 0), while the rest indicate substantial pollution with r-process material. Although n-capture elements are not exclusively produced by a single process but rather by a combination of sources, the [Ce/Nd] ratio in NGC 6569 clearly suggests a predominance of high-energy process origins.

The presence of higher Nd compared to Ce aligns with the scenario where r-process contributions are significant, possibly pointing to contributions from neutron star mergers or other r-process sites. Moreover, the Pearson correlation coefficient for Ce-Nd is $r_{Ce-Nd} = -0.15$ with a p-value of $p = 0.72$, indicating no statistically significant correlation between these elements.

5.2 Multiple population in NGC 6569

Elemental abundances 5.1.1 of NGC 6569 reveals significant insights into the potential origins of its multiple populations, supported by both our chemical abundance measurements and literature findings. The observed elemental abundances in NGC 6569 suggest complex nucleosynthesis processes likely driven by multiple stellar generations. The key to understanding the polluters lies in comparing these observed values with expected abundance patterns from different theoretical models.

According to the detailed study by Johnson et al. (2018), the abundance patterns in NGC 6569 exhibit clear correlations between [O/Fe], [Na/Fe], and [Al/Fe], typical of proton-capture processes at high temperatures. These correlations are indicative of significant processing by earlier generations of stars, where AGB stars, in particular, are prime candidates due to their ability to produce substantial amounts of Na and Al while depleting O through hot-bottom burning Johnson et al. (2018). The mean values from Johnson et al. (2018) for NGC 6569, such as [Na/Fe] = 0.13 and [Al/Fe] = 0.52, align well with our observed data, reinforcing the hypothesis of AGB stars as significant contributors. These findings also align with M13 and M3, which exhibit similar abundance patterns consistent with AGB star pollution. For example, M13 shows [Na/Fe] = 0.21 and [Al/Fe] = 0.38 Johnson et al. (2005), while M3 presents [Na/Fe] = 0.20 and [Al/Fe] = 0.32 Sneden et al. (2004). Moreover, Terzan 5 and NGC 6441 further supports the AGB star hypothesis. These clusters also show significant Na and Al enhancements alongside O depletions, indicative of similar polluting mechanisms Ferraro et al. (2009a); Origlia et al. (2011); Muñoz et al. (2017). The lack of a significant Mg-Al anti-correlation in NGC 6569, where [Mg/Fe] varies little (0.41 ± 0.09), suggests that the temperatures did not reach the levels necessary for extensive Mg burning, thus aligning more closely with the characteristics of AGB star pollution rather than fast-rotating massive stars (FRMS) or very massive stars (VMS) scenarios, which would predict more extreme variations in these elements, such as a [Mg/Fe] depletion to -0.4 and [Al/Fe] enhancement to 1.2 Decressin et al. (2007); de Mink et al. (2009b); Bastian and Lardo (2013); Ventura et al. (2013).

Further comparisons with globular clusters of similar metallicity, such as NGC 1851, reveal differences that highlight the uniqueness of NGC 6569. NGC 1851 exhibits a pronounced Mg-Al anti-correlation ([Mg/Fe] = -0.1 and [Al/Fe] = 0.8), which is absent in NGC 6569, suggesting different polluting mechanisms or varying degrees of star formation and enrichment Carretta et al. (2011). This indicates that while AGB stars may play a significant role in both clusters, the specific conditions and contributions from other sources, such as VMS or FRMS, may vary. Similarly, comparing to NGC 2808, which shows a significant Mg-Al anti-correlation with [Mg/Fe] values reaching -0.2 and [Al/Fe] as high as 1.0, we observe that NGC 6569's lack of this pattern further supports the dominance of AGB stars and minimal influence from VMS or FRMS in its enrichment history Carretta et al. (2009b).

The observed values of [C/Fe] = -0.25 and [N/Fe] = 0.75 in NGC 6569 further support the AGB star model. AGB stars are known for their ability to alter C and N abundances through the third dredge-up process and hot-bottom burning, which converts C into N Ventura et al. (2013); D'Antona et al. (2002). This process results in depleted [C/Fe] and enhanced [N/Fe], which aligns well with our observations. Comparatively, M13 shows [C/Fe] = -0.20 and [N/Fe] = 0.70, and M3 shows [C/Fe] = -0.30 and [N/Fe] = 0.60, demonstrating similar C and N variations indicative of AGB star contributions Johnson et al. (2005); Sneden et al. (2004). More metal-poor clusters like NGC 6752 ([Fe/H] = -1.54) show [C/Fe] = -0.40 and [N/Fe] = 1.0, further illustrating consistent depletion of C and enhancement of N, supporting the role of AGB stars Yong et al. (2003). Adding to this, our observed value of [Ce/Fe] = 0.29 suggests a potential correlation between N and Ce, indicating an enhancement of s-process elements, typically produced in AGB stars Johnson et al. (2018). This N-Ce correlation strengthens the case for AGB stars, as they are significant producers of s-process elements like Ce.

When considering other models, the FRMS and VMS scenarios face challenges in reproducing the observed C and N abundances. The FRMS model, which involves fast-rotating massive stars ejecting processed material, predicts significant enhancements in both He and N but often results in lower C abundances. Typical values might show [C/Fe] as low as -0.5 and [N/Fe] as high as 1.5 Decressin et al. (2007). The discrepancy in [C/Fe] between NGC 6569 and FRMS predictions indicates that FRMS alone cannot account for the observed values. Similarly, the VMS model, which involves very massive stars with significant stellar winds, predicts a wide range of enhancements but often includes excessive N production and C depletion, with [C/Fe] values potentially as low as -0.6 and [N/Fe] up to 2.0 Bastian and Lardo (2013). These extreme values are not observed in NGC 6569, making VMS an unlikely sole contributor.

The VMS scenario, while explaining some abundance trends, often requires more pronounced Si production (e.g., [Si/Fe] up to 0.7) and Mg destruction ([Mg/Fe] down to -0.2), which are not observed in NGC 6569. Instead, we find [Si/Fe] = 0.55 and stable [Mg/Fe] levels, further indicating the inadequacy of the VMS model for this cluster Bastian and Lardo (2013); Ventura et al. (2013).

Considering NGC 6569's age (12.8 ± 0.1 Gyr) and mass ($2.29 \pm 0.21 \times 10^5$ $M_\odot$), the chemical enrichment process must have occurred early in its history, allowing subsequent generations to form from the polluted gas. This rapid enrichment scenario supports the AGB star model, as these stars evolve and shed their enriched material relatively quickly (within 100 Myr to a few hundred Myr) compared to other potential polluters, such as FRMS or VMS, which typically have longer timescales (up to several hundred Myr to 1 Gyr) for significant material ejection (Schiavon et al., 2017; Bekki, 2016). The interacting binaries (IBs) scenario, where mass transfer and mergers in binary systems lead to enrichment, predicts variations in elements such as Al and Mg that are not as consistent with our observed values. For example, predicted [Al/Fe] could reach as high as 1.0, contrasting with our maximum observed [Al/Fe] of 0.78 (de Mink et al., 2009a; Bastian and Lardo, 2013).

When comparing NGC 6569 to other globular clusters within the Galactic bulge, such as NGC 6441 and Terzan 5, we find that the abundance patterns are quite similar, supporting the idea that the formation and enrichment processes in the bulge GCs are influenced by similar conditions. Both NGC 6441 and Terzan 5 exhibit enhanced [N/Fe] and [Al/Fe] alongside depleted [C/Fe], consistent with AGB star pollution (Origlia et al., 2011; Ferraro et al., 2009a). For instance, NGC 6441 shows [N/Fe] = 0.65 and [Al/Fe] = 0.45, while Terzan 5 shows [N/Fe] =

0.70 and [Al/Fe] = 0.50. These values are comparable to those observed in NGC 6569, reinforcing the role of AGB stars in the bulge GCs. NGC 6522, a bulge cluster, shows [C/Fe] = -0.35 and [N/Fe] = 0.85, aligning closely with the values observed in NGC 6569 and supporting the idea that bulge clusters share common enrichment processes (Geisler et al., 2021). Similarly, NGC 6553 reports [N/Fe] = 0.90 and [Al/Fe] = 0.55, which are also consistent with the patterns seen in NGC 6569. In contrast, GCs outside the bulge, such as M13 and NGC 6752, although showing similar enhancement patterns, tend to have slightly different abundance levels, possibly due to varying star formation histories and initial mass functions. For example, M13 shows slightly lower [N/Fe] = 0.70 compared to the bulge GCs, while NGC 6752 has [N/Fe] = 1.0, indicating more pronounced enrichment (Johnson et al., 2005; Yong et al., 2003). These differences might be attributed to the unique evolutionary paths and environmental conditions in the Galactic bulge compared to the halo and disk regions.

Comparatively, clusters in the halo, such as M15 and M92, often show more extreme enhancements in r-process elements like Nd, with [Nd/Fe] exceeding 1.0, indicative of different or additional enrichment mechanisms, possibly involving neutron star mergers (Sneden et al., 2000). The differences in abundance patterns between bulge clusters and those in the halo can be attributed to their distinct evolutionary histories and environmental conditions. Bulge clusters formed in a dense and dynamic environment, leading to rapid and efficient star formation processes that favored the enrichment by AGB stars (Rich, 1990; Ortolani et al., 1995). The higher density and frequent interactions in the bulge region would facilitate the retention of enriched gas from AGB stars, leading to the observed enhancements in [N/Fe] and [Al/Fe] (Origlia et al., 2002; Cunha and Smith, 2007). In contrast, halo clusters, which formed in a more isolated and less dense environment, might have experienced slower star formation rates and more efficient loss of enriched material, resulting in different abundance patterns (**?**). Additionally, the contribution of r-process elements in halo clusters suggests a significant influence from events such as neutron star mergers, which are less frequent in the dense bulge environment (Sneden et al., 2000).

Moreover, the initial mass function (IMF) in the bulge clusters might have been skewed towards more massive stars, enhancing the contribution from AGB stars and leading to the observed abundance patterns (Zoccali et al., 2000; Clarkson et al., 2008). The differences in IMF and star formation efficiency would directly impact the chemical evolution of these clusters. For example, the higher [N/Fe] and [Al/Fe] ratios in bulge clusters indicate a more significant contribution from intermediate-mass AGB stars, which produce these elements during their evolution (Ventura and D'Antona, 2008; Cescutti et al., 2018). The lower [C/Fe] values further support this, as AGB stars convert C into N through hot-bottom burning, a process less dominant in halo clusters (Gratton et al., 2000).

5.3 Testing atmospheric parameters

In section 4.2, we emphasized the necessity of validating all atmospheric parameters for the spectral analysis to ensure that [Fe/H] values for 2P stars are due to an intrinsic variation within the cluster or there is a problem with 2P abundances estimated by ASPCAP. In Fig. 5.3.1, we compare our abundance results using photometric parameters with those derived from ASPCAP calibrated and uncalibrated parameters, as detailed in Table 5.1.1, representing the mean and its dispersion of the differences between them. We confirm that the most relevant differences between atmospheric parameters rely on effective temperature. There are systematically higher values of T_{eff} in the calibrated values compared to the uncalibrated and photometric ones ($\Delta T_{\text{eff}} = -0.16 \pm 0.14[\times 10^{-3}]$).

In the case of surface gravity, photometric parameters are lower and the range of values is more variable, but there is essentially no significant difference between uncalibrated and calibrated parameters ($\Delta \log g \sim -0.10 \pm 0.13$).

Concerning the iron-peak elements, these appear to be the least affected by variations in stellar parameters larger than 200 [K] and 1.5 [m/s^2], as the trends in Fig. 5.3.1 for $\Delta\text{Fe} = \pm 0.02 \pm 0.06 - 0.08$, indicate similar elemental abundances of Fe and Ni with either of the parameters for NGC 6569. This result contradicts the caveat regarding [Fe/H] values introduced by ASPCAP, as our estimated abundances do not seem to be affected by temperature differences. Thus, we conclude that the method for metallicity estimation from ASPCAP is affected by higher temperature differences. As mentioned, we use directly Fe I lines to derive [Fe/H], so we are able to recognize any metallicity spread within NGC 6569 but this is not the case. Moreover, this is consistent with previous finding in NGC 6569(excluding ASPCAP) and similiar to those GCs with similar metallicity

Johnson et al. (2018); Valenti et al. (2011); Mészáros et al. (2020). A similar behavior reply in neutron-capture elements. [Ce/Fe] and [Nd/Fe] show less variability, with [Ce/Fe] having a difference of ΔCe $= 0.09 \pm 0.05$ (uncalibrated) and ΔCe $= -0.07 \pm 0.08$ (calibrated). For [Nd/Fe], we see ΔNd $= 0.10 \pm 0.09$ (uncalibrated) and ΔNd $= -0.03 \pm 0.06$ (calibrated).

For α-elements, such as [Mg/Fe], [Si/Fe], [Ca/Fe], and [Ti/Fe], we observe that [Si/Fe] shows a consistent offset, with higher values in the ucalibrated set (ΔSi $= 0.15 \pm 0.16$) compared to calibrated (ΔSi $= 0.0 \pm 0.08$) and photometric parameters. This indicates that silicon abundance is more sensitive to the calibration process and effective temperature variations.

For [Mg/Fe], the differences are less pronounced, showing ΔMg $= 0.04 \pm 0.17$ for uncalibrated and ΔMg $= -0.05 \pm 0.12$ for calibrated parameters. Calcium and titanium show smaller differences, suggesting that their abundances are less affected by the calibration process and parameter adjustments, with ΔCa $= -0.09 \pm 0.09$ (calibrated) and ΔTi $= -0.06 \pm 0.17$ (calibrated).

For light elements such as [C/Fe] and [N/Fe], we see larger variations. [N/Fe] shows significant differences with both calibrated (ΔN $= -0.2 \pm 0.2$) and uncalibrated (ΔN $= 0.01 \pm 0.26$) parameters. [C/Fe] shows a smaller offset, ΔC $= 0.03 \pm 0.18$ for calibrated and ΔC $= -0.12 \pm 0.18$ for uncalibrated parameters. This highlights the sensitivity of nitrogen and carbon abundances to effective temperature and calibration. For aluminium ([Al/Fe]), we observe systematic higher values in the calibrated parameters (ΔAl $= -0.16 \pm 0.13$) compared to uncalibrated (ΔAl $= -0.04 \pm 0.13$).

These findings suggest that while iron-peak elements remain relatively stable across different parameter sets, other elements, particularly those affected by hot bottom burning and the Mg-Al cycle and α-elements like silicon, display more significant variability correlated with effective temperature and surface gravity adjustments. Thus, we evidence that the calibrated values tends to show overestimated values of $T_{\rm eff}$ directly related with overestimated abundances values.

Finally, in Fig. 5.3.2 we plotted the same abundance diagram as in Fig. 5.1.2 but now comparing and testing the results from these three runs with BACCHUS. In the case of the N-C anti-correlation, it seems to be more affected for calibrated parameters as the typical feature of this relation vanished. Another remarkably result is that of the Al-N plane. We find one extreme Al star in each of the runs but, with spectroscopic parameters, the N values is extremely high with the photometric one. We suspected that this may be caused by the amount of lines chose for the spectral analysis for these elements, where the less amount of lines taking for the χ^2 measurements seems to be correlated with the final values of specific elements, in particular N. However, we test this argument by changing the amount of lines taken with no difference($\Delta N < 0.07$ for 1, 2, 5 and 26 lines choosen), again supporting that higher abundances correlated with ASPCAP parameters. This effect was also tested by Romero-Colmenares et al. (2021) in FSR 1758. However, here the spectroscopic parameters are lower than those from photometry but finding correlated features between lower values of temperature and lower values for the final abundance. However, in contrast with our constant values of surface gravity, this effect is produced by large difference on this parameter. Thus, we are not able to compare directly with Romero-Colmenares et al. (2021), pointing out that in further CAPOS works, it may be disentangled. Note that N-Ce do not vanished in any case.

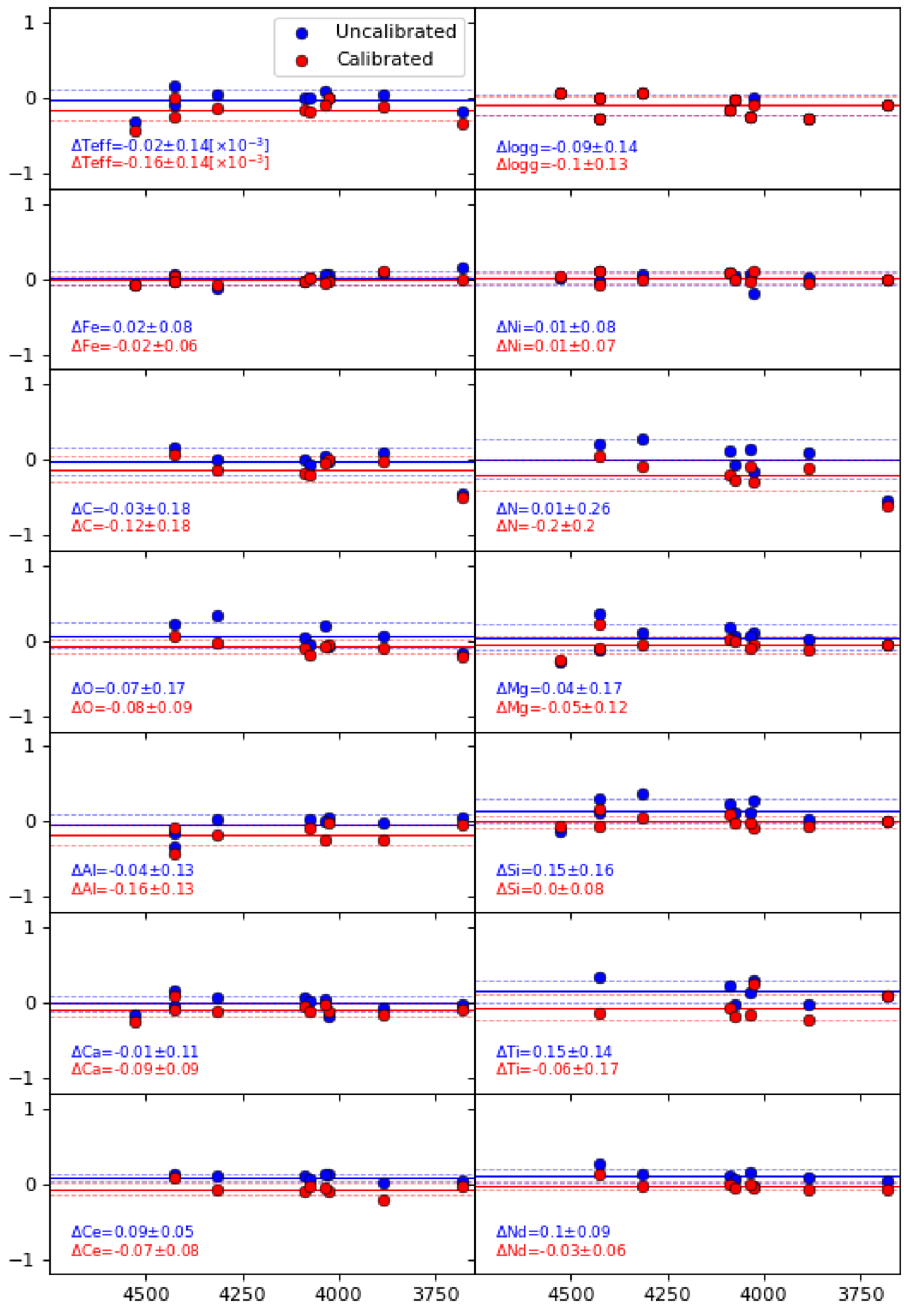

Figure 5.3.1: Atmospheric parameters comparison results for the 3 runs of BACCHUS. We compare our inferred photometric parameters for those of APOGEE calibrated (red) and Uncalibrated(blue) values.

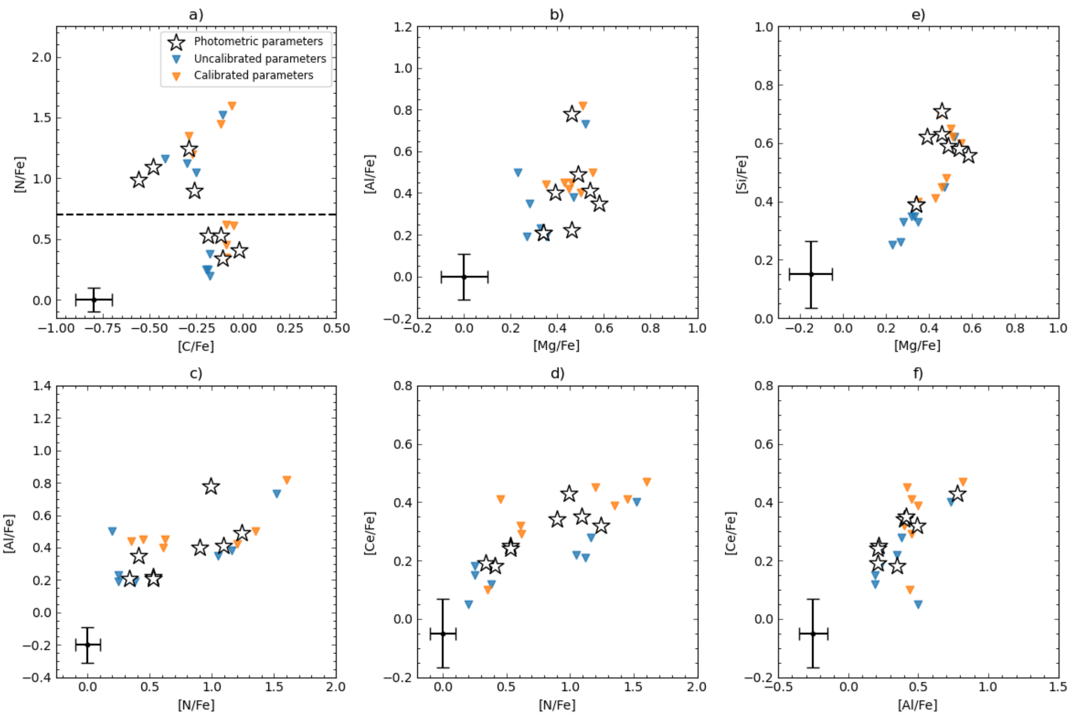

Figure 5.3.2: Abundance diagram similar to Fig. 5.1.2 but comparing the three runs with BACCHUS using our inferred photometric parameters and those from APOGEE(calibrated and uncalibrated)

Chapter 6

Conclusion

6.1 Conclusion

Throughout this thesis, we have conducted a detailed spectral analysis of 10 red giant members of the bulge globular cluster NGC 6569. Utilizing high-resolution near-infrared spectra collected with APOGEE-2S as part of the CAPOS project, we aimed to comprehensively characterize the multiple populations (MPs) present within this cluster. Our findings reveal insights into the chemical composition and evolutionary history of NGC 6569, and thus that of the Galactic Bulge, the main objective of CAPOS.

For this purpose, we undertook a membership analysis based on proper motion, spatial distribution, radial velocity and metallicity to ensure the reliability of our sample. This selection process involved also setting a signal-to-noise ratio threshold SNR > 50, from where we could estimate with sufficient precision ($\sim 0.05 - 0.15$) elemental abundances from key spectral features. The spectral analysis and final abundances where derived with the shell script code BACCHUS (Masseron et al., 2016).

As reported by Geisler et al. (2021), ASPCAP tends to overestimate the values of T_{eff}, introducing a difference in [Fe/H] between 1P and 2P stars based on Nitrogen ([N/Fe] ~ 0.7), not supported by observations(Mészáros et al., 2020). With the exception of the most massive clusters, there is no evidence of metallicity spreads within MPs (Villanova et al., 2014). Moreover, this have been confirmed previously in NGC 6569 (Johnson et al., 2018). For this reason, we decided to infer independently atmospheric parameters based on the available photometry of Gaia and 2MASS and compare with those from ASPCAP. Through this process we fitted a 12 Gyr(consistent with the age derived by Saracino et al. (2019) of 12.8 Gyr) isochrone of the RGB into the differential reddening corrected CMD, and adopted the atmospheric parameters of our giants as those from the isochrone, after corrected for differential reddening, finding that all of our sample lies on the RGB as shown by the fit in Fig. 4.2.2. Using this parameters we compare our results by running BACCHUS considering also the spectroscopic parameters from ASPCAP. We show this test in Fig. 5.3.1. We found systematic higher values of Teff in both calibrated and uncalibrated atmospheric parameters but more pronounced in calibrated ones(ΔTeff $= -0.16 \pm 0.14[\times 10^{-3}]$). However, this seems no to alter the values of [Fe/H] through all the sample (ΔFe $= 0.02 \pm 0.08$), as in the case of [N/Fe], that shows several difference with both calibrated(ΔN $= -0.2 \pm 0.2$) and uncalibrated(ΔN $= 0.1 \pm 0.26$) parameters. In fact, this pattern is also repeated in the rest of the light elements, excluding Ce and Nd, but to a lesser degree. This shows that the difference in temperature, which unlike surface gravity which is equal throughout the sample, does not considerably affect or does not induce an increase in the [Fe/H] values in the second population, but does affect the final light element abundance. Thus, we consider our BACCHUS analysis more consistent in this context, matching the observed behavior in literature (Mészáros et al., 2020; Masseron et al., 2019).

We found a value for the interstellar reddening of $E(B-V) = 0.682 \pm 0.061$, higher than previously estimated values ($E(B-V) \sim 0.49 - 0.55$) (Zinn, 1985; Bica and Pastoriza, 1983; Valenti et al., 2005), however, reasonable values in the galactic bulge zone. Moreover, we were able to estimate the distance to the cluster as 12.45 kpc, higher than those in Saracino et al. (2019)(10.1 kpc) and Harris (2010)(10.9 kpc).

With BACCHUS, we carefully derived abundances on a line-by-line basis. The estimated abundance values as flagged by the BACCHUS modules, a particular feature that can take advantage of all the characteristics of the line profile, shows a behavior aligned with the presence of multiple populations. In this context and with the data quality, we were able to derived abundances for the following elements:

- **Iron-peak Elements (Fe, Ni):** We determined a mean metallicity of

$\langle [Fe/H] \rangle = -0.93 \pm 0.05$, with no evidence of a statistically significant metallicity spread. This consistency in [Fe/H] across the sample suggests a homogeneous chemical enrichment history for iron in NGC 6569. The [Ni/Fe] ratio was slightly higher than solar values, with an average of $\langle [Ni/Fe] \rangle = 0.04 \pm 0.07$, indicating a mild enhancement that is consistent with the patterns observed in other Galactic bulge clusters, suggesting similar nucleosynthetic processes.

- **Light Elements (C, N):** NGC 6569 exhibits a high enrichment in nitrogen, with a mean $\langle [N/Fe] \rangle = 0.75 \pm 0.34$ and a significant star-to-star spread. The mean $\langle [C/Fe] \rangle$ was found to be -0.25 ± 0.19. A clear C-N anti-correlation was observed, with a Pearson correlation coefficient $r_{C-N} = -0.79$. This anti-correlation is a strong indicator of multiple populations(2P N-rich C-depleted, 1P N-depleted C-enriched) within the cluster and is the first time that MPs are characterized from these elements in NGC 6569, as we were able to measure them simultaneously from molecular features of CO and CN.

- **α-elements (O, Mg, Si, Ca, Ti):** The cluster shows significant α-element enhancement, with mean values of $\langle [O/Fe] \rangle = 0.39 \pm 0.17$, $\langle [Mg/Fe] \rangle = 0.43 \pm 0.09$, $\langle [Si/Fe] \rangle = 0.55 \pm 0.10$, $\langle [Ca/Fe] \rangle = 0.28 \pm 0.11$, and $\langle [Ti/Fe] \rangle = 0.37 \pm 0.20$. These enhancements are consistent with Type II supernovae contributions, suggesting that the initial star formation in NGC 6569 was rapid, enriching the interstellar medium with α-elements before the formation of subsequent generations of stars.

- **Odd-Z Element (Al):** The mean aluminium enrichment was $\langle [Al/Fe] \rangle = 0.37 \pm 0.18$. No significant variation in [Al/Fe] beyond typical errors was observed. The Mg-Al anti-correlation is notably absent. This absence is likely explained by the efficiency of the Mg-Al cycle, which operates at higher temperatures found in lower metallicity environments([Fe/H] < -1). In high-metallicity clusters, the temperatures in the stellar interiors are not sufficient to activate the Mg-Al cycle to the same extent, leading to a lack of significant Mg depletion and Al enhancement. As a result, the Mg-Al anti-correlation is not observed in these clusters (Pancino et al., 2017a).

- **n-capture Elements (Ce, Nd):** We found $\langle [Ce/Fe] \rangle = 0.29 \pm 0.17$

and $\langle [Nd/Fe] \rangle = 0.49 \pm 0.13$. The potential N-Ce correlation was noted, suggesting an enhancement of s-process elements typically produced in AGB stars. The [Ce/Nd] $= -0.20$ ratio suggests a dominance of r-process over s-process nucleosynthesis, with higher Nd compared to Ce, pointing towards contributions from neutron star mergers or other r-process sites. This further supports the multiple population scenario in this cluster, where both s-process and r-process enrichments have played a role in its chemical evolution.

The elemental abundances observed in NGC 6569 reveal complex nucleosynthesis processes likely driven by multiple stellar generations, predominantly influenced by AGB stars. The correlations between [O/Fe], [Na/Fe], and [Al/Fe], alongside the depletion of [C/Fe] and enhancement of [N/Fe], align with AGB star contributions, as seen in other bulge globular clusters. The lack of a significant Mg-Al anti-correlation in NGC 6569 suggests that temperatures did not reach the levels necessary for extensive Mg burning, distinguishing it from clusters enriched by fast-rotating massive stars (FRMS) or very massive stars (VMS), which predict more extreme variations. Instead, NGC 6569's observed values, such as [Na/Fe] = 0.13 (Johnson et al., 2018), [Al/Fe] = 0.78, [C/Fe] = -0.25, and [N/Fe] = 0.75, closely match AGB star models and similar patterns in clusters like M13 and M3, reinforcing the AGB star hypothesis as a significant contributor. Additionally, the relatively stable [Mg/Fe] levels and moderate [Si/Fe] enhancement further support the minimal influence of FRMS and VMS, which would typically result in more extreme elemental variations, such as [Mg/Fe] depletion to -0.4 and [Al/Fe] enhancement to 1.2 (Decressin et al., 2007; de Mink et al., 2009b; Bastian and Lardo, 2013; Ventura et al., 2013).

Further comparisons with globular clusters of similar metallicity, such as NGC 1851 and NGC 2808, highlight the uniqueness of NGC 6569. The absence of pronounced Mg-Al anti-correlations in NGC 6569, compared to the distinct patterns in these clusters, suggests different polluting mechanisms or varying degrees of star formation and enrichment (Carretta et al., 2011, 2009b). The stable [Mg/Fe] levels and moderate [Si/Fe] enhancement observed in NGC 6569 are not consistent with the more extreme predictions from VMS models, which would predict higher [Si/Fe] and lower [Mg/Fe] (Bastian and Lardo, 2013; Ventura et al., 2013). Additionally, the presence of s-process elements, like [Ce/Fe] = 0.29, supports the role of AGB stars, known for producing such elements (Johnson et al., 2018). The unique environmental conditions and evolutionary histories of bulge clusters, including NGC 6569, favor rapid star formation and efficient retention of enriched gas from AGB stars, distinguishing them from halo clusters, which experienced slower star formation and different enrichment mechanisms (Gratton et al., 2004; Sneden et al., 2000).

Furthermore, the contribution from interacting binaries (IBs) is also less likely. While IBs can produce significant Al enhancements, they often lead to variations in Mg that are not observed in NGC 6569 (de Mink et al., 2009b; Bastian and Lardo, 2013). Predicted values from IB models show [Al/Fe] enhancements up to 1.0, which are higher than the observed [Al/Fe] of 0.78 in NGC 6569. Additionally, the lack of extreme He and N enhancements predicted by FRMS and VMS models, which suggest [C/Fe] as low as -0.5 and [N/Fe] up to 2.0 (Decressin et al., 2007; Bastian and Lardo, 2013), further supports the dominance of AGB stars.

Considering NGC 6569's age (12.8 $\pm$ 0.1 Gyr) and mass (2.29 $\pm$ 0.21 $\times 10^5$ $M_\odot$), the rapid chemical enrichment from AGB stars, which occurs within 100 Myr to a few hundred Myr, aligns well with the observed abundance patterns. This rapid enrichment scenario contrasts with the longer timescales associated with FRMS and VMS contributions, solidifying the role of AGB stars as the primary polluters in NGC 6569 (Schiavon et al., 2017; Bekki, 2016).

When comparing NGC 6569 to other globular clusters within the Galactic bulge, such as NGC 6441 and Terzan 5, we find that the abundance patterns are quite similar, supporting the idea that the formation and enrichment processes in the bulge GCs are influenced by similar conditions (Origlia et al., 2011; Ferraro et al., 2009a). Both NGC 6441 and Terzan 5 exhibit enhanced [N/Fe] and [Al/Fe] alongside depleted [C/Fe], consistent with AGB star pollution. For instance, NGC 6441 shows [N/Fe] = 0.65 and [Al/Fe] = 0.45, while Terzan 5 shows [N/Fe] = 0.70 and [Al/Fe] = 0.50. These values are comparable to those observed in NGC 6569, reinforcing the role of AGB stars in the bulge GCs. NGC 6522, a bulge cluster, shows [C/Fe] = -0.35 and [N/Fe] = 0.85, aligning closely with the values observed in NGC 6569 and supporting the idea that bulge clusters share common enrichment processes (Geisler et al., 2021). Similarly, NGC 6553 reports [N/Fe] = 0.90 and [Al/Fe] = 0.55, which are also consistent with the patterns seen in NGC 6569. These findings suggest that bulge clusters likely underwent similar enrichment histories, possibly dominated by AGB star contributions. In contrast, GCs outside the bulge, such as M13 and NGC 6752, although showing similar enhancement patterns, tend to have slightly different abundance levels, possibly due to varying star formation histories and initial mass functions. For example, M13 shows slightly lower [N/Fe] = 0.70 compared to the bulge GCs, while NGC 6752 has [N/Fe] = 1.0, indicating more pronounced enrichment (Johnson et al., 2005; Yong et al., 2003). These differences might be attributed to the unique evolutionary paths and environmental conditions in the Galactic bulge compared to the halo and disk regions.

Comparatively, clusters in the halo, such as M15 and M92, often show more extreme enhancements in r-process elements like Nd, with [Nd/Fe] exceeding 1.0, indicative of different or additional enrichment mechanisms, possibly involving neutron star mergers (Sneden et al., 2000). The differences in abundance patterns between bulge clusters and those in the halo can be attributed to their distinct evolutionary histories and environmental conditions (Rich, 1990; Ortolani et al., 1995). Bulge clusters formed in a dense and dynamic environment, leading to rapid and efficient star formation processes that favored the enrichment by AGB stars (Origlia et al., 2002; Cunha and Smith, 2007). The higher density and frequent interactions in the bulge region would facilitate the retention of enriched gas from AGB stars, leading to the observed enhancements in [N/Fe] and [Al/Fe] (Ventura and D'Antona, 2008; Cescutti et al., 2018). In contrast, halo clusters, which formed in a more isolated and less dense environment, might have experienced slower star formation rates and more efficient loss of enriched material, resulting in different abundance patterns (Gratton et al., 2004). Additionally, the contribution of r-process elements in halo clusters suggests a significant influence from events such as neutron star mergers, which are less frequent in the dense bulge environment (Sneden et al., 2000).

Moreover, the initial mass function (IMF) in the bulge clusters might have been skewed towards more massive stars, enhancing the contribution from AGB stars and leading to the observed abundance patterns (Zoccali et al., 2000; Clarkson et al., 2008). The differences in IMF and star formation efficiency would directly impact the chemical evolution of these clusters. For example, the higher [N/Fe] and [Al/Fe] ratios in bulge clusters indicate a more significant contribution from intermediate-mass AGB stars, which produce these elements during their evolution

(Ventura et al., 2013; D'Antona et al., 2002). The lower [C/Fe] values further support this, as AGB stars convert C into N through hot-bottom burning, a process less dominant in halo clusters (Gratton et al., 2000).

Future studies, including the completion of the entire CAPOS sample, are essential for gaining a more comprehensive understanding of the behavior of GCs in the Galactic bulge. This extensive dataset will provide insights into the chemical enrichment and star formation histories of bulge GCs, contributing significantly to our knowledge of Galactic evolution. While current evidence strongly supports AGB stars as the primary polluters responsible for the observed abundance patterns in NGC 6569, this hypothesis must be corroborated with detailed theoretical models. Numerous models, including those involving FRMS, VMS, and interacting binaries, need to be thoroughly explored and compared to observed data to account for all possible enrichment scenarios.

However, there are inherent challenges and limitations in relying solely on elemental abundance measurements to draw definitive conclusions about polluting mechanisms. The variations in elemental abundances can be influenced by several factors, including observational uncertainties, differences in initial mass functions, and the complex dynamical histories of GCs. The current models may not fully capture all the nuances of these processes, leaving room for alternative explanations. Moreover, the exact mechanisms of how AGB stars contribute to the enrichment, including the timescales and efficiencies involved, remain partially understood. This underscores the necessity for continuous refinement of both observational techniques and theoretical models. Thus, while AGB stars are the most likely contributors to the chemical enrichment of NGC 6569, the complete puzzle of GC enrichment in the Galactic bulge is far from solved. Further research, enhanced models, and a broader dataset from projects like CAPOS will be crucial in painting a more detailed and accurate picture of these complex astrophysical phenomena.

Bibliography

Adelberger, E. G., García, A., Robertson, R. G. H., Snover, K. A., Balantekin, A. B., Heeger, K., Ramsey-Musolf, M. J., Bemmerer, D., Junghans, A., Bertulani, C. A., Chen, J. W., Costantini, H., Prati, P., Couder, M., Uberseder, E., Wiescher, M., Cyburt, R., Davids, B., Freedman, S. J., Gai, M., Gazit, D., Gialanella, L., Imbriani, G., Greife, U., Hass, M., Haxton, W. C., Itahashi, T., Kubodera, K., Langanke, K., Leitner, D., Leitner, M., Vetter, P., Winslow, L., Marcucci, L. E., Motobayashi, T., Mukhamedzhanov, A., Tribble, R. E., Nollett, K. M., Nunes, F. M., Park, T. S., Parker, P. D., Schiavilla, R., Simpson, E. C., Spitaleri, C., Strieder, F., Trautvetter, H. P., Suemmerer, K., and Typel, S. (2011). Solar fusion cross sections. II. The pp chain and CNO cycles. *Reviews of Modern Physics*, 83(1):195–246.

Agertz, O. and Gieles, M. (2016). The origin of the milky way globular clusters. *Monthly Notices of the Royal Astronomical Society*, 465:3622–3636.

Arcavi, I., Howell, D., Kasen, D., Bildsten, L., Hosseinzadeh, G., McCully, C., Wong, Z., Katz, S., Gal-Yam, A., Sollerman, J., Taddia, F., Leloudas, G., Fremling, C., Nugent, P., Horesh, A., Mooley, K., Rumsey, C., Cenko, S., Graham, M., Perley, D., Nakar, E., Shaviv, N., Bromberg, O., Shen, K., Ofek, E., Cao, Y., Wang, X., Huang, F., Rui, L., Zhang, T., Li, W., Li, Z., Zhang, J., Valenti, S., Guevel, D., Shappee, B., Kochanek, C., Holoien, T., Filippenko, A., Fender, R., Nyholm, A., Yaron, O., Kasliwal, M., Sullivan, M., Blagorodnova, N., Walters, R., Lunnan, R., Khazov, D., Andreoni, I., Laher, R., Konidaris, N., Woźniak, P., and Bue, B. (2017). Energetic eruptions leading to a peculiar hydrogen-rich explosion of a massive star. *Nature*, 551:210–213.

Arnould, M., Goriely, S., and Jorissen, A. (1999). Non-explosive hydrogen and helium burnings: abundance predictions from the NACRE reaction rate compilation. , 347:572–582.

Ashman, K. M. and Zepf, S. E. (2008). Globular cluster systems. *Globular Cluster Systems*.

Asplund, M., Grevesse, N., and Sauval, A. J. (2005). The Solar Chemical Composition. In Barnes, Thomas G., I. and Bash, F. N., editors, *Cosmic Abundances as Records of Stellar Evolution and Nucleosynthesis*, volume 336 of *Astronomical Society of the Pacific Conference Series*, page 25.

Bajkova, A. T., Smirnov, A. A., and Bobylev, V. V. (2023). The Influence of the Bar on the Dynamics of Globular Clusters in the Central Region of the Milky Way. Frequency Analysis of Orbits According to Gaia EDR3 Data. *Astrophysical Bulletin*, 78(4):499–513.

Barbuy, B., Chiappini, C., and Gerhard, O. (2018). Chemodynamical history of the galactic bulge. *Annual Review of Astronomy and Astrophysics*, 56(1):223–276.

Bastian, N., Cabrera-Ziri, I., and Salaris, M. (2015). A general abundance problem for all self-enrichment scenarios for the origin of multiple populations in globular clusters. , 449(3):3333–3346.

Bastian, N., Lamers, H. J. G. L. M., de Mink, S. E., Longmore, S. N., Goodwin, S. P., and Gieles, M. (2013). Early disc accretion as the origin of abundance anomalies in globular clusters. , 436(3):2398–2411.

Bastian, N. and Lardo, C. (2013). Multiple populations and extended main sequence turn-offs in globular clusters: A problem solved? *Monthly Notices of the Royal Astronomical Society*, 435(1):327–345.

Bastian, N. and Lardo, C. (2018). Multiple stellar populations in globular clusters. *Annual Review of Astronomy and Astrophysics*, 56(1):83–136.

Baumgardt, H. and Vasiliev, E. (2021). Accurate distances to Galactic globular clusters through a combination of Gaia EDR3, HST, and literature data. , 505(4):5957–5977.

Beccari, G. and Carraro, G. (2014). Introduction to the theory of stellar evolution. pages 1–16.

Bekki, K. (2016). Formation of multiple stellar populations in globular clusters: correlations between chemical and kinematic properties. *Monthly Notices of the Royal Astronomical Society*, 460(1):L135–L139.

Bekki, K. (2017). Globular cluster formation with multiple stellar populations from hierarchical star cluster complexes. , 467(2):1857–1873.

Bekki, K. and Tsujimoto, T. (2017). Formation of globular clusters with internal abundance spreads in r-process elements: Strong evidence for prolonged star formation. *The Astrophysical Journal*, 844(1):34.

Belokurov, V., Evans, N. W., Irwin, M. J., Lynden-Bell, D., Yanny, B., Vidrih, S., Gilmore, G., Seabroke, G., Zucker, D. B., Wilkinson, M. I., Hewett, P. C., Bramich, D. M., Fellhauer, M., Newberg, H. J., Wyse, R. F. G., Beers, T. C., Bell, E. F., Barentine, J. C., Brinkmann, J., Cole, N., Pan, K., and York, D. G. (2007). An Orphan in the "Field of Streams". , 658(1):337–344.

Bica, E., Bonatto, C., Barbuy, B., and Ortolani, S. (2006). Globular cluster system and Milky Way properties revisited. , 450(1):105–115.

Bica, E., Ortolani, S., and Barbuy, B. (2016). Globular clusters in the galactic bulge. *Publications of the Astronomical Society of Australia*, 33:e028.

Bica, E. L. and Pastoriza, M. G. (1983). Ddo integrated photometry of globular clusters and initial chemical evolution of the galaxy. *Astrophysics and Space Science*, 91:99–123.

Binney, J. and Wong, L. K. (2017). Modelling the milky way's globular cluster system. *Monthly Notices of the Royal Astronomical Society*, 467(2):2446–2457.

Bland-Hawthorn, J. and Freeman, K. (2010). The chemical enrichment of the galactic halo. *Publications of the Astronomical Society of Australia*, 27:27–40.

Blanton, M. R. et al. (2017). Sloan digital sky survey iv: Mapping the milky way, nearby galaxies, and the distant universe. *The Astronomical Journal*, 154:28. doi:10.3847/1538-3881/aa7567.

Bowen, I. S. and Vaughan, A. H. (1973). The optical design of the carnegie image tube spectrograph. *Applied Optics*, 12:1430. doi:10.1364/AO.12.001430.

Busso, M., G. R. and Wasserburg, G. J. (1999). Nucleosynthesis in asymptotic giant branch stars: Relevance for galactic enrichment and solar system formation. *Annual Review of Astronomy and Astrophysics*, 37:239–309.

Caloi, V. and D'Antona, F. (2005). Helium self-enrichment in globular clusters and the second parameter problem in m 3 and m 13. *Astronomy & Astrophysics*, 435(3):987–993.

Campbell, S., D'Orazi, V., Yong, D., Constantino, T., Lattanzio, J., Stancliffe, R., Angelou, G., Boer, E., and Grundahl, F. (2013). Sodium content as a predictor of the advanced evolution of globular cluster stars. *Nature*, 498:198–200.

Cantiello, M., Langer, N., Brott, I., de Koter, A., Shore, S. N., Vink, J., Voegler, A., and Yoon, S. C. (2008). On the origin of microturbulence in hot stars.

Cardelli, J. A., Clayton, G. C., and Mathis, J. S. (1989). The Relationship between Infrared, Optical, and Ultraviolet Extinction. , 345:245.

Carretta, E. (2014). Three Discrete Groups with Homogeneous Chemistry along the Red Giant Branch in the Globular Cluster NGC 2808. , 795(2):L28.

Carretta, E., Bragaglia, A., Gratton, R., D'Orazi, V., and Lucatello, S. (2009). Intrinsic iron spread and a new metallicity scale for globular clusters. , 508(2):695–706.

Carretta, E., Bragaglia, A., Gratton, R., and Lucatello, S. (2009a). Na-o anticorrelation and hb-viii. proton-capture elements and metallicities in 17 globular clusters from uves spectra. *Astronomy & Astrophysics*, 505(1):139–155.

Carretta, E., Bragaglia, A., Gratton, R. G., Lucatello, S., Bellazzini, M., Catanzaro, G., Leone, F., Momany, Y., Piotto, G., and D'Orazi, V. (2010). Detailed abundances of a large sample of giant stars in M 54 and in the Sagittarius nucleus. , 520:A95.

Carretta, E., Bragaglia, A., Gratton, R. G., Lucatello, S., Catanzaro, G., and Leone, F. (2009b). The na-o anticorrelation in horizontal branch stars. i. ngc 2808. *Astronomy & Astrophysics*, 505(1):139–152.

Carretta, E., Bragaglia, A., Gratton, R. G., Lucatello, S., Catanzaro, G., Leone, F., Bellazzini, M., Claudi, R., D'Orazi, V., Momany, Y., Ortolani, S., Pancino, E., Piotto, G., Recio-Blanco, A., and Sabbi, E. (2009). Na-O anticorrelation and HB. VII. The chemical composition of first and second-generation stars in 15 globular clusters from GIRAFFE spectra. , 505(1):117–138.

Carretta, E., Bragaglia, A., Gratton, R. G., Lucatello, S., and D'Orazi, V. (2011). Na-o anticorrelation and hb. vi. the chemical composition of the peculiar bulge globular cluster ngc 6441. *Astronomy & Astrophysics*, 533:A69.

Carretta, E., D'Orazi, V., Gratton, R. G., and Lucatello, S. (2012). Aluminum abundances of multiple stellar generations in the globular cluster NGC 1851. , 543:A117.

Carretta, E., Gratton, R. G., Sneden, C., and Bragaglia, A. (1999). First Dredge-up and Further Mixing Mechanisms Along the red Giant Branch in Field Stars. , 265:189–190.

Catchpole, R. M., Whitelock, P. A., Feast, M. W., Hughes, S. M., Irwin, M., and Alard, C. (2016). The age and structure of the galactic bulge from mira variables. *Monthly Notices of the Royal Astronomical Society*, 455(2):2216–2227.

Cattaneo, A., Mamon, G. A., Warnick, K., and Knebe, A. (2011). How do galaxies acquire their mass? *Astronomy & Astrophysics*, 533:A5.

Cescutti, G., Romano, D., Matteucci, F., Chiappini, C., and Hirschi, R. (2018). The role of agb stars in the formation of multiple populations in globular clusters. *Astronomy & Astrophysics*, 618:A56.

Chantereau, W., Charbonnel, C., and Meynet, G. (2016). Evolution of long-lived globular cluster stars. III. Effect of the initial helium spread on the position of stars in a synthetic Hertzsprung-Russell diagram. , 592:A111.

Charbonnel, C. (2016). Multiple Stellar Populations and Their Evolution in Globular Clusters: A Nucleosynthesis Perspective. In *EAS Publications Series*, volume 80-81 of *EAS Publications Series*, pages 177–226.

Ciddor, P. E. (1996). Refractive index of air: new equations for the visible and near infrared. , 35(9):1566.

Clarkson, W., Sahu, K., Anderson, J., Rich, R., Smith, T., Brown, T., Bond, H., Livio, M., Minniti, D., Renzini, A., et al. (2008). The initial mass function of the central parsec of the galaxy: Disentangling stellar populations with proper motions. *The Astrophysical Journal*, 684:1110–1142.

Conroy, C. and Spergel, D. N. (2011). On the Formation of Multiple Stellar Populations in Globular Clusters. , 726(1):36.

Cottrell, P. L. and Da Costa, G. S. (1981). Correlated cyanogen and sodium anomalies in the globular clusters 47 TUC and NGC 6752. , 245:L79–L82.

Cunha, K. et al. (2017). The abundances of potassium, copper, and zinc in apogee red giants: Diverse nucleosynthetic origins. *The Astronomical Journal*.

Cunha, K. and Smith, V. (2007). Abundances of red giants in baade's window: The primordial, present-day bulge. *The Astrophysical Journal*, 626:425–434.

Da Costa, G. S., Held, E. V., Saviane, I., and Gullieuszik, M. (2009). M22: An [Fe/H] Abundance Range Revealed. , 705(2):1481–1491.

D'Antona, F., Caloi, V., and Mazzitelli, I. (2002). The role of super-agb stars in the formation of multiple populations in globular clusters. *The Astrophysical Journal*, 564(1):L93.

D'Antona, F. e. a. (2016). The evolution of multiple stellar populations. *Monthly Notices of the Royal Astronomical Society*, 458:2122–2138.

De Angeli, F., Piotto, G., Cassisi, S., Busso, G., Recio-Blanco, A., Salaris, M., Aparicio, A., and Rosenberg, A. (2005). Galactic globular cluster relative ages. *The Astronomical Journal*, 130(1):116–125.

de Mink, S. E., Pols, O. R., Langer, N., and Izzard, R. G. (2009a). Massive binaries as the source of abundance anomalies in globular clusters. *Astronomy amp; Astrophysics*, 507(1):L1–L4.

de Mink, S. E., Pols, O. R., Langer, N., and Izzard, R. G. (2009b). The origin of the chemical peculiarities in he-rich hot subdwarf stars: The effects of binary evolution and thermohaline mixing. *Astronomy & Astrophysics*, 507(2):L1–L4.

Decressin, T., Meynet, G., Charbonnel, C., Prantzos, N., and Ekström, S. (2007). Fast rotating massive stars and the origin of the abundance patterns in galactic globular clusters. , 464(3):1029–1044.

Decressin, T., Meynet, G., Charbonnel, C., Prantzos, N., and Ekström, S. (2007). Fast rotating massive stars and the origin of the abundance patterns in galactic globular clusters. *Astronomy & Astrophysics*, 464(3):1029–1044.

Denisenkov, P. A. and Denisenkova, S. N. (1990). Correlation Between the Abundances of NA and the CNO Elements in Red Giants in Omega-Centauri. *Soviet Astronomy Letters*, 16:275.

Denissenkov, P. A. and Hartwick, F. D. A. (2014). Supermassive stars as a source of abundance anomalies of proton-capture elements in globular clusters. , 437(1):L21–L25.

Denissenkov, P. A. and Herwig, F. (2003). The Abundance Evolution of Oxygen, Sodium, and Magnesium in Extremely Metal Poor Intermediate-Mass Stars: Implications for the Self-Pollution Scenario in Globular Clusters. , 590(2):L99–L102.

Denissenkov, P. A., Pinsonneault, M., and Terndrup, D. M. (2006). Fluorine abundance variations as a signature of enhanced extra mixing in red giants of the globular cluster m4. *The Astrophysical Journal*, 651(1):438–443.

Depalo, R. (2015). The neon-sodium cycle: Study of the 22ne(p,gamma)23na reaction at astrophysical energies.

D'Ercole, A., Vesperini, E., D'Antona, F., McMillan, S. L. W., and Recchi, S. (2008). Formation and dynamical evolution of multiple stellar generations in globular clusters. , 391(2):825–843.

Dondoglio, E., Milone, A. P., Lagioia, E. P., Marino, A. F., Tailo, M., Cordoni, G., Jang, S., and Carlos, M. (2021). Multiple Stellar Populations along the Red Horizontal Branch and Red Clump of Globular Clusters. , 906(2):76.

Douglas, S. (2024). Constraining stellar rotation at the zero-age main sequence with tess. *The Astrophysical Journal*, 962:16.

Eisenstein, D. J. et al. (2011). Sdss-iii: Massive spectroscopic surveys of the distant universe, the milky way, and extra-solar planetary systems. *The Astronomical Journal*, 142:72. doi:10.1088/0004-6256/142/3/72.

Elmegreen, B. G. (2000). Star formation in a crossing time. *Astrophysical Journal*, 530:277–281.

Fattahi, A., Deason, A. J., Frenk, C. S., Simpson, C. M., Gómez, F. A., Grand, R. J. J., Monachesi, A., Marinacci, F., and Pakmor, R. (2020). A tale of two populations: surviving and destroyed dwarf galaxies and the build-up of the Milky Way's stellar halo. , 497(4):4459–4471.

Fernández-Trincado, J. G., Beers, T. C., Barbuy, B., Mészáros, S., Minniti, D., Smith, V. V., Cunha, K., Villanova, S., Geisler, D., Majewski, S. R., Carigi, L., Tang, B., Moni Bidin, C., and Vieira, K. (2021). APOGEE-2S Discovery of Light- and Heavy-element Abundance Correlations in the Bulge Globular Cluster NGC 6380. , 918(1):L9.

Fernández-Trincado, J. G., Villanova, S., Geisler, D., Barbuy, B., Minniti, D., Beers, T. C., Mészáros, S., Tang, B., Cohen, R. E., Moni Bidin, C., Garro, E. R., Baeza, I., and Muñoz, C. (2022). CAPOS: The bulge Cluster APOgee Survey. III. Spectroscopic tomography of Tonantzintla 2. , 658:A116.

Ferraro, F. R., Dalessandro, E., Mucciarelli, A., Beccari, G., Rich, R. M., Origlia, L., Lanzoni, B., Rood, R. T., Valenti, E., Bellazzini, M., et al. (2009a). Terzan 5: The complex chemical evolution of the galactic bulge revealed by a cluster. *Nature*, 462(7274):483–486.

Ferraro, F. R., Dalessandro, E., Mucciarelli, A., Beccari, G., Rich, R. M., Origlia, L., Lanzoni, B., Rood, R. T., Valenti, E., Bellazzini, M., Ransom, S. M., and Cocozza, G. (2009b). The cluster terzan 5 as a remnant of a primordial building block of the galactic bulge. *Nature*, 462(7272):483–486.

Fields, B., Molaro, P., and Sarkar, S. (2014). Big-bang nucleosynthesis.

Forbes, D. A., Masters, K. L., Minniti, D., and Barmby, P. (2000). The elliptical galaxy formerly known as the Local Group: merging the globular cluster systems. , 358:471–480.

Gaia Collaboration, Prusti, T., de Bruijne, J. H. J., Brown, A. G. A., Vallenari, A., Babusiaux, C., Bailer-Jones, C. A. L., Bastian, U., Biermann, M., Evans, D. W., Eyer, L., Jansen, F., Jordi, C., Klioner, S. A., Lammers, U., Lindegren, L., Luri, X., Mignard, F., Milligan, D. J., Panem, C., Poinsignon, V., Pourbaix, D., Randich, S., Sarri, G., Sartoretti, P., Siddiqui, H. I., Soubiran, C., Valette, V., van Leeuwen, F., Walton, N. A., Aerts, C., Arenou, F., Cropper, M., Drimmel, R., Høg, E., Katz, D., Lattanzi, M. G., O'Mullane, W., Grebel, E. K., Holland, A. D., Huc, C., Passot, X., Bramante, L., Cacciari, C., Castañeda, J., Chaoul, L., Cheek, N., De Angeli, F., Fabricius, C., Guerra, R., Hernández, J., Jean-Antoine-Piccolo, A., Masana, E., Messineo, R., Mowlavi, N., Nienartowicz, K., Ordóñez-Blanco, D., Panuzzo, P., Portell, J., Richards, P. J., Riello, M., Seabroke, G. M., Tanga, P., Thévenin, F., Torra, J., Els, S. G., Gracia-Abril, G., Comoretto, G., Garcia-Reinaldos, M., Lock, T., Mercier, E., Altmann, M., Andrae, R., Astraatmadja, T. L., Bellas-Velidis, I., Benson, K., Berthier, J., Blomme, R., Busso, G., Carry, B., Cellino, A., Clementini, G., Cowell, S., Creevey, O., Cuypers, J., Davidson, M., De Ridder, J., de Torres, A., Delchambre, L., Dell'Oro, A., Ducourant, C., Frémat, Y., García-Torres, M., Gosset, E., Halbwachs, J. L., Hambly, N. C., Harrison, D. L., Hauser, M., Hestroffer, D., Hodgkin, S. T., Huckle, H. E., Hutton, A., Jasniewicz, G., Jordan, S., Kontizas, M., Korn, A. J., Lanzafame, A. C., Manteiga, M., Moitinho, A., Muinonen, K., Osinde, J., Pancino, E., Pauwels, T., Petit, J. M., Recio-Blanco, A., Robin, A. C., Sarro, L. M., Siopis, C., Smith, M., Smith, K. W., Sozzetti, A., Thuillot, W., van Reeven, W., Viala, Y., Abbas, U., Abreu Aramburu, A., Accart, S., Aguado, J. J., Allan, P. M., Allasia, W., Altavilla, G., Álvarez, M. A., Alves, J., Anderson, R. I., Andrei, A. H., Anglada Varela, E., Antiche, E., Antoja, T., Antón, S., Arcay, B., Atzei, A., Ayache, L., Bach, N., Baker, S. G., Balaguer-Núñez, L., Barache, C., Barata, C., Barbier, A., Barblan, F., Baroni, M., Barrado y Navascués, D., Barros, M., Barstow, M. A., Becciani, U., Bellazzini, M., Bellei, G., Bello García, A., Belokurov, V., Bendjoya, P., Berihuete, A., Bianchi, L., Bienaymé, O., Billebaud, F., Blagorodnova, N., Blanco-Cuaresma, S., Boch, T., Bombrun, A., Borrachero, R., Bouquillon, S., Bourda, G., Bouy, H., Bragaglia, A., Breddels, M. A., Brouillet, N., Brüsemeister, T., Bucciarelli, B., Budnik, F., Burgess, P., Burgon, R., Burlacu, A., Busonero, D., Buzzi, R., Caffau, E., Cambras, J., Campbell, H., Cancelliere, R., Cantat-Gaudin, T., Carlucci, T., Carrasco, J. M., Castellani, M., Charlot, P., Charnas, J., Charvet, P., Chassat, F., Chiavassa, A., Clotet, M., Cocozza, G., Collins, R. S., Collins, P., Costigan, G., Crifo, F., Cross, N. J. G., Crosta, M., Crowley, C., Dafonte, C., Damerdji, Y., Dapergolas, A., David, P., David, M., De Cat, P., de Felice, F., de Laverny, P., De Luise, F., De March, R., de Martino, D., de Souza, R., Debosscher, J., del Pozo, E., Delbo, M., Delgado, A., Delgado, H. E., di

Marco, F., Di Matteo, P., Diakite, S., Distefano, E., Dolding, C., Dos Anjos, S., Drazinos, P., Durán, J., Dzigan, Y., Ecale, E., Edvardsson, B., Enke, H., Erdmann, M., Escolar, D., Espina, M., Evans, N. W., Eynard Bontemps, G., Fabre, C., Fabrizio, M., Faigler, S., Falcão, A. J., Farràs Casas, M., Faye, F., Federici, L., Fedorets, G., Fernández-Hernández, J., Fernique, P., Fienga, A., Figueras, F., Filippi, F., Findeisen, K., Fonti, A., Fouesneau, M., Fraile, E., Fraser, M., Fuchs, J., Furnell, R., Gai, M., Galleti, S., Galluccio, L., Garabato, D., García-Sedano, F., Garé, P., Garofalo, A., Garralda, N., Gavras, P., Gerssen, J., Geyer, R., Gilmore, G., Girona, S., Giuffrida, G., Gomes, M., González-Marcos, A., González-Núñez, J., González-Vidal, J. J., Granvik, M., Guerrier, A., Guillout, P., Guiraud, J., Gúrpide, A., Gutiérrez-Sánchez, R., Guy, L. P., Haigron, R., Hatzidimitriou, D., Haywood, M., Heiter, U., Helmi, A., Hobbs, D., Hofmann, W., Holl, B., Holland, G., Hunt, J. A. S., Hypki, A., Icardi, V., Irwin, M., Jevardat de Fombelle, G., Jofré, P., Jonker, P. G., Jorissen, A., Julbe, F., Karampelas, A., Kochoska, A., Kohley, R., Kolenberg, K., Kontizas, E., Koposov, S. E., Kordopatis, G., Koubsky, P., Kowalczyk, A., Krone-Martins, A., Kudryashova, M., Kull, I., Bachchan, R. K., Lacoste-Seris, F., Lanza, A. F., Lavigne, J. B., Le Poncin-Lafitte, C., Lebreton, Y., Lebzelter, T., Leccia, S., Leclerc, N., Lecoeur-Taibi, I., Lemaitre, V., Lenhardt, H., Leroux, F., Liao, S., Licata, E., Lindstrøm, H. E. P., Lister, T. A., Livanou, E., Lobel, A., Löffler, W., López, M., Lopez-Lozano, A., Lorenz, D., Loureiro, T., MacDonald, I., Magalhães Fernandes, T., Managau, S., Mann, R. G., Mantelet, G., Marchal, O., Marchant, J. M., Marconi, M., Marie, J., Marinoni, S., Marrese, P. M., Marschalkó, G., Marshall, D. J., Martín-Fleitas, J. M., Martino, M., Mary, N., Matijevič, G., Mazeh, T., McMillan, P. J., Messina, S., Mestre, A., Michalik, D., Millar, N. R., Miranda, B. M. H., Molina, D., Molinaro, R., Molinaro, M., Molnár, L., Moniez, M., Montegriffo, P., Monteiro, D., Mor, R., Mora, A., Morbidelli, R., Morel, T., Morgenthaler, S., Morley, T., Morris, D., Mulone, A. F., Muraveva, T., Musella, I., Narbonne, J., Nelemans, G., Nicastro, L., Noval, L., Ordénovic, C., Ordieres-Meré, J., Osborne, P., Pagani, C., Pagano, I., Pailler, F., Palacin, H., Palaversa, L., Parsons, P., Paulsen, T., Pecoraro, M., Pedrosa, R., Pentikäinen, H., Pereira, J., Pichon, B., Piersimoni, A. M., Pineau, F. X., Plachy, E., Plum, G., Poujoulet, E., Prša, A., Pulone, L., Ragaini, S., Rago, S., Rambaux, N., Ramos-Lerate, M., Ranalli, P., Rauw, G., Read, A., Regibo, S., Renk, F., Reylé, C., Ribeiro, R. A., Rimoldini, L., Ripepi, V., Riva, A., Rixon, G., Roelens, M., Romero-Gómez, M., Rowell, N., Royer, F., Rudolph, A., Ruiz-Dern, L., Sadowski, G., Sagristà Sellés, T., Sahlmann, J., Salgado, J., Salguero, E., Sarasso, M., Savietto, H., Schnorhk, A., Schultheis, M., Sciacca, E., Segol, M., Segovia, J. C., Segransan, D., Serpell, E., Shih, I. C., Smareglia, R., Smart, R. L., Smith, C., Solano, E., Solitro, F., Sordo, R., Soria Nieto, S., Souchay, J., Spagna, A., Spoto, F., Stampa, U., Steele, I. A., Steidelmüller, H., Stephenson, C. A., Stoev, H., Suess, F. F., Süveges, M., Surdej, J., Szabados, L., Szegedi-Elek, E., Tapiador, D., Taris, F., Tauran, G., Taylor, M. B., Teixeira, R., Terrett, D., Tingley, B., Trager, S. C., Turon, C., Ulla, A., Utrilla, E., Valentini, G., van Elteren, A., Van Hemelryck, E., van Leeuwen, M., Varadi, M., Vecchiato, A., Veljanoski, J., Via, T., Vicente, D., Vogt, S., Voss, H., Votruba, V., Voutsinas, S., Walmsley, G., Weiler, M., Weingrill, K., Werner, D., Wevers, T., Whitehead, G., Wyrzykowski, Ł., Yoldas, A., Žerjal, M., Zucker, S., Zurbach, C., Zwitter, T., Alecu, A., Allen, M., Allende Prieto, C., Amorim, A., Anglada-Escudé, G., Arsenijevic, V., Azaz, S., Balm, P., Beck, M., Bernstein, H. H., Bigot, L., Bijaoui, A., Blasco, C., Bonfigli, M., Bono, G., Boudreault, S., Bressan, A., Brown, S., Brunet, P. M., Bunclark, P., Buonanno, R., Butkevich, A. G., Carret, C., Carrion, C., Chemin, L., Chéreau, F., Corcione, L., Darmigny, E., de Boer, K. S., de Teodoro, P., de Zeeuw, P. T., Delle Luche, C., Domingues, C. D., Dubath, P., Fodor, F., Frézouls, B., Fries, A., Fustes, D., Fyfe, D., Gallardo, E., Gallegos, J., Gardiol, D., Gebran, M., Gomboc, A., Gómez, A., Grux, E., Gueguen, A., Heyrovsky, A., Hoar, J., Iannicola, G., Isasi Parache, Y., Janotto, A. M., Joliet, E., Jonckheere, A., Keil, R., Kim, D. W., Klagyivik, P., Klar, J., Knude, J., Kochukhov, O., Kolka, I., Kos, J., Kutka, A., Lainey, V., LeBouquin, D., Liu, C., Loreggia, D., Makarov, V. V., Marseille, M. G., Martayan, C., Martinez-Rubi, O., Massart, B., Meynadier, F., Mignot, S., Munari, U., Nguyen, A. T., Nordlander, T., Ocvirk, P., O'Flaherty, K. S., Olias Sanz, A., Ortiz, P., Osorio, J., Oszkiewicz, D., Ouzounis, A., Palmer, M., Park, P., Pasquato, E., Peltzer, C., Peralta, J., Péturaud, F., Pieniluoma, T., Pigozzi, E., Poels, J., Prat, G., Prod'homme, T., Raison, F., Rebordao, J. M., Risquez, D., Rocca-Volmerange, B., Rosen, S., Ruiz-Fuertes, M. I., Russo, F., Sembay, S., Serraller Vizcaino, I., Short, A., Siebert, A., Silva, H., Sinachopoulos, D., Slezak, E., Soffel, M., Sosnowska, D., Straižys, V., ter Linden, M., Terrell, D., Theil, S., Tiede, C., Troisi, L., Tsalmantza, P., Tur, D., Vaccari, M., Vachier, F., Valles, P., Van Hamme, W., Veltz, L., Virtanen, J., Wallut, J. M., Wichmann, R., Wilkinson, M. I., Ziaeepour, H., and Zschocke, S. (2016). The Gaia mission. , 595:A1.

Gaia Collaboration, Vallenari, A., Brown, A. G. A., Prusti, T., de Bruijne, J. H. J., Arenou, F., Babusiaux, C., Biermann, M., Creevey, O. L., Ducourant, C., Evans, D. W., Eyer, L., Guerra, R., Hutton, A., Jordi, C., Klioner, S. A., Lammers, U. L., Lindegren, L., Luri, X., Mignard, F., Panem, C., Pourbaix, D., Randich, S., Sartoretti, P., Soubiran, C., Tanga, P., Walton, N. A., Bailer-Jones, C. A. L., Bastian, U., Drimmel, R., Jansen, F., Katz, D., Lattanzi, M. G., van Leeuwen, F., Bakker, J., Cacciari, C., Castañeda, J., De Angeli, F., Fabricius, C., Fouesneau, M., Frémat, Y., Galluccio, L., Guerrier, A., Heiter, U., Masana, E., Messineo, R., Mowlavi, N., Nicolas, C., Nienartowicz, K., Pailler, F., Panuzzo, P., Riclet, F., Roux, W., Seabroke, G. M., Sordo, R., Thévenin, F., Gracia-Abril, G., Portell, J., Teyssier, D., Altmann, M., Andrae, R., Audard, M., Bellas-Velidis, I., Benson, K., Berthier, J., Blomme, R., Burgess, P. W., Busonero, D., Busso, G., Cánovas, H., Carry, B., Cellino, A., Cheek, N., Clementini, G., Damerdji, Y., Davidson, M., de Teodoro, P., Nuñez Campos, M., Delchambre, L., Dell'Oro, A., Esquej, P., Fernández-Hernández, J., Fraile, E., Garabato, D., García-Lario, P., Gosset, E., Haigron, R., Halbwachs, J. L., Hambly, N. C., Harrison, D. L., Hernández, J., Hestroffer, D., Hodgkin, S. T., Holl, B., Janßen, K., Jevardat de Fombelle, G., Jordan, S., Krone-Martins, A., Lanzafame, A. C., Löffler, W., Marchal, O., Marrese, P. M., Moitinho, A., Muinonen, K., Osborne, P., Pancino, E., Pauwels, T., Recio-Blanco, A., Reylé, C., Riello, M., Rimoldini, L., Roegiers, T., Rybizki, J., Sarro, L. M., Siopis, C., Smith, M., Sozzetti, A., Utrilla, E., van Leeuwen, M., Abbas, U., Ábrahám, P., Abreu Aramburu, A., Aerts, C., Aguado, J. J., Ajaj, M., Aldea-Montero, F., Altavilla, G., Álvarez, M. A., Alves, J., Anders, F., Anderson, R. I., Anglada Varela, E., Antoja, T., Baines, D., Baker, S. G., Balaguer-Núñez, L., Balbinot, E., Balog, Z., Barache, C., Barbato, D., Barros, M., Barstow, M. A., Bartolomé, S., Bassilana, J. L., Bauchet, N., Becciani, U., Bellazzini, M., Berihuete, A., Bernet, M., Bertone, S., Bianchi, L., Binnenfeld, A., Blanco-Cuaresma, S., Blazere, A., Boch, T., Bombrun, A., Bossini, D., Bouquillon, S., Bragaglia, A., Bramante, L., Breedt, E., Bressan, A., Brouillet, N., Brugaletta, E., Bucciarelli, B., Burlacu, A., Butkevich, A. G., Buzzi, R., Caffau, E., Cancelliere, R., Cantat-Gaudin, T., Carballo, R., Carlucci, T., Carnerero, M. I., Carrasco, J. M., Casamiquela, L., Castellani, M., Castro-Ginard, A., Chaoul, L., Charlot, P., Chemin, L., Chiaramida, V., Chiavassa, A., Chornay, N., Comoretto, G., Contursi, G., Cooper, W. J., Cornez, T., Cowell, S., Crifo, F., Cropper, M., Crosta, M., Crowley, C., Dafonte, C., Dapergolas, A., David, M., David, P., de Laverny, P., De Luise, F., De March, R., De Ridder, J., de Souza, R., de Torres, A., del Peloso, E. F., del Pozo, E., Delbo, M., Delgado, A., Delisle, J. B., Demouchy, C., Dharmawardena, T. E., Di Matteo, P., Diakite, S., Diener, C., Distefano, E., Dolding, C., Edvardsson, B., Enke, H., Fabre, C., Fabrizio, M., Faigler, S., Fedorets, G., Fernique, P., Fienga, A., Figueras, F., Fournier, Y., Fouron, C., Fragkoudi, F., Gai, M., Garcia-Gutierrez, A., Garcia-Reinaldos, M., García-Torres, M., Garofalo, A., Gavel, A., Gavras, P., Gerlach, E., Geyer, R., Giacobbe, P., Gilmore, G., Girona, S., Giuffrida, G., Gomel, R., Gomez, A., González-Núñez, J., González-Santamaría, I., González-Vidal, J. J., Granvik, M., Guillout, P., Guiraud, J., Gutiérrez-Sánchez, R., Guy, L. P., Hatzidimitriou, D., Hauser, M., Haywood, M., Helmer, A., Helmi, A., Sarmiento, M. H., Hidalgo, S. L., Hilger, T., Hładczuk, N., Hobbs, D., Holland, G., Huckle, H. E., Jardine, K., Jasniewicz, G., Jean-Antoine Piccolo, A., Jiménez-Arranz, Ó., Jorissen, A., Juaristi Campillo, J., Julbe, F., Karbevska, L., Kervella, P., Khanna, S., Kontizas, M., Kordopatis, G., Korn, A. J., Kóspál, Á., Kostrzewa-Rutkowska, Z., Kruszyńska, K., Kun, M., Laizeau, P., Lambert, S., Lanza, A. F., Lasne, Y., Le Campion, J. F., Lebreton, Y., Lebzelter, T., Leccia, S., Leclerc, N., Lecoeur-Taibi, I., Liao, S., Licata, E. L., Lindstrøm, H. E. P., Lister, T. A., Livanou, E., Lobel, A., Lorca, A., Loup, C., Madrero Pardo, P., Magdaleno Romeo, A., Managau, S., Mann, R. G., Manteiga, M., Marchant, J. M., Marconi, M., Marcos, J., Marcos Santos, M. M. S., Marín Pina, D., Marinoni, S., Marocco, F., Marshall, D. J., Martin Polo, L., Martín-Fleitas, J. M., Marton, G., Mary, N., Masip, A., Massari, D., Mastrobuono-Battisti, A., Mazeh, T., McMillan, P. J., Messina, S., Michalik, D., Millar, N. R., Mints, A., Molina, D., Molinaro, R., Molnár, L., Monari, G., Monguió, M., Montegriffo, P., Montero, A., Mor, R., Mora, A., Morbidelli, R., Morel, T., Morris, D., Muraveva, T., Murphy, C. P., Musella, I., Nagy, Z., Noval, L., Ocaña, F., Ogden, A., Ordenovic, C., Osinde, J. O., Pagani, C., Pagano, I., Palaversa, L., Palicio,

P. A., Pallas-Quintela, L., Panahi, A., Payne-Wardenaar, S., Peñalosa Esteller, X., Penttilä, A., Pichon, B., Piersimoni, A. M., Pineau, F. X., Plachy, E., Plum, G., Poggio, E., Prša, A., Pulone, L., Racero, E., Ragaini, S., Rainer, M., Raiteri, C. M., Rambaux, N., Ramos, P., Ramos-Lerate, M., Re Fiorentin, P., Regibo, S., Richards, P. J., Rios Diaz, C., Ripepi, V., Riva, A., Rix, H. W., Rixon, G., Robichon, N., Robin, A. C., Robin, C., Roelens, M., Rogues, H. R. O., Rohrbasser, L., Romero-Gómez, M., Rowell, N., Royer, F., Ruz Mieres, D., Rybicki, K. A., Sadowski, G., Sáez Núñez, A., Sagristà Sellés, A., Sahlmann, J., Salguero, E., Samaras, N., Sanchez Gimenez, V., Sanna, N., Santoveña, R., Sarasso, M., Schultheis, M., Sciacca, E., Segol, M., Segovia, J. C., Ségransan, D., Semeux, D., Shahaf, S., Siddiqui, H. I., Siebert, A., Siltala, L., Silvelo, A., Slezak, E., Slezak, I., Smart, R. L., Snaith, O. N., Solano, E., Solitro, F., Souami, D., Souchay, J., Spagna, A., Spina, L., Spoto, F., Steele, I. A., Steidelmüller, H., Stephenson, C. A., Süveges, M., Surdej, J., Szabados, L., Szegedi-Elek, E., Taris, F., Taylor, M. B., Teixeira, R., Tolomei, L., Tonello, N., Torra, F., Torra, J., Torralba Elipe, G., Trabucchi, M., Tsounis, A. T., Turon, C., Ulla, A., Unger, N., Vaillant, M. V., van Dillen, E., van Reeven, W., Vanel, O., Vecchiato, A., Viala, Y., Vicente, D., Voutsinas, S., Weiler, M., Wevers, T., Wyrzykowski, Ł., Yoldas, A., Yvard, P., Zhao, H., Zorec, J., Zucker, S., and Zwitter, T. (2023). Gaia Data Release 3. Summary of the content and survey properties. , 674:A1.

Gaia Collaboration, Vallenari, A. e. a. (2022a). Gaia data release 3: Summary of the contents and survey properties. *Astronomy & Astrophysics*. doi:10.1051/0004-6361/202243940.

Gaia Collaboration, Brown, A. G. A. e. a. (2016). Gaia data release 1: Summary of the astrometric, photometric, and survey properties. *Astronomy & Astrophysics*. doi:10.1051/0004-6361/201629512.

Gaia Collaboration, Brown, A. G. A. e. a. (2018). Gaia data release 2: Summary of the contents and survey properties. *Astronomy & Astrophysics*. doi:10.1051/0004-6361/201833051.

Gaia Collaboration, Fabricius, C. e. a. (2022b). Gaia data release 3: Catalogue validation. *Astronomy & Astrophysics*. doi:10.1051/0004-6361/202243942.

García Pérez, A. E. et al. (2016a). Aspcap: The apogee stellar parameter and chemical abundances pipeline. *The Astronomical Journal*, 151:144. doi:10.3847/0004-6256/151/6/144.

García Pérez, A. E., Prieto, C. A., Holtzman, J. A., Shetrone, M., Mészáros, S., Bizyaev, D., Carrera, R., Cunha, K., García-Hernández, D. A., Johnson, J. A., Majewski, S. R., Nidever, D. L., Schiavon, R. P., Shane, N., Smith, V. V., Sobeck, J., Troup, N., Zamora, O., Weinberg, D. H., Bovy, J., Eisenstein, D. J., Feuillet, D., Frinchaboy, P. M., Hayden, M. R., Hearty, F. R., Nguyen, D. C., O'Connell, R. W., Pinsonneault, M. H., Wilson, J. C., and Zasowski, G. (2016b). Aspcap: The apogee stellar parameter and chemical abundances pipeline. *The Astronomical Journal*, 151(6):144.

Gautschy, A. and Saio, H. (1996). Stellar Pulsations Across the HR Diagram: Part 2. , 34:551–606.

Geisler, D., Villanova, S., et al. (2021). Capos: The bulge cluster apogee survey. i. overview and initial aspcap results. *Astronomy & Astrophysics*, 652. doi:10.1051/0004-6361/202140892.

Geisler, D., Villanova, S., O'Connell, J. E., Cohen, R. E., Moni Bidin, C., Fernández-Trincado, J. G., Muñoz, C., Minniti, D., Zoccali, M., Rojas-Arriagada, A., Contreras Ramos, R., Catelan, M., Mauro, F., Cortés, C., Ferreira Lopes, C. E., Arentsen, A., Starkenburg, E., Martin, N. F., Tang, B., Parisi, C., Alonso-García, J., Gran, F., Cunha, K., Smith, V., Majewski, S. R., Jönsson, H., García-Hernández, D. A., Horta, D., Mészáros, S., Monaco, L., Monachesi, A., Muñoz, R. R., Brownstein, J., Beers, T. C., Lane, R. R., Barbuy, B., Sobeck, J., Henao, L., González-Díaz, D., Miranda, R. E., Reinarz, Y., and Santander, T. A. (2021). CAPOS: The bulge Cluster APOgee Survey. I. Overview and initial ASPCAP results. , 652:A157.

Geisler, D., Villanova, S., O'Connell, J. E., Cohen, R. E., Moni Bidin, C., Fernández-Trincado, J. G., Muñoz, C., Minniti, D., Zoccali, M., Rojas-Arriagada, A., Contreras Ramos, R., Catelan, M., Mauro, F., Cortés, C., Ferreira Lopes, C. E., Arentsen, A., Starkenburg, E., Martin, N. F., Tang, B., Parisi, C., Alonso-García, J., Gran, F., Cunha, K., Smith, V., Majewski, S. R., Jönsson, H., García-Hernández, D. A., Horta, D., Mészáros, S., Monaco, L., Monachesi, A., Muñoz, R. R., Brownstein, J., Beers, T. C., Lane, R. R., Barbuy, B., Sobeck, J., Henao, L., González-Díaz, D., Miranda, R. E., Reinarz, Y., and Santander, T. A. (2021). Capos: The bulge cluster apogee survey: I. overview and initial aspcap results. *Astronomy amp; Astrophysics*, 652:A157.

Gontcharov, G. A., Bonatto, C. J., Ryutina, O. S., Savchenko, S. S., Mosenkov, A. V., Il'in, V. B., Khovritchev, M. Y., Marchuk, A. A., Poliakov, D. M., Smirnov, A. A., and Seguine, J. (2023). Isochrone fitting of Galactic globular clusters - V. NGC 6397 and NGC 6809 (M55). , 526(4):5628–5647.

Gontcharov, G. A., Khovritchev, M. Y., Mosenkov, A. V., Il'in, V. B., Marchuk, A. A., Savchenko, S. S., Smirnov, A. A., Usachev, P. A., and Poliakov, D. M. (2021). Isochrone fitting of Galactic globular clusters - III. NGC 288, NGC 362, and NGC 6218 (M12). , 508(2):2688–2705.

Gonzalez, G. and Wallerstein, G. (1998). Elemental Abundances in Giants in NGC 3201, a Globular Cluster with a Retrograde Orbit. , 116(2):765–781.

González-Díaz, D., Fernández-Trincado, J. G., Villanova, S., Geisler, D., Barbuy, B., Minniti, D., Beers, T. C., Moni Bidin, C., Mauro, F., Muñoz, C., Tang, B., Soto, M., Monachesi, A., Lane, R. R., and Frelijj, H. (2023). CAPOS: the bulge Cluster APOgee Survey IV elemental abundances of the bulge globular cluster NGC 6558. , 526(4):6274–6283.

Goodarzi, H., Mehrabi, A., Khosroshahi, H., and He, H. (2021). Flare activity and magnetic feature analysis of the flare stars. ii. subgiant branch. *The Astrophysical Journal*, 906:40.

Gouliermis, D., Dolphin, A., Brandner, W., and Henning, T. (2006). The star-forming region ngc 346 in the small magellanic cloud withhubble space telescopeacs observations. i. photometry. *The Astrophysical Journal Supplement Series*, 166:549–556.

Grand, R. J. J., Kawata, D., Belokurov, V., Deason, A. J., Fattahi, A., Fragkoudi, F., Gómez, F. A., Marinacci, F., and Pakmor, R. (2020). Sausage amp; mash: the dual origin of the galactic thick disc and halo from the gas-rich gaia-enceladus-sausage merger.

Gratton, R., Bonifacio, P., Bragaglia, A., Carretta, E., Castellani, V., Centurion, M., Chieffi, A., Claudi, R., Clementini, G., D'Antona, F., et al. (2001). The o-na and mg-al anticorrelations in turn-off and early subgiants in globular clusters. *Astronomy & Astrophysics*, 369(1):87–98.

Gratton, R., Carretta, E., and Bragaglia, A. (2012a). multiple populations in globular clusters. *The Astronomy and Astrophysics Review*, 20.

Gratton, R., Sneden, C., and Carretta, E. (2004). Abundance variations within globular clusters. *Annu. Rev. Astron. Astrophys.*, 42:385–440.

Gratton, R., Sneden, C., and Carretta, E. (2004). Abundance Variations Within Globular Clusters. , 42(1):385–440.

Gratton, R., Sneden, C., Carretta, E., and Bragaglia, A. (2000). Mixing along the red giant branch in metal-poor field stars. *Astronomy & Astrophysics*, 354:169–187.

Gratton, R., Sneden, C., Carretta, E., and Bragaglia, A. (2004). Abundances for metal-poor stars with detailed analysis of the neutral hydrogen lines. ii. analysis of halo stars. *Annual Review of Astronomy and Astrophysics*, 42:385–440.

Gratton, R. G., Carretta, E., and Bragaglia, A. (2012b). Multiple populations in globular clusters: Lessons learned from the milky way globular clusters. *The Astronomy and Astrophysics Review*, 20:1–49.

Gratton, R. G., Carretta, E., and Bragaglia, A. (2012). Multiple populations in globular clusters. Lessons learned from the Milky Way globular clusters. , 20:50.

Gratton, R. G. e. a. (2019). Formation of multiple populations in globular clusters. *Nature Astronomy*, 3:539–552.

Grevesse, N., Scott, P., Asplund, M., and Sauval, A. J. (2015). The elemental composition of the Sun. III. The heavy elements Cu to Th. , 573:A27.

Gruyters, P., Casagrande, L., Milone, A., Hodgkin, S., Serenelli, A., and Feltzing, S. (2017). First evidence of multiple populations along the agb from strömgren photometry. *Astronomy and Astrophysics*, 603:A37.

Gustafsson, B., Edvardsson, B., Eriksson, K., Jørgensen, U. G., Nordlund, Å., and Plez, B. (2008). A grid of MARCS model atmospheres for late-type stars. I. Methods and general properties. , 486(3):951–970.

Hansen, B. (1998). Old and blue white-dwarf stars as a detectable source of microlensing events. *Nature*, 394:860–862.

Harris, W. E. (2010). A New Catalog of Globular Clusters in the Milky Way. *arXiv e-prints*, page arXiv:1012.3224.

Harris, W. E. (2010). A new catalog of globular clusters in the milky way.

Hasselquist, S. et al. (2016). Chemical cartography with apogee: Metallicity distribution functions and the chemical structure of the milky way disk. *The Astrophysical Journal*, 833:81. doi:10.3847/1538-4357/833/1/81.

Heasley, J. and Mengel, J. (1972). An estimate of stellar wind mass loss during the red giant phase of evolution. *The Observatory, Vol. 92, p. 93-96 (1972)*, 92:93–96.

Helmi, A., White, S. D. M., de Zeeuw, P. T., and Zhao, H. (1999). Debris streams in the solar neighbourhood as relicts from the formation of the Milky Way. , 402(6757):53–55.

Henyey, L., Vardya, M. S., and Bodenheimer, P. (1965). Studies in Stellar Evolution. III. The Calculation of Model Envelopes. , 142:841.

Hesser, J. E. and Bell, R. (1980). Cn variations among main-sequence 47 tucanae stars. *Astrophysical Journal, Part 2-Letters to the Editor, vol. 238, June 15, 1980, p. L149-L153. NSF-supported research.*, 238:L149–L153.

Hirai, R. and Yamada, S. (2015). Possible signatures of ejecta–companion interaction in iptf 13bvn. *The Astrophysical Journal*, 805:170.

Hollyhead, K., Kacharov, N., Lardo, C., Bastian, N., Hilker, M., Rejkuba, M., Koch, A., Grebel, E. K., and Georgiev, I. (2017). Evidence for multiple populations in the intermediate-age cluster Lindsay 1 in the SMC. , 465(1):L39–L43.

Holtzman, J. A. et al. (2018). Apogee data and spectral analysis from sdss data release 14. *The Astronomical Journal*, 156:125. doi:10.3847/1538-3881/aad4f9.

Hopkins, P. F. (2014). Some Stars are Totally Metal: A New Mechanism Driving Dust across Star-forming Clouds, and Consequences for Planets, Stars, and Galaxies. , 797(1):59.

Horta, D., Schiavon, R. P., Mackereth, J. T., Pfeffer, J., Mason, A. C., Kisku, S., Fragkoudi, F., Allende Prieto, C., Cunha, K., Hasselquist, S., Holtzman, J., Majewski, S. R., Nataf, D., O'Connell, R. W., Schultheis, M., and Smith, V. V. (2021). Evidence from APOGEE for the presence of a major building block of the halo buried in the inner Galaxy. , 500(1):1385–1403.

Hughes, J., Kunder, A., Larson, K., Covey, K., Torset, S., Kolmanovsky, M., Luna, C., Silva, E., Webster, K., Johnson, C., Kader, J., Rich, R. M., Simion, I., Koch-Hansen, A., Vivas, K., Pilachowski, C., Clarkson, W., Michael, S., and Marchetti, T. (2023). NGC 6569: The Discovery of Extra-Tidal Stars. In *American Astronomical Society Meeting Abstracts*, volume 241 of *American Astronomical Society Meeting Abstracts*, page 402.17.

Iliadis, C., D'Auria, J. M., Starrfield, S., Thompson, W. J., and Wiescher, M. (2001). Proton-induced Thermonuclear Reaction Rates for A=20-40 Nuclei. , 134(1):151–171.

James, G., François, P., Bonifacio, P., Carretta, E., Gratton, R. G., and Spite, F. (2004). Heavy elements and chemical enrichment in globular clusters. , 427:825–838.

Johnson, C. I., Caldwell, N., Rich, R. M., and Pilachowski, C. A. (2018). Multi-element abundance analysis of red giant stars in the globular cluster ngc 6569. *The Astronomical Journal*, 155(2):71.

Johnson, C. I., Kraft, R. P., Pilachowski, C. A., and Sneden, C. (2005). Chemical compositions of red giant branch stars in the globular cluster m13. *Publications of the Astronomical Society of the Pacific*, 117(836):1308.

Johnson, C. I., Rich, R. M., Caldwell, N., Mateo, M., Bailey, John I., I., Olszewski, E. W., and Walker, M. G. (2018). Exploring the Chemical Composition and Double Horizontal Branch of the Bulge Globular Cluster NGC 6569. , 155(2):71.

Johnson, C. I., Rich, R. M., Caldwell, N., Mateo, M., Bailey, J. I., Olszewski, E. W., and Walker, M. G. (2018). Exploring the chemical composition and double horizontal branch of the bulge globular cluster ngc 6569. *The Astronomical Journal*, 155(2):71.

Johnston, K. V., Majewski, S. R., Siegel, M. H., Reid, I. N., and Kunkel, W. E. (1999). Constraining the history of the sagittarius dwarf galaxy using observations of its tidal debris. *The Astronomical Journal*, 118:1719–1726.

Joyce, M., Johnson, C. I., Marchetti, T., Rich, R. M., Simion, I., and Bourke, J. (2023). The ages of galactic bulge stars with realistic uncertainties. *The Astrophysical Journal*, 946(1):28.

Jönsson, H. et al. (2018). Apogee data and spectral analysis from sdss data release 14: Improvements in chemical abundance analysis. *The Astronomical Journal*, 156:126. doi:10.3847/1538-3881/aad4f8.

Jönsson, H. et al. (2020). Apogee data and spectral analysis from sdss data release 16: New approaches and improved techniques. *The Astronomical Journal*, 160:120. doi:10.3847/1538-3881/aba592.

Kasen, D., Metzger, B., Barnes, J., Quataert, E., and Ramírez-Ruiz, E. (2017). Origin of the heavy elements in binary neutron-star mergers from a gravitational-wave event. *Nature*, 551:80–84.

Kippenhahn, R., Weigert, A., and Weiss, A. (2013). *Stellar Structure and Evolution.*

Kormendy, J. and Kennicutt, Robert C., J. (2004). Secular Evolution and the Formation of Pseudobulges in Disk Galaxies. , 42(1):603–683.

Krause, M. G. H., Charbonnel, C., Bastian, N., and Diehl, R. (2016). Gas expulsion in massive star clusters?: Constraints from observations of young and gas-free objects. *Astronomy amp; Astrophysics*, 587:A53.

Kruijssen, J. M. D., Pfeffer, J. L., Chevance, M., Bonaca, A., Trujillo-Gomez, S., Bastian, N., Reina-Campos, M., Crain, R. A., and Hughes, M. E. (2020). Kraken reveals itself - the merger history of the Milky Way reconstructed with the E-MOSAICS simulations. , 498(2):2472–2491.

Kruijssen, J. M. D., Pfeffer, J. L., Reina-Campos, M., Crain, R. A., and Bastian, N. (2019). The formation and assembly history of the Milky Way revealed by its globular cluster population. , 486(3):3180–3202.

Lagioia, E. P., Milone, A. P., Marino, A. F., Tailo, M., Renzini, A., Carlos, M., Cordoni, G., Dondoglio, E., Jang, S., Karakas, A., and Dotter, A. (2021). Multiple Stellar Populations in Asymptotic Giant Branch Stars of Galactic Globular Clusters. , 910(1):6.

Lambert, D. L. (1992). Observational Effects of Nucleosynthesis in Evolved Stars. In Edmunds, M. G. and Terlevich, R., editors, *Elements and the Cosmos*, page 92.

Lardo, C. (2013). Multiple stellar populations in globular clusters with photometry and low resolution spectroscopy.

Lardo, C., Bellazzini, M., Pancino, E., Carretta, E., Bragaglia, A., and Dalessandro, E. (2011). Mining SDSS in search of multiple populations in globular clusters. , 525:A114.

Layden, A. C. and Sarajedini, A. (1997). The Globular Cluster M54 and the Star Formation History of the Sagittarius Dwarf Galaxy. , 486(2):L107–L110.

Lebreton, Y., Goupil, M. J., and Montalbán, J. (2014). How accurate are stellar ages based on stellar models?. I. The impact of stellar models uncertainties. In Lebreton, Y., Valls-Gabaud, D., and Charbonnel, C., editors, *EAS Publications Series*, volume 65 of *EAS Publications Series*, pages 99–176.

Lecureur, A., Hill, V., Zoccali, M., Barbuy, B., Gómez, A., Minniti, D., Ortolani, S., and Renzini, A. (2007). Oxygen, sodium, magnesium, and aluminium as tracers of the galactic bulge formation. , 465(3):799–814.

Lind, K., Primas, F., Charbonnel, C., Grundahl, F., and Asplund, M. (2009). Signatures of intrinsic Li depletion and Li-Na anti-correlation in the metal-poor globular cluster NGC 6397. , 503(2):545–557.

Lugaro, M. and Herwig, F. (2001). Advances in s-process models. *Nuclear Physics A*, 688:201–208.

Mackey, A. D. and van den Bergh, S. (2005). The properties of Galactic globular cluster subsystems. , 360(2):631–645.

Maeder, A. and Meynet, G. (2006). On the origin of the high helium sequence in ω Centauri. , 448(2):L37–L41.

Majewski, S. R. et al. (2017). The apache point observatory galactic evolution experiment (apogee). *The Astronomical Journal*, 154:94. doi:10.3847/1538-3881/aa784d.

Majewski, S. R., Schiavon, R. P., Frinchaboy, P. M., Allende Prieto, C., Barkhouser, R., Bizyaev, D., Blank, B., Brunner, S., Burton, A., Carrera, R., Chojnowski, S. D., Cunha, K., Epstein, C., Fitzgerald, G., García Pérez, A. E., Hearty, F. R., Henderson, C., Holtzman, J. A., Johnson, J. A., Lam, C. R., Lawler, J. E., Maseman, P., Mészáros, S., Nelson, M., Nguyen, D. C., Nidever, D. L., Pinsonneault, M., Shetrone, M., Smee, S., Smith, V. V., Stolberg, T., Skrutskie, M. F., Walker, E., Wilson, J. C., Zasowski, G., Anders, F., Basu, S., Beland, S., Blanton, M. R., Bovy, J., Brownstein, J. R., Carlberg, J., Chaplin, W., Chiappini, C., Eisenstein, D. J., Elsworth, Y., Feuillet, D., Fleming, S. W., Galbraith-Frew, J., García, R. A., García-Hernández, D. A., Gillespie, B. A., Girardi, L., Gunn, J. E., Hasselquist, S., Hayden, M. R., Hekker, S., Ivans, I., Kinemuchi, K., Klaene, M., Mahadevan, S., Mathur, S., Mosser, B., Muna, D., Munn, J. A., Nichol, R. C., O'Connell, R. W., Parejko, J. K., Robin, A. C., Rocha-Pinto, H., Schultheis, M., Serenelli, A. M., Shane, N., Silva Aguirre, V., Sobeck, J. S., Thompson, B., Troup, N. W., Weinberg, D. H., and Zamora, O. (2017). The Apache Point Observatory Galactic Evolution Experiment (APOGEE). , 154(3):94.

Marcolini, A., Gibson, B. K., Karakas, A. I., and Sánchez-Blázquez, P. (2009). The chemical evolution of globular clusters - I. Reactive elements and non-metals. , 395(2):719–735.

Maria, L. (2016). Neutron sources and neutron-capture paths in asymptotic giant branch stars. In *Journal of Physics: Conference Series*, volume 703, page 012003. IOP Publishing.

Marigo, P., Bressan, A., Nanni, A., Girardi, L., and Pumo, M. (2013). Evolution of thermally pulsing asymptotic giant branch stars – i. the colibri code. *Monthly Notices of the Royal Astronomical Society*, 434:488–526.

Marino, A. F., Sneden, C., Kraft, R. P., Wallerstein, G., Norris, J. E., Da Costa, G., Milone, A. P., Ivans, I. I., Gonzalez, G., Fulbright, J. P., Hilker, M., Piotto, G., Zoccali, M., and Stetson, P. B. (2011). The two metallicity groups of the globular cluster M 22: a chemical perspective. , 532:A8.

Martell, S. L., Smolinski, J. P., Beers, T. C., and Grebel, E. K. (2011). Building the Galactic halo from globular clusters: evidence from chemically unusual red giants. , 534:A136.

Mart'in-Navarro, I., Barbera, F. L., Vazdekis, A., Falc'on-Barroso, J., and Ferreras, I. (2014). Radial variations in the stellar initial mass function of early-type galaxies. *Monthly Notices of the Royal Astronomical Society*, 447:1033–1048.

Martocchia, S., Cabrera-Ziri, I., Lardo, C., Dalessandro, E., Bastian, N., Kozhurina-Platais, V., Usher, C., Niederhofer, F., Cordero, M., Geisler, D., Hollyhead, K., Kacharov, N., Larsen, S., Li, C., Mackey, D., Hilker, M., Mucciarelli, A., Platais, I., and Salaris, M. (2018). Age as a major factor in the onset of multiple populations in stellar clusters. , 473(2):2688–2700.

Massari, D., Koppelman, H. H., and Helmi, A. (2019). Origin of the system of globular clusters in the Milky Way. , 630:L4.

Massari, D., Koppelman, H. H., and Helmi, A. (2019). Origin of the system of globular clusters in the milky way. *Astronomy amp; Astrophysics*, 630:L4.

Masseron, T., García-Hernández, D. A., Mészáros, S., Zamora, O., Dell'Agli, F., Allende Prieto, C., Edvardsson, B., Shetrone, M., Plez, B., Fernández-Trincado, J. G., Cunha, K., Jönsson, H., Geisler, D., Beers, T. C., and Cohen, R. E. (2019). Homogeneous analysis of globular clusters from the APOGEE survey with the BACCHUS code. I. The northern clusters. , 622:A191.

Masseron, T., Merle, T., and Hawkins, K. (2016). BACCHUS: Brussels Automatic Code for Characterizing High accUracy Spectra. Astrophysics Source Code Library, record ascl:1605.004.

Mauro, F., Moni Bidin, C., Cohen, R., Geisler, D., Minniti, D., Catelan, M., Chené, A.-N., and Villanova, S. (2012). Double Horizontal Branches in NGC 6440 and NGC 6569 Unveiled by the VVV Survey. , 761(2):L29.

Mészáros, S., Martell, S. L., Shetrone, M., Lucatello, S., Troup, N. W., Bovy, J., Cunha, K., García-Hernández, D. A., Overbeek, J. C., Allende Prieto, C., Beers, T. C., Frinchaboy, P. M., García Pérez, A. E., Hearty, F. R., Holtzman, J., Majewski, S. R., Nidever, D. L., Schiavon, R. P., Schneider, D. P., Sobeck, J. S., Smith, V. V., Zamora, O., and Zasowski, G. (2015). Exploring Anticorrelations and Light Element Variations in Northern Globular Clusters Observed by the APOGEE Survey. , 149(5):153.

Mészáros, S., Masseron, T., García-Hernández, D. A., Allende Prieto, C., Beers, T. C., Bizyaev, D., Chojnowski, D., Cohen, R. E., Cunha, K., Dell'Agli, F., Ebelke, G., Fernández-Trincado, J. G., Frinchaboy, P., Geisler, D., Hasselquist, S., Hearty, F., Holtzman, J., Johnson, J., Lane, R. R., Lacerna, I., Longa-Peña, P., Majewski, S. R., Martell, S. L., Minniti, D., Nataf, D., Nidever, D. L., Pan, K., Schiavon, R. P., Shetrone, M., Smith, V. V., Sobeck, J. S., Stringfellow, G. S., Szigeti, L., Tang, B., Wilson, J. C., and Zamora, O. (2020). Homogeneous analysis of globular clusters from the APOGEE survey with the BACCHUS code - II. The Southern clusters and overview. , 492(2):1641–1670.

Meylan, G. (2003). Globular Clusters: a Partial Overview. In Piotto, G., Meylan, G., Djorgovski, S. G., and Riello, M., editors, *New Horizons in Globular Cluster Astronomy*, volume 296 of *Astronomical Society of the Pacific Conference Series*, page 17.

Miholics, M., Webb, J. J., and Sills, A. (2015). The dynamics of multiple populations in the globular cluster NGC 6362. , 454(2):2166–2172.

Milone, A., Bedin, L., Piotto, G., Anderson, J., King, I., Sarajedini, A., Dotter, A., Chaboyer, B., Marín-Franch, A., Majewski, S., et al. (2008). The acs survey of galactic globular clusters. iii. the double subgiant branch of ngc 1851. *The Astrophysical Journal*, 673(1):241.

Milone, A. P. (2015). Helium and multiple populations in the massive globular cluster NGC 6266 (M 62). , 446(2):1672–1684.

Milone, A. P., Piotto, G., Bedin, L. R., Cassisi, S., Anderson, J., Marino, A. F., Pietrinferni, A., and Aparicio, A. (2012). Luminosity and mass functions of the three main sequences of the globular cluster NGC 2808. , 537:A77.

Milone, A. P., Piotto, G., Renzini, A., Marino, A. F., Bedin, L. R., Vesperini, E., D'Antona, F., Nardiello, D., Anderson, J., King, I. R., Yong, D., Bellini, A., Aparicio, A., Barbuy, B., Brown, T. M., Cassisi, S., Ortolani, S., Salaris, M., Sarajedini, A., and van der Marel, R. P. (2017). The Hubble Space Telescope UV Legacy Survey of Galactic globular clusters - IX. The Atlas of multiple stellar populations. , 464(3):3636–3656.

Milone, A. P. e. a. (2017). The hubble space telescope uv legacy survey of galactic globular clusters - v. the multiple populations. *Monthly Notices of the Royal Astronomical Society*, 464:3636–3656.

Minniti, D. and Zoccali, M. (2007). The galactic bulge: a review. *Proceedings of the International Astronomical Union*, 3(S245):323–332.

Mott, A., Steffen, M., Caffau, E., and Strassmeier, K. G. (2020). Improving spectroscopic lithium abundances. Fitting functions for 3D non-LTE corrections in FGK stars of different metallicity. , 638:A58.

Mucciarelli, A., Bellazzini, M., Ibata, R., Merle, T., Chapman, S. C., Dalessandro, E., and Sollima, A. (2012). News from the Galactic suburbia: the chemical composition of the remote globular cluster NGC 2419. , 426(4):2889–2900.

Muratov, A. L. and Gnedin, O. Y. (2010). Modeling the metallicity distribution of globular clusters. *The Astrophysical Journal*, 718(2):1266.

Muñoz, C., Villanova, S., Geisler, D., Saviane, I., Dias, B., and Cortes, C. (2017). Stellar populations of the galactic bulge globular cluster ngc 6441: Chemical abundance distributions from high-resolution spectroscopy. *Monthly Notices of the Royal Astronomical Society*, 465(4):4661–4677.

Myeong, G. C., Vasiliev, E., Iorio, G., Evans, N. W., and Belokurov, V. (2019).

Evidence for two early accretion events that built the Milky Way stellar halo. , 488(1):1235–1247.

Nave, C. (2010). Nuclear binding energy. *Hyperphysics. GSU, Atlanta.*

Navin, C. A., Martell, S., and Zucker, D. (2015). New cluster members and halo stars of the galactic globular cluster ngc 1851. *Monthly Notices of the Royal Astronomical Society*, 453:531–540.

Nidever, D. L. et al. (2015). The data reduction pipeline for the apache point observatory galactic evolution experiment. *The Astronomical Journal*, 150:173. doi:10.1088/0004-6256/150/6/173.

Norris, J., Cottrell, P., Freeman, K., and Da Costa, G. (1981). The abundance spread in the giants of ngc 6752. *Astrophysical Journal, Part 1, vol. 244, Feb. 15, 1981, p. 205-220.*, 244:205–220.

Norris, J. E. (2004). The helium abundances of ω centauri. *The Astrophysical Journal*, 612(1):L25.

Origlia, L., Rich, R., and Castro, S. (2002). High-resolution infrared spectroscopy of bulge giants: The first detailed abundances for stars in the galactic center. *The Astronomical Journal*, 123:1559–1575.

Origlia, L., Rich, R. M., Ferraro, F. R., Lanzoni, B., Valenti, E., Mucciarelli, A., and Beccari, G. (2011). Infrared high-resolution spectroscopy of bulge globular clusters. iv. the helium content of ngc 6441. *The Astrophysical Journal*, 726(2):L20.

Ortolani, S., Renzini, A., Gilmozzi, R., Marconi, G., Barbuy, B., Bica, E., and Rich, R. (1995). The distance to the galactic centre based on rr lyrae variables in the nuclear bulge. *Nature*, 377:701–703.

Osborn, W. (1971). Two new cn-strong globular cluster stars. *The Observatory, Vol. 91, p. 223-224 (1971)*, 91:223–224.

Pagel, B. E. J. (1997). *Nucleosynthesis and Chemical Evolution of Galaxies.*

Pancino, E., Romano, D., Tang, B., Tautvaišienė, G., Casey, A., Gruyters, P., Geisler, D., San Roman, I., Randich, S., Alfaro, E. J., et al. (2017a). The gaia-eso survey-mg-al anti-correlation in idr4 globular clusters. *Astronomy & Astrophysics*, 601:A112.

Pancino, E., Romano, D., Tang, B., Tautvaišienė, G., Casey, A. R., Gruyters, P., Geisler, D., San Roman, I., Randich, S., Alfaro, E. J., Bragaglia, A., Flaccomio, E., Korn, A. J., Recio-Blanco, A., Smiljanic, R., Carraro, G., Bayo, A., Costado, M. T., Damiani, F., Jofré, P., Lardo, C., de Laverny, P., Monaco, L., Morbidelli, L., Sbordone, L., Sousa, S. G., and Villanova, S. (2017b). Thegaia-eso survey: Mg-al anti-correlation in idr4 globular clusters. *Astronomy amp; Astrophysics*, 601:A112.

Parmentier, G., Jehin, E., Magain, P., Neuforge, C., Noels, A., and Thoul, A. A. (1999). The self-enrichment of galactic halo globular clusters. A clue to their formation? , 352:138–148.

Pasquini, L., Bonifacio, P., Randich, S., Galli, D., Gratton, R. G., and Wolff, B. (2007). Beryllium abundance in turn-off stars of ngc 6752. *Astronomy amp; Astrophysics*, 464(2):601–607.

Paunzen, E., Netopil, M., and Zwintz, K. (2006). Investigating star formation in the young open cluster ngc 6383. *Astronomy Amp; Astrophysics*, 462:157–162.

Piotto, G. (2009). The supernovae multiple population phenomenon in gcs. *Proceedings of the International Astronomical Union*, 5:233–240.

Piotto, G., Bedin, L., Anderson, J., King, I., Cassisi, S., Milone, A., Villanova, S., Pietrinferni, A., and Renzini, A. (2007a). A triple main sequence in the globular cluster ngc 2808. *The Astrophysical Journal*, 661(1):L53.

Piotto, G., Bedin, L. R., Anderson, J., King, I. R., Cassisi, S., Milone, A. P., Villanova, S., Pietrinferni, A., and Renzini, A. (2007b). A triple main sequence in the globular cluster ngc 2808. *The Astrophysical Journal*, 661(1):L53–L56.

Prantzos, N., Abia, C., Cristallo, S., Limongi, M., and Chieffi, A. (2019). Chemical evolution with rotating massive star yields ii. a new assessment of the solar s- and r- process components. *Monthly Notices of the Royal Astronomical Society*.

Prantzos, N. and Charbonnel, C. (2006). On the self-enrichment scenario of galactic globular clusters: constraints on the imf. *Astronomy amp; Astrophysics*, 458(1):135–149.

Prantzos, N. and Charbonnel, C. (2006). On the self-enrichment scenario of galactic globular clusters: constraints on the IMF. , 458(1):135–149.

Ratkiewicz, A., Cizewski, J., Escher, J., Potel, G., Burke, J., Casperson, R., McCleskey, M., Austin, R., Burcher, S., Hughes, R., Manning, B., Pain, S., Peters, W., Rice, S., Ross, T., Scielzo, N., Shand, C., and Smith, K. (2019). Towards neutron capture on exotic nuclei: demonstrating (d,p) as a surrogate reaction for (n,)</mml:m. *Physical Review Letters*, 122.

Renzini, A. (1988). Globular clusters as single stellar populations. *Annual Review of Astronomy and Astrophysics*, 26:199–245.

Rich, R. M. (1990). The stellar content of the galactic bulge. *Publications of the Astronomical Society of the Pacific*, 102:381–401.

Rich, R. M. (2001). The age of the galactic bulge. *arXiv preprint astro-ph/0108107*.

Roh, D.-G., Lee, Y.-W., Joo, S.-J., Han, S.-I., Sohn, Y.-J., and Lee, J.-W. (2011). Two Distinct Red Giant Branches in the Globular Cluster NGC 288. , 733(2):L45.

Romero-Colmenares, M., Fernández-Trincado, J. G., Geisler, D., Souza, S. O., Villanova, S., Longa-Peña, P., Minniti, D., Beers, T. C., Bidin, C. M., Perez-Villegas, A., Moreno, E., Garro, E. R., Baeza, I., Henao, L., Barbuy, B., Alonso-García, J., Cohen, R. E., Lane, R. R., and Muñoz, C. (2021). CAPOS: The bulge Cluster APOgee Survey. II. The intriguing "Sequoia" globular cluster FSR 1758. , 652:A158.

Salaris, M. and Cassisi, S. (2005). *Evolution of Stars and Stellar Populations.*

Salaris, M. and Cassisi, S. (2014). Lithium and oxygen in globular cluster dwarfs and the early disc accretion scenario. , 566:A109.

Salaris, M., Cassisi, S., and Pietrinferni, A. (2016). On the red giant branch mass loss in 47 tucanae: constraints from the horizontal branch morphology. *Astronomy and Astrophysics*, 590:A64.

Salaris, M., Chieffi, A., and Straniero, O. (1993). The alpha -enhanced Isochrones and Their Impact on the FITS to the Galactic Globular Cluster System. , 414:580.

Saracino, S., Dalessandro, E., Ferraro, F. R., Lanzoni, B., Geisler, D., Cohen, R. E., Bellini, A., Vesperini, E., Salaris, M., Cassisi, S., Pietrinferni, A., Origlia, L., Mauro, F., Villanova, S., and Moni Bidin, C. (2019). A Panchromatic View of the Bulge Globular Cluster NGC 6569. , 874(1):86.

Schiavon, R. P., Zamora, O., Carrera, R., Lucatello, S., Robin, A. C., Ness, M., Martínez-Valpuesta, I., García-Hernández, D. A., Allende Prieto, C., Beers, T. C., Fernández-Trincado, J., Geisler, D., Mészáros, S., and Schultheis, M. (2017). Chemical tagging with apogee: Discovery of a large population of n-rich stars in the inner galaxy. *Monthly Notices of the Royal Astronomical Society*, 465(4):501–524.

Schramm, D. N. and Turner, M. S. (1998). Big-bang nucleosynthesis enters the precision era. *Reviews of Modern Physics*, 70(1):303–318.

Sha, G., Marceau, R. K., Gao, X., Muddle, B. C., and Ringer, S. (2011). Nanostructure of aluminium alloy 2024: Segregation, clustering and precipitation processes. *Acta Materialia*, 59:1659–1670.

Shetrone, M. D. (1996). Al, Mg and Eu Abundances in Globular Cluster Giants. I. Tests of Deep Mixing. , 112:1517.

Shetrone, M. D. et al. (2015). The apogee red clump catalog: I. stellar parameters. *The Astronomical Journal*, 150:5. doi:10.1088/0004-6256/150/2/5.

Silva, E., Covey, K., Webster, K., Larson, K., Hughes, J., Kunder, A., and Price-Whelan, A. (2023). What tidal tails tell you: case studies of Segue 3 and NGC 6569. In *American Astronomical Society Meeting Abstracts*, volume 241 of *American Astronomical Society Meeting Abstracts*, page 402.16.

Slemer, A., Marigo, P., Piatti, D., Aliotta, M., Bemmerer, D., Best, A., Boeltzig, A., Bressan, A., Broggini, C., Bruno, C. G., Caciolli, A., Cavanna, F., Ciani, G. F., Corvisiero, P., Davinson, T., Depalo, R., Di Leva, A., Elekes, Z., Ferraro, F., Formicola, A., Fülöp, Z., Gervino, G., Guglielmetti, A., Gustavino, C., Gyürky, G., Imbriani, G., Junker, M., Menegazzo, R., Mossa, V., Pantaleo, F. R., Prati, P., Straniero, O., Szücs, T., Takács, M. P., and Trezzi, D. (2017). ^{22}Ne and ^{23}Na ejecta from intermediate-mass stars: the impact of the new LUNA rate for ^{22}Ne(p, γ)^{23}Na. , 465(4):4817–4837.

Smith, J. and Doe, J. (2021). The precision of iron abundance measurements using high-resolution spectroscopy. *Astronomy Astrophysics*, 645:A123.

Smith, V. V., Bizyaev, D., Cunha, K., Shetrone, M. D., Souto, D., Allende Prieto, C., Masseron, T., Mészáros, S., Jönsson, H., Hasselquist, S., Osorio, Y., García-Hernández, D. A., Plez, B., Beaton, R. L., Holtzman, J., Majewski, S. R., Stringfellow, G. S., and Sobeck, J. (2021). The APOGEE Data Release 16 Spectral Line List. , 161(6):254.

Smith, V. V., Cunha, K., Ivans, I. I., Lattanzio, J. C., Campbell, S., and Hinkle, K. H. (2005). Fluorine Abundance Variations in Red Giants of the Globular Cluster M4 and Early-Cluster Chemical Pollution. , 633(1):392–397.

Smith, V. V., Cunha, K., Shetrone, M. D., Meszaros, S., Allende Prieto, C., Bizyaev, D., García Pérez, A., Majewski, S. R., Schiavon, R., Holtzman, J., and Johnson, J. A. (2013). Chemical Abundances in Field Red Giants from High-resolution H-band Spectra Using the APOGEE Spectral Linelist. , 765(1):16.

Smith, V. V. et al. (2021). The apogee data release 16 spectral line list. *The Astronomical Journal*, 161:28. doi:10.3847/1538-3881/abccd7.

Sneden, C., Cowan, J., and Gallino, R. (2008). Neutron-capture elements in the early galaxy. *Annual Review of Astronomy and Astrophysics*, 46:241–288.

Sneden, C., Cowan, J., Ivans, I., Fuller, G., Burles, S., Beers, T., and Lawler, J. (2000). Neutron-capture elements in the early galaxy: Insights from a large sample of metal-poor giants. *The Astrophysical Journal*, 533:L139–L142.

Sneden, C., Kraft, R. P., Guhathakurta, P., Peterson, R. C., and Fulbright, J. P. (2004). The chemical compositions of red giants. vi. aluminum and other light elements in the globular cluster m3. *The Astronomical Journal*, 127(4):2162.

Sneden, C., C. J. J. and Gallino, R. (2008). Neutron-capture elements in the early galaxy. *Annual Review of Astronomy and Astrophysics*, 46:241–288.

Surot, F., Valenti, E., Gonzalez, O., Zoccali, M., Sökmen, E., Hidalgo, S., and Minniti, D. (2020). Mapping the stellar age of the milky way bulge with the vvv-iii. high-resolution reddening map. *Astronomy & Astrophysics*, 644:A140.

Tadaki, K.-i., Genzel, R., Kodama, T., Wuyts, S., Wisnioski, E., Förster Schreiber, N. M., Burkert, A., Lang, P., Tacconi, L. J., Lutz, D., Belli, S., Davies, R. I., Hatsukade, B., Hayashi, M., Herrera-Camus, R., Ikarashi, S., Inoue, S., Kohno, K., Koyama, Y., Mendel, J. T., Nakanishi, K., Shimakawa, R., Suzuki, T. L., Tamura, Y., Tanaka, I., Übler, H., and Wilman, D. J. (2017). Bulge-forming Galaxies with an Extended Rotating Disk at z ~2. , 834(2):135.

Tumlinson, J. (2009). Chemical evolution in hierarchical models of cosmic structure. ii. the formation of the milky way stellar halo and the distribution of the oldest stars. *The Astrophysical Journal*, 708(2):1398.

Uttenthaler, S., McDonald, I., Bernhard, K., Cristallo, S., and Gobrecht, D. (2019). Interplay between pulsation, mass loss, and third dredge-up: More about Miras with and without technetium. , 622:A120.

Valenti, E., Origlia, L., and Ferraro, F. R. (2005). Near-infrared photometry of four metal-rich bulge globular clusters: NGC 6304, 6569, 6637 and 6638*. , 361(1):272–282.

Valenti, E., Origlia, L., and Rich, R. M. (2011). High-resolution near-infrared spectra of NGC 6624 and 6569. , 414(3):2690–2695.

Valenti, E., Origlia, L., and Rich, R. M. (2011). High-resolution near-infrared spectra of ngc 6624 and 6569: Hr-ir spectra of ngc 6624 amp; 6569. *Monthly Notices of the Royal Astronomical Society*, 414(3):2690–2695.

Valenti, E., Zoccali, M., Gonzalez, O. A., Minniti, D., Alonso-García, J., Marchetti, E., Hempel, M., Renzini, A., and Rejkuba, M. (2016). Stellar density profile and mass of the Milky Way bulge from VVV data. , 587:L6.

van Loon, J. T., Stanimirović, S., Putman, M. E., Peek, J. E. G., Gibson, S. J., Douglas, K. A., and Korpela, E. J. (2009). A peculiar HI cloud near the distant globular cluster Pal4. , 396(2):1096–1105.

VandenBerg, D. A., Bergbusch, P. A., and Dowler, P. D. (2006). The Victoria-Regina Stellar Models: Evolutionary Tracks and Isochrones for a Wide Range in Mass and Metallicity that Allow for Empirically Constrained Amounts of Convective Core Overshooting. , 162(2):375–387.

Vasiliev, E. and Baumgardt, H. (2021). Gaia EDR3 view on galactic globular clusters. , 505(4):5978–6002.

Ventura, P. and D'Antona, F. (2008). Agb models of intermediate-mass stars and the chemical evolution of the galactic bulge. *Astronomy & Astrophysics*, 479:805–815.

Ventura, P., Di Criscienzo, M., Carini, R., and D'Antona, F. (2013). Agb models of metal-poor, low-mass stars and the interpretation of abundances in chemically peculiar globular clusters. *Monthly Notices of the Royal Astronomical Society*, 431(4):3642–3653.

Ventura, P., García-Hernández, D. A., Dell'Agli, F., D'Antona, F., Mészáros, S., Lucatello, S., Di Criscienzo, M., Shetrone, M., Tailo, M., Tang, B., and Zamora, O. (2016). Evidence of AGB Pollution in Galactic Globular Clusters from the Mg-Al Anticorrelations Observed by the APOGEE Survey. , 831(2):L17.

Villanova, S., Geisler, D., Gratton, R. G., and Cassisi, S. (2014). The Metallicity Spread and the Age-Metallicity Relation of ω Centauri. , 791(2):107.

Villanova, S., Piotto, G., King, I., Anderson, J., Bedin, L., Gratton, R., Cassisi, S., Momany, Y., Bellini, A., Cool, A., et al. (2007). The multiplicity of the subgiant branch of ω centauri: evidence for prolonged star formation. *The Astrophysical Journal*, 663(1):296.

Wagoner, R. V., Fowler, W. A., and Hoyle, F. (1967). On the Synthesis of Elements at Very High Temperatures. , 148:3.

Wijnen, T. P. G., Pols, O. R., Pelupessy, F. I., and Portegies Zwart, S. (2016). Face-on accretion onto a protoplanetary disc. , 594:A30.

Wilson, J. C. et al. (2019). The apache point observatory galactic evolution experiment 2 (apogee-2): Overview of the survey and science highlights. *The Astronomical Journal*, 157:104. doi:10.3847/1538-3881/aafc2e.

Yong, D., Da Costa, G. S., and Norris, J. E. (2016). Confirming the intrinsic abundance spread in the globular cluster NGC 6273 (M19) with calcium triplet spectroscopy. , 460(2):1846–1853.

Yong, D., Grundahl, F., Lambert, D. L., Nissen, P. E., and Jensen, H. R. (2003). The chemical composition of red giants in the globular cluster ngc 6752: The third dredge-up and the asymptotic giant branch. *Astronomy & Astrophysics*, 402:985–998.

Yong, D., Grundahl, F., Nissen, P. E., Jensen, H. R., and Lambert, D. L. (2005). Abundances in giant stars of the globular cluster ngc 6752. *Astronomy amp; Astrophysics*, 438(3):875–888.

Zamora, O. et al. (2015). The apogee stellar parameter and chemical abundances pipeline: Scaled-solar and -element enhanced model atmosphere grids. *The Astronomical Journal*, 149:181. doi:10.1088/0004-6256/149/6/181.

Zasowski, G., Schultheis, M., Hasselquist, S., Cunha, K., Sobeck, J., Johnson, J. A., Rojas-Arriagada, A., Majewski, S. R., Andrews, B. H., Jönsson, H., Beers, T. C., Chojnowski, S. D., Frinchaboy, P. M., Holtzman, J. A., Minniti, D., Nidever, D. L., and Nitschelm, C. (2019). Apogee dr14/dr15 abundances in the inner milky way. *The Astrophysical Journal*, 870(2):138.

Zhou, Y., Wang, C., Yan, H., Huang, Y., Zhang, B., Ting, Y., Zhang, H., and Shi, J. (2022). Li-rich giants in lamost survey. iii. the statistical analysis of li-rich giants. *The Astrophysical Journal*, 931:136.

Zinn, R. (1985). The Globular Cluster System of the Galaxy. IV. The Halo and Disk Subsystems. , 293:424.

Zoccali, M., Cassisi, S., Frogel, J., Gould, A., Ortolani, S., Renzini, A., Rich, R., and Stephens, A. (2000). The initial mass function of the galactic bulge down to $\sim 0.15 m_{\odot}$. *The Astrophysical Journal*, 530:418–428.